DEVELOPMENT OF NANOPARTICLE BASED NUCLEATING AGENTS FOR POLYOLEFINS

Thesis Submitted to AcSIR For the Award of the Degree of

DOCTOR OF PHILOSOPHY

In **Chemical Sciences**

By

Mohan Raj Mani

Registration Number: 10CC11J26053

Under the guidance of

Dr. Ashish K. Lele

Dr. Vijayamohanan K. Pillai

CSIR-National Chemical Laboratory
Pune-411008, India

July 2016

Dedicated to.....

my loving parents, sister, wife and daughter

सीएसआयआर–राष्ट्रीय रासायनिक प्रयोगशाला
(वैज्ञानिक तथा औद्योगिक अनुसंधान परिषद)
डॉ. होमी भाभा मार्ग, पुणे – 411 008. भारत
CSIR-NATIONAL CHEMICAL LABORATORY
(Council of Scientific & Industrial Research)
Dr. Homi Bhabha Road, Pune - 411008. India

CERTIFICATE

This is to certify that the work incorporated in this Ph.D. thesis entitled **Development of Nanoparticle Based Nucleating Agents for Polyolefins** submitted by **Mr. Mohan Raj Mani** to Academy of Scientific and Innovative Research (AcSIR) in fulfillment of the requirements for the award of the Degree of **Doctor of Philosophy in Chemical Sciences** embodies original research work under my supervision. I further certify that this work has not been submitted to any other University or Institution in part or full for the award of any degree or diploma. Research material obtained from other sources has been duly acknowledged in the thesis. Any text, illustration, table etc., used in the thesis from other sources, have been duly cited and acknowledged.

Research Guide
(Dr. Ashish K. Lele)

Research Co-Guide
(Dr. Vijayamohanan K. Pillai)

Date: 15-07-2016

Pune

Communications Channels
NCL Level DID : 2590
NCL Board No. : +91-20-25902000
Four PRI Lines : +91-20-25902000
FAX
Director's Office : +91-20-25902601
COA's Office : +91-20-25902660
SPO's Office : +91 20 25902664
WEBSITE
www.ncl-india.org

DECLARATION

I, hereby declare that all the experiments in this thesis entitled, "**Development of Nanoparticle Based Nucleating Agents for Polyolefins**" submitted for the degree of **Doctor of Philosophy in Chemical Sciences** to Academy of Scientific and Innovative Research (AcSIR), has been carried out by me at the Polymer Science and Engineering Division of CSIR-National Chemical Laboratory, Pune, India under the guidance of **Dr. Ashish K. Lele** and **Dr. Vijayamohanan K. Pillai**. Research material obtained from other sources has been duly cited and acknowledged in the thesis. This work is original and has not been submitted in part or full by me for any degree or diploma to this or any other University.

M. Mohan

(Mohan Raj Mani)

Date: 15-07-2016

CSIR-NCL

Pune, India

Acknowledgements

I wish to express my sincere gratitude to all those peoples who have contributed and supported with their professional and personal support to the successful completion of my thesis.

Firstly, my heartfelt gratitude to Dr. C. Ramesh, my research supervisor, mentor, for his invaluable guidance, constant support and encouragement during the course of this work. I am extremely grateful to him for being an ideal nucleator for my career growth. My sincere regards and reverence are for him, forever.

My sincere thanks to Dr. K. Vijayamohanan, my research co-supervisor, for his constant support and guidance during the course of this work.

I am extremely grateful to Dr. Ashish K. Lele (Head of the Polymer Science and Engineering Division) for his financial support and encouragement in the final year. My sincere gratitude to him for accepting me as his student after the retirement of Dr.C. Ramesh from service.

I am fortunate to have a nice colleague, Mr. Yogesh Marathe who is like my brother and very kind person. My heartfelt thanks to him for assisting me with the preparation and melt-mixing of some of the compounds. Without his help it would have been difficult for me to do melt compounding alone.

I am grateful to Dr. K. Guruswamy for scientific discussions and suggestions. I am also thankful to Drs. P. A. Joy, M. V. Badiger. Suresh Bhat, C. V. Avadhani, D. Baskaran, B.B. Idage, S. B. Idage, P. P. Wadgaonkar, Dr (Mrs). Deepa Dhoble, Dr (Mrs) S. B. Idage, Mr. S. K. Menon for their help during the course of the work. My sincere thanks to Dr. E. Bhoje Gowd, NIIST, for SAXS measurements on few of the samples.

I am indeed grateful to Drs. Mallikarjuna, Kannan, Dharmaraja who were instrumental in bringing me to NCL. All these friends are my senior, classmate and junior at Bharathidasan university respectively, and my heartfelt thanks to them for helping me in every respects when I started my career at NCL.

I take this opportunity to express my gratitude to Dr. K. Panchanatheswaran, my M.Sc project supervisor. I started my research career with him and the research experience which I gained from him tremendously useful for my Ph.D thesis work. My sincere thanks to Mr. K. A. Venkatesan for mentoring my M. Sc research project at IGCAR, kalpakkam.

My special thanks to Dr. Anyya Nisal (NCL) and Mrs. Shoba (IIT Bombay) for helping me with the staining of my polymer samples.

I am blessed with a friend, Dr. Edwin who is like one of my family members and helped me in times of need. I thank him for his moral support and guidance during my stay at NCL.

I thank my close friend Dr. R. Saravanakumar for keeping me vibrant at all the stages of my career eversince we met in M.Sc. I have shared all the moments with him and many of the times he had been the one to know first.

I am fortunate to have senior friends Drs. Jose Kavitha, B.S. Krishnamurthy, Baby Mariyatra, Mothi Mohamed, Sakthivel, Hemamalini, Balasubramanium, Kannan, Naresh, Venkatachalam, Thanigaimani. I thank all of them for being kind, caring and affectionate during my masters degree at Bharathidasan university. I acknowledge the help and support of Dr. Kumaresan and Giridhar at IGCAR.

I deeply acknowledge my lab friends K. J. Kiran, Sudhakar, Karthika, Manojkumar, Soumyajyothi, Prakash, Mega, Yogesh, Amrutha, Dr. Samruthi, Jithinraj, Raja, for keeping the lab with pleasant atmosphere.

On this occasion, I must thank all the friends who made the life at NCL a very cheerful one. Drs. Ramesh, Hemant Nair, Lalitha, Kaja, Vijayanand, Arul Kashmir, Dhanalakshmi, Murugesan, Senthil Kumar, Rajambal, Senthil Kumar, Sivaranjani, Lenin, Ramsundhar, Mohan, Devaraji, Ashok, Manikandan, Mohasin, Ravi, Punith, Pandiaraj, Suresh, Raja Perumal, Nagaraj, Selvakumar, Ramesh Kumar, Immanuel, Victor Paulraj and many more.

I wish to thank all the church friends who made my stay in pune a comfortable one. Mr. Ashir selvaraj, Mr. Deva, Mr. Jayaprakash, Dr.Samuel Lasaras, Christo, Sudhan, Shyam, Jabastin, Alwin, John Aruldoss, Sathish, Francis, Abraham, Emmanuvel, David, John, and many more.

I am overwhelmed when I want to right about my parents. I find no words to express my feeling for them. Their infallible love and support always been my strength. Their patience and sacrifice will remain my inspiration throughout my life. The untiring work of my father, Mr. Mani helped me grow up to this stage. My mother Mrs. Inbavalli is hard working and deserves the Ph. D as I do. In this place I must mention about my loving sister Mrs. Vidhya Srinivasan who always stand behind me to support with love and affection which one needs the most to grow up in the life. Also, I thank my uncle G. Rengaswamy for motivating me to aim for high.

I express deep sense of gratitude to my lovely wife Mrs. Sathiya and my sweet daughter Yohanya for their patience and constant support during the final years of the research work.

Above all I thank God the Almighty for guiding me in my life. Only because of His grace this work was made possible.

Though, many have not been mentioned, none is forgotten.

M. Mani

(Mohan Raj Mani)

CONTENTS

ABSTRACT

The thesis presents the results on the nucleation of isotactic polypropylene (iPP) by various carboxylate-alumoxanes and metal organic frameworks (MOFs) based on the aluminium dicarboxylates. The lamellar morphology of the α- and the β-phases of iPP crystallized under controlled non-isothermal conditions are studied by wide-angle X-ray scattering (WAXS), small-angle X-ray scattering (SAXS) and differential scanning calorimetry (DSC). The thesis also discusses the nucleating ability of carboxylate-alumoxane in polyolefin having different side group, i.e., syndiotactic polystyrene.

Carboxylate-alumoxane nano particles and used as nucleating agent for iPP. The structures of the nucleating agents (NAs) are characterized using MALDI–TOF mass spectrometry (MS) and FT-IR spectroscopy analyses. The key molecular feature of carboxylate-alumoxanes is the bicyclic ring structure having aluminum centers linked with two carboxylate groups and the oxo ligand. The carboxylate-alumoxane with butterfly-like conformation correlates well with the nucleation characteristics of iPP and, for the first time, the impact of a thermally induced, crystalline transition of carboxylate-alumoxanes, which alters neither the structural conformation nor the nucleation efficiency of the transformed material, is demonstrated. Further, the butterfly-like structure has been subtly disturbed by appropriately choosing carboxylic acid in order to confirm its profound influence in the nucleation of iPP. The structure of *p*-*t*-butylbenzoate (PTBBA)-galloxane is isomorphic with PTBBA-alumoxane and exhibits similar crystalline transition behaviour and nucleation efficiency as that of PTBBA-alumoxane supporting the butterfly-like structure in controlling nucleation of iPP.

Preparation of carboxylate-alumoxane using dicarboxylic acids leads to the formation of metal organic framework (MOF) which exhibit a unique butterfly-like structure similar to that of carboxylate-alumoxanes due to the similar ligation around Al centers and correlates well with the nucleation characteristics of iPP. A subtle change in the structure of ligand backbone (fumarate/ succinate) does not alter the framework, nevertheless impacts the hydrophilic/hydrophobic character of the network and its subsequent nucleation characteristics. This suggests that nucleating agent should facilitate favourable interaction with hydrophobic iPP for efficient nucleation. Further, a systematic variation of the alkyl chain length in the Al-dicarboxylate does not change

the nucleation efficiency considerably, even though it increases the distance between the octahedral alumina chains in the metal-organic framework, suggesting that the butterfly-like structure present in the framework is a key aspect for nucleation. Further, the significance of the orientational conformation of the dicarboxylate around the metal centre for the nucleation is confirmed by the poor nucleation efficiency of chromium and zirconium suberates MOF where the orientation of suberate would be different from that of aluminium suberate due to difference in the ligation of carboxylate group.

Isotactic polypropylene exhibits various polymorphs depending on the experimental conditions. Among various crystalline modifications, the *β*-phase attracts attention as much as that of the *α*-phase. The *β*-phase exhibits higher ductility and impact strength compared to the *α*-phase. The iPP can be crystallized in the *β*-phase by *β*-selective nucleating agents. Carboxylate-alumoxane derived from *p*-*n*-alkylbenzoic acids, where length of the *n*-alkyl group varies from 2-8 carbon atoms, exhibits dual nucleating ability and nucleates isotactic polypropylene (iPP) into predominantly in the *β*-phase under specific conditions. The selectivity of the *β*-phase nucleation depends on the concentration of the nucleating agent, end melting temperature and cooling rate. The *β*-phase obtained from *p*-*n*-alkylbenzoate-alumoxanes is compared with the *β*-phase obtained from calcium pimelate (CaP), an efficient *β*-phase selective nucleating agent, using the results from DSC, WAXS and SAXS analysis. The lamellar morphology of iPP nucleated with different nucleating agents crystallized at different crystallization temperatures (T_C) under controlled non-isothermal conditions are evaluated using SAXS analysis. The long period increases with increasing crystallization temperature and the long period of the *β*-phase is always larger than that of the *α*-phase for a given crystallization temperature. Furthermore, the variation of long period with crystallization temperature clearly brings out two crystallization temperature ranges; the low temperature range and the high temperature range. The one-dimensional correlation analysis of the *β*-phase shows that the thickness of the crystal lamellae (*l*c) increases with T_C and exhibits the low and high crystallization temperature ranges. The morphological difference between the *α*- and the *β*-phases are discussed and attributed to the differences in the impact properties and the melting temperature.

The influence of carboxylate-alumoxane on the crystallization and morphology of syndiotactic polystyrene (sPS) has been studied to understand the efficacy of these

particles in the nucleation of sPS. Syndiotactic polystyrene is a polyolefin, analogous to iPP, having pendent phenyl groups along the polymer backbone. Nucleation efficiency studies show that the PTBBA-alumoxane is a highly efficient nucleating agent for sPS and nucleates predominantly in the α-phase as revealed by WAXS analysis. The poor nucleating ability of zirconium PTBBA complex signifies the critical role of the orientational conformation of PTBBA around metal centre in the nucleation of sPS. Aluminium succinate MOF shows coordination linkages around aluminium similar to PTBBA-alumoxane and shows high thermal stability above 300 °C but exhibits poor nucleation efficiency. This is attributed to poor interaction of sPS with alkyl groups of MOF due to difference in the polarity. The self nucleating ability of the α- and the β-crystals was evaluated by self-seeding experiments. For both the α- and the β-seeded sPS, the T_C increase with decreasing end melting temperature (T_{max}) as expected. However, α-seeded sPS always crystallizes at higher temperature compared to β-seeded sPS for a given T_{max}. Also, the dependence of T_C on T_{max} shows different temperature ranges which is attributed due to homogeneous, heterogeneous and self nucleation mechanisms. Further, crystalline morphology of the sPS non-isothermally crystallized from different T_{max} are analysed using WAXS analysis. Interestingly, the α-phase is formed from the β-seeded sPS when the T_{max} range is between 277 to 271 °C. This suggests that either the β-nuclei acts itself as heterogeneous α-nucleator or the β-nuclei transforms in to α nuclei and subsequently crystallizes in to the α-phase at this temperature range. The self-nucleation studies based on pure α- and the β-crystals suggest that under non isothermal conditions, the end melting temperature controls the final crystalline form not the crystallization temperature.

The present results thus provides valuable pathways for developing new nucleating agents based on carboxylate-alumoxanes and Al-dicarboxylate MOFs with appropriate selection and orientation of the organic linkers around the metal centre.

GLOSSARY

Al-FumA	Aluminium fumarate
Al-SubA	Aluminium suberate
Al-SucA	Aluminium succinate
BA	Benzoate
BET	Brunauer–Emmett–Teller
CaP	Calcium pimelate
Cr-SubA	Chromium suberate
DBS	dibenzylidene sorbitol
DFT	Density functional theory
DMDBS (Millad 3988)	1,3:2,4-bis(3,4-dimethylbenzylidene) sorbitol
DSC	Differential scanning calorimetry
FT-IR	Fourier transform infrared spectroscopy
GNs	Ggraphene nano sheets
GPC	Gel permeation chromatography
h	hour
HexBA	*p*-*n*-Hexylbenzoate
HPN-68	Bicyclo [2.2.1] heptane dicarboxylate salt
HT	High temperature
HTWAXS	High temperature Wide-angle X-ray scattering
iPP	Isotactic polypropylene
l_a	Amorphous layer thickness
l_C	Lamellar thickness
LT	Low temperature
LTQ	Linear trans-γ-quinacridone
MALDI-TOF MS	Matrix-assisted laser desorption/ionization Time-of-flight mass spectrometry
min	minutes
mL	Millilitre
MOF	Metal organic framework
NA11	Sodium 2,2'-methylene bis-(4,6-di-tert-butylphenyl)phosphate
NAs	Nucleating agents
NE	Nucleation efficiency

NJS	N,N-dicyclohexyl-2,6-naphthalenedicarboxamide
nm	Nanometer
NMR	Nuclear magnetic resonance
PA	Phenylacetate
*pn*ABA	*p*-*n*-alkylbezoate
POSS	polyhedral oligomeric silsesquioxane
PTBBA	*p*-*t*-butylbenzoate
PVCH	Polyvinylcyclohexane
RCP	Random copolymer
SAXS	Small-angle X-ray scattering
sPS	Syndiotactic polystryrene
T_C	Crystallization temperature upon cooling
TEM	Transmission electron microscopy
T_g	Glass transition temperature
TGA	Thermogravimetric analysis
T_m	Melting temperature
TMB-5	An aromatic amide derivative
TT	Crystalline phase transition temperature
WAXS	Wide-angle X-ray scattering
Zr-SubA	Zirconium suberate
ΔH_C	Enthalpy of crystallization
ΔH_f	Enthalpy of fusion
ν_{as}	Asymmetric stretching vibration
ν_s	Symmetric stretching vibration

List of Tables

List of Schemes

List of Figures

CHAPTER 1

General Introduction

1.1 Polypropylene

Polypropylene is invented in 1954 by Natta, by following the pioneering work of Ziegler for the preparation of "stereoregular" polymers. Polypropylene is a thermoplastic and a single largest consumed polymer in the world due to its versatility. Polypropylene possesses beneficial properties such as high surface hardness, good tensile strength, and strong chemical resistance.[1] It is used in packaging, automobile, construction, electrical & electronics, and medical industries. Today's global PP production capacity is about 60 million mt per year and is expected to reach 75 million mt per year in 2022.[2] Global polypropylene market was valued at USD 77.46 billion in 2012 and is expected to reach USD 133.3 billion by 2023 owing to the rising demand for lightweight vehicles.[1] It can be easily realized that polypropylene is one of the most important commodity thermoplastics with a deep commercial penetration and continuous research to improve/modify its properties.[3]

Depending on the ordering in the stereospecific placement of the methyl group along polymer backbone, polypropylene is classified into three different forms viz., isotactic, syndiotactic and atactic. Nevertheless, all the above forms are derived from the head to tail addition of monomer units which is referred as regiospecificity. Atactic form is referred when there is no stereo consistency in the placement of methyl group consequently it is amorphous. The pendent methyl groups in the other two forms are stereospecifically ordered (methyl group have the same configuration (isotactic) or alternating configuration (syndiotactic) with respect to the polymer backbone) which allows polymer chain pack in to the crystalline lattice during the crystallization process.[4] Among the two stereoregular forms, isotactic polypropylene is widely used thermoplastic compared to the syndiotactic polypropylene. Isotactic polypropylene is produced in different grades viz., homopolymer, random copolymer and impact copolymers. Homopolymer represents the polymers made with single type of monomers, while polymers containing a mixture of monomers are called copolymers. If the comonomer units are distributed randomly along the polymer chain then it is known as random copolymers (RCP). PP random copolymers are produced by random insertion of ethylene (up to 6 wt%) or other comonomers within the polymer chain resulting defects in the polymer chain. Due to defects the polymeric material shows

lower crystallinity, melting point, modulus and higher clarity which are desired for specific applications. The impact copolymers are molecular level intimate mixtures of propylene homopolymer and *ca.* 40 wt% ethylene-propylene rubber.[5]

1.2 Crystalline modifications of isotactic polypropylene (iPP)

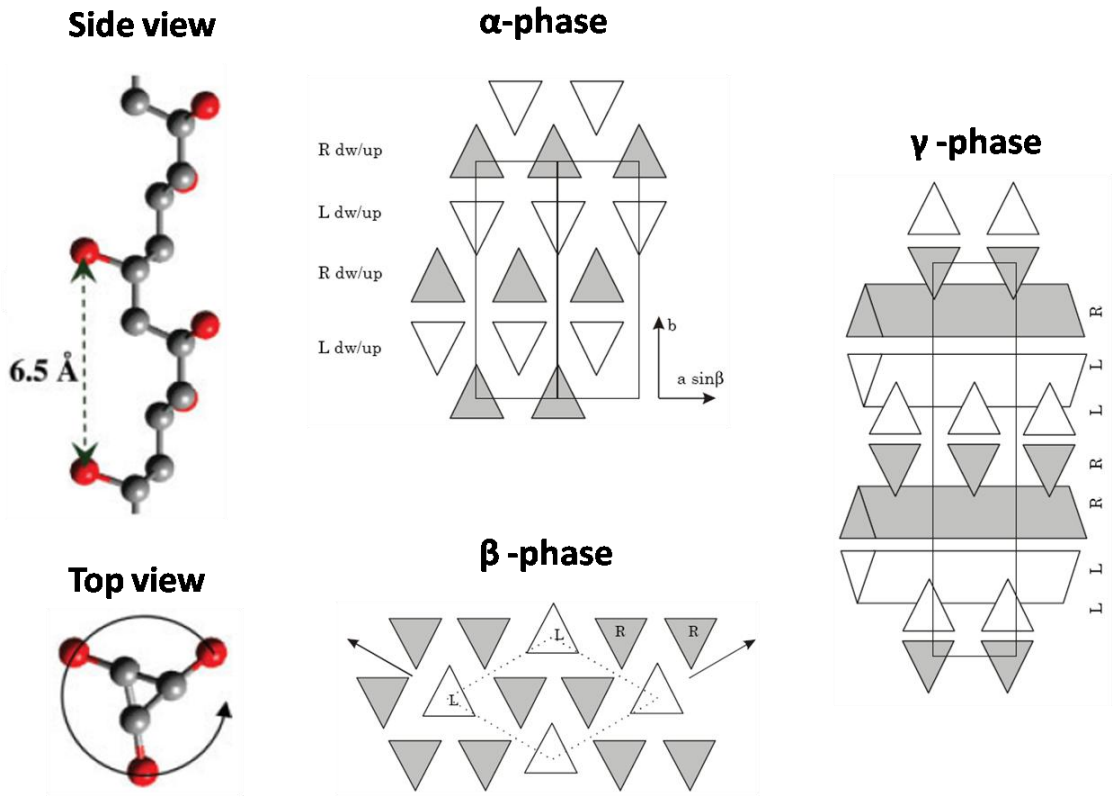

Figure 1.1: Side and top views of 3_1-helical conformation[6,7] and its molecular packing and orientations in the crystalline lattices of *α*-, *β*-, *γ*-phases of isotactic polypropylene.[8-10]

Isotactic polypropylene (iPP) is a semicrystalline polymer that exhibits wide range of structure and morphology depending on the experimental conditions. Padden and Keith made detailed study on the different types of spherulitic morphology exhibited by iPP.[11] Furthermore, iPP also exhibits different crystalline modifications, such as monoclinic (*α*), trigonal (*β*), orthorhombic (*γ*), smectic and ε forms. The *α*-phase is thermodynamically more stable and commonly found under melt crystallization conditions. In all the crystalline phases the polymer chain takes 3_1-helix conformation although the packing (left or right handed helix or both) and orientation (either up

(Figure 1.1) or down positioning of methyl groups) of the helical chain differs in their respective crystal lattice. The α-phase is thermodynamically more stable and commonly found under melt crystallization conditions. However, two limiting structures (disordered $\alpha 1$ and ordered $\alpha 2$) has been postulated for α-form depending on the various degrees of disorder in up and down positioning of chains.[12] The β-phase is obtained by certain specific nucleating agents[13,14] and is the most efficient route. It has also been found in the sheared polymer,[15-18] crystallization in a temperature gradient,[19] quenching the polymer melt rapidly to 100−130 °C.[18-20] The γ form has been obtained in low molecular weight polymer specimens and the use of bicyclo [2.2.1] heptane dicarboxylate salt (HPN-68) nucleating agent.[21-24] It has also been observed in high molecular weight PP crystallized under high pressure,[10] irregular iPP,[25] and propene/ethene random copolymers.[26] The ε form has been reported by Lotz in stereo defective iPP films.[27]

1.3 Nucleating agents for polypropylene

Development of nucleating agents for the semi-crystalline polymers is an active area of research in both industry as well as academia because of its key role as additive during polymer processing. The most studied polymer is isotactic polypropylene due to the combination of moderately slow crystal growth at high degree of supercoolings along with the practical absence of sporadic nucleation.[36] The production of polypropylene is increasing exponentially and the need for the nucleating agents is also increasing proportionately. There are varieties of materials that are tested for their nucleation effect in iPP during early 1970 and extensive search had been conducted by Beck and Binsbergen.[34,38]

1.4 Role of nucleating agents in the iPP crystallization

In general, the properties of semi-crystalline polymers are governed by their structure and morphology and in turn are controlled by the crystallization characteristics of the polymer. Therefore, regulating and controlling the crystallization process is of great interest to polymer scientists and materials engineers. Solidification in polymers occur only at high degrees of supercooling (at well below their equilibrium melting temperature) due to long chain length and associated high viscosities.[28] The

crystallization process in polymer melt starts with nucleation followed by crystal growth. The homogeneous nucleation occurs due to the density fluctuation within the polymer melt during cooling to well below their melting temperature where the energy barrier is lowered. The difference in the crystallization temperature (T_C) from the equilibrium melting temperature (T^0_m) (the melting point of the thermodynamically stable extended chain crystal) is defined as degree of supercooling $\Delta T = T^o_m - T_C$. Nucleating agents reduces the degree of supercooling (ΔT) by increasing the crystallization temperature of the polymer. This is because NAs disperse evenly in the polymer matrix and provide heterogeneous nucleation site around which polymer chain can adhere and crystallize into spherulites, at temperatures higher than the non-nucleated polymer. Therefore, parts made from nucleated polymer resins can be removed from the mold at higher temperatures consequently, cycle time is reduced and productivity is raised. Due to high density of heterogeneous nucleating sites, nucleated polymer shows smaller spherulitic size with narrow size range compared to the non-nucleated polymer. The nucleating agents which improve the optical properties of the polymer to are called clarifying agents.[28] Nucleated polymers also show improved stiffness of the end product and slightly lower the impact strength. The typical DSC thermogram of the nucleated and non-nucleated isotactic polypropylene is shown in Figure 1.2.

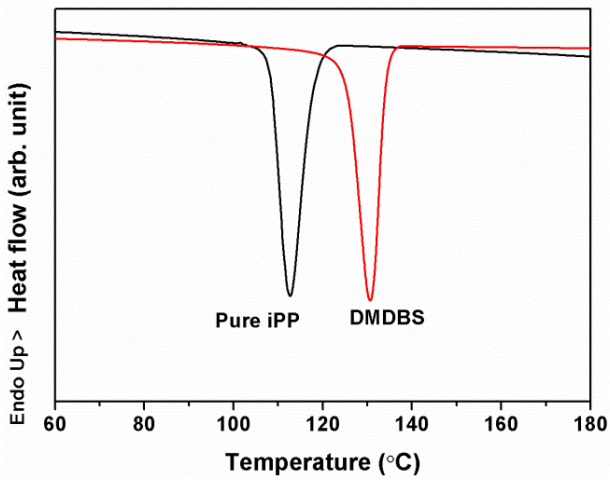

Figure 1.2: Differential scanning calorimetry (DSC) thermographs of pure iPP and iPP nucleated with DMDBS recorded at 10 °C/min cooling rate.

1.5 Nucleation mechanism

Nucleating agents fall under the class of additives, they are being used in extremely low levels (<2000 ppm) or varies up to 1 wt% depending on the active nucleation concentration of the additive. Since NAs are added in minute amounts, probing the nature of interaction between the nucleating agent and the polymer or the nucleation mechanism are very difficult to establish by experimental techniques.[29]

Frequent attempts are being made to understand the mechanism of heterogeneous nucleation. For example, nucleation via the epitaxial growth due to lattice matching is one aspect of polymer crystallization in which crystal growth occurs on the nucleating substance especially when the lattice dimension of nucleating agent matches well with the polymer unit cell dimensions.[30,31] For example, earlier investigations on epitaxial crystallization shown that the interaction of 010 plane of iPP which contains lozenge shaped array of methyl group can interact with nucleating agents having periodicities of ≈ 5, ≈ 4.2 and ≈ 6.6 Å.[30] Mathieu et al., found that the NAs with an ≈6.5Å lattice parameter induces both α- and β-phases of iPP. For example, 4-fluorobenzoic acid and dicyclohexaylterepthalamide (DCHT) are having 6.5Å periodicity but former induces exclusive α-phase while later gives β-phase. They also showed that the formation of particular crystalline phase of iPP is not only NAs specific but also depend on crystallization temperature (Tc). For example, γ-quinacridone induces either β-iPP or α-iPP when Tc is below or above ≈140 °C.

A recent theoretical study on nucleation activity has demonstrated that the attractive interaction between the polymer and the adsorbing surface is crucial for lowering the thermodynamic potential for nucleation.[32] This has been further confirmed by Smith et al.[33] by demonstrating the correlation between the nucleation ability and the van der Waals interaction of the nucleating substance with a helical form of polypropylene using molecular modelling. Binsbergen suggested after studying the nucleation ability of various metal salts of carboxylic acid that the alignment of polymer molecules along the rows of hydrocarbon domain sandwiched between polar groups cause the nucleation.[34]

Although a vast number of compounds has been shown to nucleate iPP,[35-37] only few are commercially successful, which includes sodium benzoate,[38] sorbitol derivatives,[39-41] 1,3,5-benzenetrisamide derivatives[42-44] and phenylene phosphate derivatives.[45,46] Polyvinyl cyclohexane[37] have also been shown to be efficient nucleating agent for isotactic polypropylene. This structural diversity of the known nucleating agents pose major problem in finding new nucleating agents based on chemical structures and functionalities.

1.6 *α*-Nucleating agents

1.6.1 Inorganic minerals

Development of nano size materials is attracting more interest because of high surface area and new properties which otherwise not possible with bulk materials. In respect of nucleation, many metal and metal oxide nano particles have been tested as nucleating agents.[47-54] Although many nanoparticulate systems have been tested, none of them turned out to be good nucleant as that of conventional nucleating agents.[38-46] Only marginal improvement in the crystallization temperature of polypropylene observed. For example, nucleation studies based on silver and gold nanoparticles, ZnO, Al_2O_3 and SiO_2 nanoparticles showed $T_{C,}$ increase only *ca.* 4-7 °C higher than pure polymer even with higher particle loading.[50,51,54] It has also been noticed that the nucleation of iPP by a particular material depends on its particle size. Gold particles of 4.3 nm nucleate iPP while larger particles are ineffective.[55]

Inorganic fillers such as talc, wollastonite and mica (*ca.* 0.5 -5 wt%) were the first materials studied in the nucleation of polypropylene although their primary role was to improve the mechanical properties, flame retardancy, warpage and shrinkage.[56] The nucleating efficacy of above inorganic particles follows the order talc > wollastonite > mica, which is based on the crystallization temperature (T_C) achieved with these materials in comparison with non-nucleated polymer. These inorganic fillers has different shapes (for example, talc and mica are lamellae shaped while wollastonite is acicular shaped) and were shown to induce morphological heterogeneity across the molded specimen. This effect increases with increasing nucleating ability of the filler. However, the nucleation efficiency and the subsequent reinforcement effect of these

minerals are also determined by a number of factors, including concentration, surface modification of the filler, particle size and distribution and particle shape.[36] Medeiros et al., studied the nucleation efficiency of polypropylene with talc at various concentration which shows 40% nucleation efficiency at 5 wt% loading.[57] The dependence of nucleation efficiency of polypropylene with the particle size of talc and pyrophyllites was studied by Ferrage et al. The finest particle of talc showed higher efficiency while the pyrophyllites were inactive at all sizes.[58]

Inorganic mineral nucleating agents added in excess amount have been shown to improve the mechanical properties of the polymers. This improvement is correlated to the alteration in the microstructure due to the nucleation induced by inorganic fillers in combination with their reinforcing effect due to more rigidness. For example, Perkalite improves the modulus, impact strength, thermal stability and heat deflection temperature.[59]

1.6.2 Surface modified inorganic nanoparticles

The overall efficiency of nucleation results from a combination of epitaxy quality and dispersion quality which are dictated by the surface of the nucleating particles.[36] The nucleation of polypropylene by surface functionalized nanoparticles has been explored.[59-64] Obviously, the surface modification would alter the nature of interaction of the inorganic minerals with the polymer consequently the nanofiller can exhibit either positive or negative effect on the nucleation efficiency. For example, maleated polypropylene coated $CaCO_3$ nanoparticles can successfully promote nucleation of iPP crystals, whereas the addition of nanosized calcium carbonate covered with fatty acids delays crystallization of iPP.[60] Similarly, the nucleating efficacy of the $CaCO_3$ particles has been shown to decrease with surface modification by dialkyl hydrogen phosphate as reported by Mitsuishi et al.[61] Yong Lin et al. studied the nucleation effect of stearate coated $CaCO_3$ nanoparticles.[62] They found noticeable nucleation effect for $CaCO_3$ nanoparticles with monolayer coverage while moderate or excessive coating diminishes the nucleating ability. They suggest that moderate coating lead to the formation of agglomerates while excessive coating would form a soft layer at the PP/CaCO3 interface at high temperatures, consequently weak nucleating ability. Polypropylene composites prepared using boehmite nanoparticles covered with various phosphonic

acids having different alkyl chain lengths have been reported.[63] Nano boehmite without surface modification showed better nucleation effect at 6 wt% loading compared to octyl phosphinic acid coated boehmite particles. However, the nucleation efficiency decreases drastically when it is covered with bis(2,4,4-trimethylpentyl)phosphinic acid. Perkalite, an organically modified synthetic layered double hydroxide, intercalated by polypropylene increases the crystallization temperature by 15 °C higher than pure iPP at 3 wt% loading.[59] In some cases the nanoparticles has been used as carrier for dispersing the nucleating agents. For example, 1,3,5-benzene tricarboxylic-(N-2-methylcyclohexyl)triamine (*ca.* 0.06 wt%) coated on to ZnO nanoparticles showed additional increase in T_C of 7 °C when compared to its pure form.[64]

1.6.3 Carbon based nanomaterials

In addition to inorganic nano particles, the nucleation effect of carbon based nanomaterials such as single walled carbon nanotubes (SWCNTs),[49,65,66] multiwalled carbon nanotubes (MWCNTs),[49,67] carbon nanofibers,[68] graphene nanosheets (GNSs),[69] carbon blacks[70] have been studied in polypropylene along with their reinforcement effect and electrical conductivity effect in polymer composites.[71-74] X-ray diffraction analysis on the nucleated polymers revealed these carbon based nanomaterials act as *α*-nucleators.[49,67,75] Miltner et al. studied the crystallization of iPP in the presence of single-wall and multiwall carbon nanotubes (SWCNTs and MWCNTs). At 1 wt% loading, SWCNTs and MWCNTs increased crystallization temperature by *ca.* 15 °C and *ca.* 10 °C respectively. The difference in the nucleating ability between single-wall and multiwall carbon nanotubes has been related to the surface area of the CNTs. Unfilled iPP exhibit double endothermic peak during heating which has been ascribed to the fusion of polymer crystals with varying lamellar thicknesses, either simultaneously present or as a result of recrystallization phenomena. However, CNTs filled iPP show single melting peak which has been explained due to the inhibition of recrystallization by CNTs on the chain segment mobility of the matrix. Further, the microstructure analysis revealed the transcrystalline morphology in the polypropylene nucleated with CNTs and is considerably different from that of spherulitic morphology commonly found in the iPP.[49] Assouline et al. suggested that the transcrystalline growth has been associated with fiber surface having high density of heterogeneous nucleating

sites, restricting crystal growth to the direction perpendicular to the fiber, with the c-axis aligned in the fiber direction.[67] Zhang et al. studied the transcrystallinity in the presence of CNTs. Interestingly, they observed composite microstructure during careful analysis of the interfacial morphology of CNTs fiber/polypropylene matrix; i.e., close to the nanotube fiber surface a cross-hatched lamellar structure consisting mother lamellae and daughter lamella and at the far away distance mother lamellae only.[75] Liu et al. improved the dispersion of MWCNTs in polypropylene with assistance of α-zirconium phosphate. As a result iPP showed enhanced modulus and strength only at 0.1 wt% loading of MWCNTs.[71] Similar effect has been observed in polypropylene /MWCNTs nanocomposites synthesized via the in situ polymerization approach.[72]

Lu et al. demonstrated the transcrystalline growth of iPP around the surface of the SWCNTs and MWCNTs. The growth has been induced by nucleation caused by the interaction of protruding methyl group with the graphitic layer of the CNTs. They showed that the transcrystalline layer was highly oriented around the nucleating CNTs. In addition, they demonstrated that the crystallographic c-axes of the lamellae were oriented perpendicular to the long axis of the CNT.[76] In contrast, Liu et al. showed that the c-axis of the polymer chain aligned parallel to the MWCNTs fiber.[71] Lee et al. reported that the organic modification by octadecylamine improved the dispersibility of MWNTs consequently showed enhanced electrical conductance at 2 wt% loading and improved mechanical properties at 1 wt% loading.[77] Similarly, ODA functionalised CNTs showed enhanced dispersibility in iPP matrix during solvent mixing method as reported by Grady et al.[65]

1.6.4 Organic nucleating agents

1.6.4.1 Sorbitol platform

Different types of organic compounds have been shown to be efficient nucleating agents for iPP.[35,36] Based on the core structure of the known efficient organic nucleating agents, it can be divided into three major platforms viz. sorbitol, benzenetrisamides and organophosphates. In contrast to inorganic minerals, organic nucleating agents disperse well in the polymer matrix due to better compatibility. However, the dispersion mechanism differs with respect to particular platform type. More specifically, these

nucleating agents can either be sensitive or insensitive to the polymer melt.[4] Melt insensitive nucleators do not dissolve at processing temperatures but disperse well in the polymer. Sorbitol and benzenetrisamides derivatives are melt sensitive nucleating agents while organophosphates are insensitive to the polymer melt. Melt sensitive nucleating agents dissolve in the polymer melt and on subsequent cooling phase separates into highly interconnected nanofibrillar network.[78] These nanofibrillar networks with uniform size provide very high nucleation density for the polymer to adhere and crystallize. Nogales et al. demonstrated the three-dimensional network formation by X-ray scattering which showed an anisotropic pattern for the sheared PP/DBS melt, while crystals formed in the sheared pure PP showed isotropic texture.[79] Sorbitol based effective nucleating agents are 1,3:2,4-dibenzylidene sorbitol (DBS), 1,3:2,4-bis(4-methylbenzylidene)sorbitol (MDBS), 1,3:2,4-bis(3,4-dimethylbenzylidene)sorbitol (DMDBS). The new addition to this type is nonitol based 1,2,3-tridesoxy-4,6:5,7-bis-O-[(4-propylphenyl)methylene]nonitol (TBPMN). These are chiral low molecular weight amphiphiles having a butterfly-shape/V-shape conformation in which sorbitol backbone is considered to be the 'body' and the phenyl rings are the 'wings' and the self-assembly is driven by the interplay of non-covalent

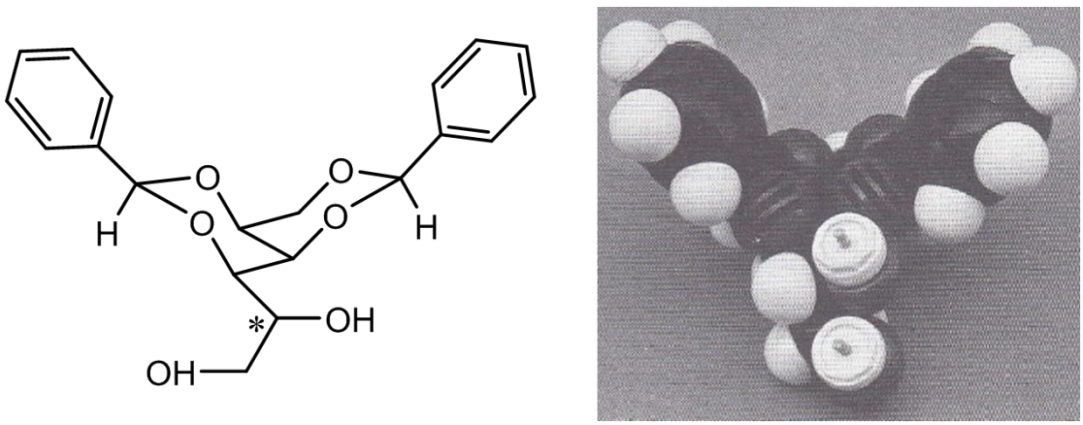

Figure 1.3: Molecular structure (left) and its 3D-model of 1,3:2,4-dibenzylidene sorbitol exhibiting the 'butterfly' shape due to the configuration of the asymmetric carbons in the parent D-glucitol. Note the apolar 'wings' (aromatic rings) and the polar sugar 'body'.[81]

interactions, predominantly hydrogen bonding and π-π stacking.[80] The molecular and 3D model of DBS is shown in Figure 1.3.

Smith et el. demonstrated the correlation between nucleation ability of V-shaped conformation and its van der Waals interaction with a helical form of polypropylene using molecular modelling. They suggested that the role of nucleator is to reduce the entropy barrier by stabilizing the helical chain which otherwise prefers to be in random coil conformation.[33] There is not much variation in the nucleation efficiency within sorbitol family. However, the active nucleation concentration varies depending on their solubility in iPP melt and is dictated by alkyl content attached to DBS. The critical concentration at which maximum efficiency is achieved for DBS, MDBS, DMDBS and DOPMN is 1000, 1500-1700, 1700-2000 and 4000 ppm respectively and above this concentration the solubility starts to decrease.[36] The role of solubility and critical temperatures for the efficiency of sorbitol clarifiers in polypropylene was studied by Horv´ath at al.[82] The phase behaviour, nucleation and optical properties of the binary system consisting of isotactic polypropylene consists of DMDBS[83] and TBPMN[84] was investigated by Paul Smith and co-workers.

1.6.4.2 Benzenetrisamide platform

Another family of efficient nucleating agents are based on benzene-1,3,5-tricarboxamide (BTA) platform.[42-44] Supramolecular chemistry of benzene-1,3,5-tricarboxamide was critically reviewed by Cantekin et al. [85] The amide group attached to a benzene core can be either three N-centred or three C=O centred amides (Figure 1.4). The three amide groups are capable of forming N-H···O=C hydrogen binding interactions to form one-dimensional growth of the monomers into supramolecular assembly under selected conditions (Figure 1.4). These compounds showed higher thermal stability (> 300 °C) or were found to undergo sublimation at those elevated temperatures, prior to melting due to the extensive H-bonding interactions (six strong H-bonds per molecule) during the formation of single columnar structure. Schmidt et al. characterized 1,3,5-Tris(2,2-dimethylpropionylamino)benzene using a combined approach based on X-ray powder diffraction and solid-state NMR spectroscopy which explained that BTA molecules were arranged in a pseudohexagonal rod packing with medium-strong hydrogen bonds and π-stacking.[86] BTA showed dispersion mechanism

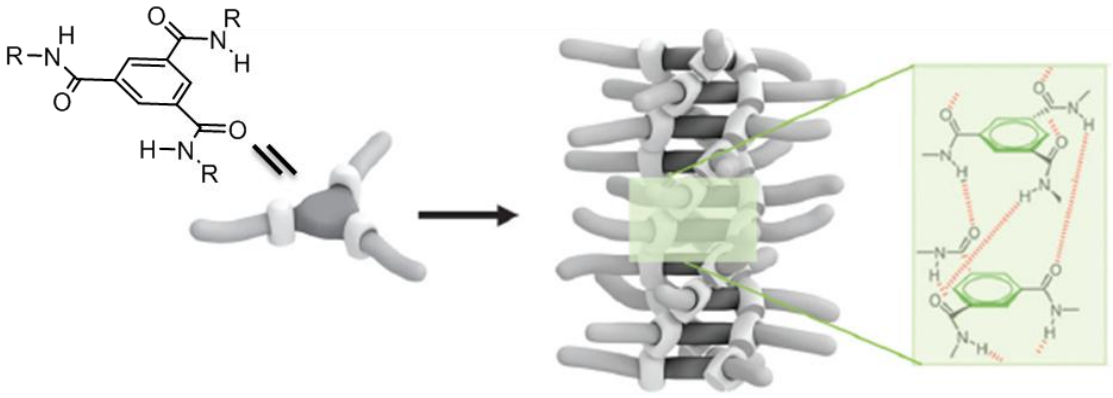

Figure 1.4: Schematic representation of benzene-1,3,5-tricarboxamide and its self-assembled helical one-dimensional aggregates, which are stabilised by threefold intermolecular N-H...O hydrogen bonding interactions and π-π stacking of the aromatic cores with distances of about 3.4 Å.[85]

similar to sorbitol derivatives, i.e., dissolution in the polymer melt followed by phase separation prior to polymer solidification. It was shown that the nucleating and clarifying abilities of BTA were strongly dependent on the additive concentration and governed by the phase behaviour of the binary system as well as solidification kinetics. The phase behavior of the binary system consisting of isotactic polypropylene and N,N',N''-tris-isopentyl-1,3,5-benzenetricarboxamide, a selected member of BTA family nucleating/clarifying agents had been investigated by Kristiansen et al.[87] BTA dissolved and self-assembled into helical columnar aggregates which provide high surface area for heterogeneous nucleation for iPP. In contrast to sorbitol based nucleating agents, BTA active nucleation concentration is very low, i.e., 0.0002 wt%. Depending on the subtle change in their chemical structure, BTA showed variation in the solid-state order, morphology and nucleation efficiency and the ability to induce specific polymorph of iPP. [42-44] The nature of the side chain was important for the BTA molecules to show nucleation effect because the exposed side groups of one single columnar helical aggregates formed a one-dimensional lattice and thereby a regular pattern on the crystal surface of the compound.[43] The repeat distance in the c-direction was 6.93 Å which was close to 6.5 Å, the spacing between the two pendent methyl groups exposed in iPP 3_1-helix, favouring epitaxial growth of the polymer on the BTA crystal lattice. Typically, when BTAs crystallized into needle like crystals of high aspect ratios (>50), an increase in crystallisation temperature of iPP (from 10 to 20 °C) was observed which was often

accompanied by a significant reduction in the haze.[43] N-centered BTA with *t*-butyl group was found to be the most effective in reducing the haze and improving the clarity of iPP.[42] This ability is now commercialised and the most effective BTA is available as Irgaclear XT 386 from BASF.[85] Abraham et al. presented a new family of 2,4,6-trimethyl-1,3,5-benzenetrisamides in which peripheral substituent varied systematically with aliphatic, aromatic and cycloaliphatic moieties. With selected derivatives of these benzenetrismides promotes α-phase formation and showed excellent nucleation performance even at a concentration of 0.00003 wt%.[45]

1.6.4.3 Organic phosphate platform

Sodium benzoate salts,[38,89] organic phosphates[88,90] and bicyclo [2.2.1] heptane dicarboxylate salt (HPN-68)[23,24] are melt insensitive nucleating agents. These compounds melt well above the polypropylene processing temperature and disperse homogeneously in the polymer matrix and provide a single point nucleation sites which accelerate α-phase crystallization. The addition of the sodium benzoate up to its saturation concentration increased the crystallization temperature by 15 °C and shortened both the isothermal and nonisothermal crystallization half-times.[89] Next to sodium benzoate, sodium 2,2′-methylene-bis-(4,6-di-t-butylphenylene)phosphate (NA-11) is widely used nucleating agent in this category. To reveal its nucleating act on iPP, NA-11 was crystallized on the oriented, thin iPP film, as well as, iPP was crystallized from the melt on NA-11 crystals. Electron microscopy analysis revealed that NA-11 epitaxially crystallized on the iPP substrate at high temperatures. This epitaxial growth was explained by the existence of lattice matching between two crystal lattices, [010]

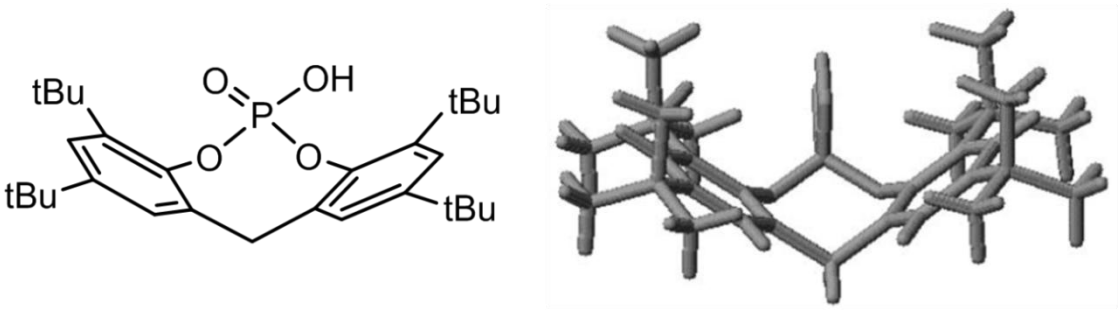

Figure 1.5: Molecular structure and model of 2,2'-methylene-bis(4,6-di-tert-butylphenyl) phosphoric acid.[88]

NA-11//[001]iPP and (001)NA-11//(010)iPP and iPP on the NA-11 crystals with the same orientational relationship.[45] Similarly, the nucleation efficiency of Lithium(I) derivative of 2,2'-methylene-bis-(4,6-di-t-butylphenylene) phosphate complex was correlated to the crystallographic matching with iPP, i.e., a cell dimension of nucleant geometry was about two times to the value of cell edge of (010)iPP.[46] Recently, ultrafine dispersion of a phosphate nucleating agent in a polypropylene matrix via the microemulsion method was reported by Guo et al.[91] They showed NA11 microemulsion disperses better in the PP matrix and improve the nucleation efficiency compared to its powder form.

The hydroxyl group in the 2,2-methylene-bis(4,6-di-tert-butylphenyl) phosphoric acid (Figure 1.5) had been modified as ethyl ester, glycol ester, phenyl ester, pentaerythritol ester, sodium salt, and triglyceride ester. Nucleation studies showed that among all the above organic phosphate derivatives, only sodium salt, and triglyceride ester increased the crystallization peak temperature of PP by 15 °C and 11 °C, respectively at 0.4 wt% nucleant concentration.[88,90] Subsequently, Zhang et al. studied the nucleation effect various metal salts of 2,2-methylene-bis(4,6-di-tert-butylphenyl) phosphoric acid derived from Na, Li, K, Ca, Mg, Zn and Al metal cations. In this series, the monovalent metal salts such as sodium, lithium and potassium salts showed a good nucleation performance. These monovalent salts incorporated into iPP at 0.2 wt% increased the crystallization peak temperature of iPP by 13.5, 13.6, and 15.0°C, respectively. But bivalent and trivalent metal salts of substituted aromatic heterocyclic phosphate showed little effect on properties of iPP.

Bicyclo [2.2.1] heptane dicarboxylate salt (HPN-68) was shown to increase the γ-phase in the PP.[23] Libster et al. improved the nucleation efficiency of HPN-68 through the incorporation into the molten polymer using a microemulsion as a nanovehicle. HPN-68 exhibited nucleation efficiency of 42% when mixed as powder at 600 ppm concentration. At lower concentration (250 ppm), mixing via microemulsion method enhanced the nucleation efficiency to 66%. This advantage was achieved by solubilizing the HPN-68 in a microemulsion to decrease its size from micro- to nanoscale. [23,24,35]

1.6.4.4 Polymeric nucleating agents

Poly(vinylcyclohexane) (PVCH) was shown to be efficient nucleating agent for isotactic polypropylene (iPP) and crystallizes iPP in the α-crystalline modifications at extremely low concentration (<200 ppm).[37] This PVCH falls in the soluble nucleating category as that of sorbitol and benzene trisamide derivatives. Lotz and co-workers investigated the cause of the its nucleation activity by growing single crystals of iPP on to the single crystals of PVCH and subjected to electron microscopy analysis. Single-crystal electron diffraction patterns and dark-field imaging demonstrated that the epitaxial relationship between α-iPP and PVCH resulted not only from a dimensional matching but also from a topographic matching of the contact faces.[31] Phillips et al. studied the effect of isotactic polystyrene (iPS) in the nucleation of polypropylene. The iPS morphology had been tuned to either crystalline or amorphous by *in-situ* heat treatment. iPS crystalline form was found to nucleate the iPP into the β-phase while iPS amorphous form induced the α-phase of iPP.[92] Reactive liquid crystal (RLC), a novel polymeric nucleating agent, was also shown to promote of the nucleation efficiency of isotactic polypropylene (iPP).[93]

Quan et al. compared the heterogeneous nucleation of isotactic polypropylene by its own fiber and other α-nucleating agents viz., DBS and NA11. Like α-nucleating agents, PP fiber showed high nucleating ability toward the iPP matrix and was demonstrated by the formation of transcrystalline layers which does not get affected by the α-nucleating agents, indicating better nucleation ability toward iPP than the nucleating agents.[94]

1.7 β-Nucleating agents

Development of β-phase iPP utilizing β-phase selective nucleating agents is also attractive area of research. The main advantage with the β-crystalline modification is that it manifests higher ductility and impact strength as compared to that of the α-phase.[95] Further, within the β-phase, Luo et al. demonstrated the connection between the β-crystal morphology and the toughening of iPP.[96] Hence, there is a constant search for finding new efficient β-nucleators although many have been reported in the literature with varying efficiencies.[1,13] The incorporation of β-selective nucleating agents are the most reliable method for the preparation of samples rich in β-modification or of pure β-

iPP. The preparation methods and supermolecular structure of the *β*-phase have been reviewed by Varga[13] and all the nucleating agents pertaining to *β*-phase nucleation have been listed in the recent review by Papageorgiou et al. The selectivity and nucleation efficiency of different nucleating agents was studied by Menyhárd et al.[97]

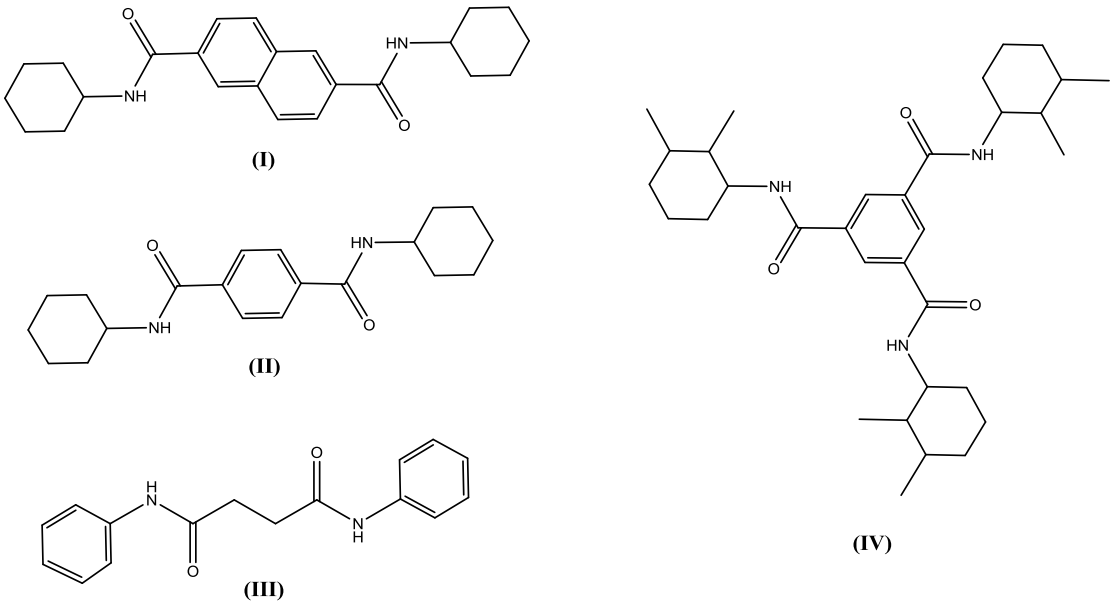

Figure 1.6: Molecular structures *β*-nucleating agents based on amide functionalities. (I) N,N'-dicyclohexyl-2,6-naphthalenedicarboxamide (NJS),[98] (II) N,N'-dicyclohexylterephthalamide,[99] (III) N,N'-Diphenylbisamides[100] and (IV) 2,3-dimethylcyclohexyl substituted 1,3,5-benzenetrisamide.[42,101]

The γ quinacridone pigment (permanent Red E3B) was found to nucleate iPP in the *β*-phase.[102,103] The *β*-nucleating ability increased with increasing γ quinacridone concentration and 85% *β*-content was obtained with 100 ppm concentration. However, the *β*-content decreased with further loading. Nearly pure *β*-polypropylene was obtained with calcium salts of suberic acid and pimelic acid.[104] Subsequently, Xiaojun Li et al. used the various calcium dicarbaoxylates for the preparation *β*-polypropylene. X-ray diffraction pattern showed high *β*-content for the ca-pimelate, ca-suberate, ca-phthalate and ca-terephthalate nucleated iPP samples.[105] Varieties *β*-nucleating agents based on amide functionalities was reported viz., N,N'-dicyclohexyl-2,6-naphthalenedicarboxamide (NJS)23[98] N,N'-dicyclohexylterephthalamide,[99] and N,N'-Diphenylbisamides[100] 2,3-dimethylcyclohexyl substituted 1,3,5-benzenetrisamide,[42,101] and TMB-5 (an aromatic amide derivative).[106,107] The molecular structures of these

compounds are shown in Figure 1.6. In addition, the *β*-phase nucleation of the derivatives each amide compound have also been studied. Menyhárd et al. studied super molecular structure of iPP in the presence of NJS that showed solubility and nucleating duality, which refers to nucleation of both the *α*- and the *β*-phases. Further, they showed the formation of final structure were influenced by the factors viz., concentration of NJS, end temperature of heating and crystallization conditions during cooling.[98] Chvátalová at al. found that the *β*-nucleation efficiency of NJS decreased with increasing molecular weight of iPP, processing time and temperature.[108] Mohmeyer et al. explored the *β*-nucleating performance of N,N'-dicyclohexylterephthalamide by tuning the chemical structure and solubility. The first modification was based on the amide linkage to benzene ring; it can be either via C=O or N-centered or combination of both. The second variation was the introduction of asymmetry by replacing of one of the cyclohexyl groups by *n*-alkyl substituent having different chain lengths. [99] Quliang LU et al. made similar studies based on N,N'-diphenyl bisamides (Figure 1.6), derived from aniline and aliphatic dicarboxylic acid in which the number of intervening methylene groups were varied from 1 to 8. Among these compounds, N,N'-diphenyl succinamide, N,N'-diphenyl glutaramide and N,N'-diphenyl adipamide were efficient *β*-nucleators for iPP and were having periodic length of ≈0.65 nm along b-axis.[100] Dong et al. studied the effect of TMB-5 on the crystallization behavior and morphological development of iPP. They found that at higher concentrations, the recrystallized TMB-5 aggregates into needle-like structure, which induced iPP with mixed polymorphic phases on the lateral surface and large amount of *β*-modification around the tip.[101]

Lanthanum complex of *β*-cyclodextrin-maleicanhydride (*β*-CDMAH-La),[109] heteronuclear dimetal complexes of lanthanum and calcium containing some specific ligands[110] also shown to nucleate iPP in the *β*-phase. However, a correlation of the molecular structure with *β*-nucleating ability was not available although preliminary efforts did not yield concrete result on their elusive role in controlling the morphology.[111]

The main characteristic of the *β*-phase, apart from its crystalline structure, is its melting temperature. The *β*-phase melts at a lower temperature (~154 °C) compared to the *α*-phase (~165 °C) and after melting it can recrystallize into the *α*-phase.[112] The *β*-

to the α-phase transformation was investigated by Forgács et al.[113] Vleeshouwers studied the behaviour of β-phase during heating by simultaneous in-situ WAXS, SAXS and DSC.[114] Cho et al. captured the transformation of the β- to the α-phase by real-time in situ X-ray diffraction using a synchrotron source. They found that the final melt temperature and hold time greatly affect the crystallization behavior during cooling and the phase transformation behavior during heating.[115] Wei Xu et al. observed the β- to the α-phase transformation during the compression of β-phase.[116] This transformation also happened due to strain induced by uniaxial-drawing as reported by Cai et al.[117] Varga demonstrated that the melting characteristics of β-polymorph depend on the previous thermal history.[118] He found no development of α-phase during heating of β-phase to the melt when the sample heated from the temperature of crystallization without cooling to room temperature. Menyhárd et al. adapted this method for finding the selectivity of various β-nucleating agents.[97] Accordingly, ca-pimelate and ca-suberate were extremely selective β-nucleators as revealed from melting endotherm which showed only melting of β-phase and no trace of α-phase melting peak. Linear trans-γ-quinacridone (LTQ) and an experimental product (CGX-220) nucleated samples showed considerable amount of α-phase along with β-phase, indicating moderate selectivity. NJS is not completely selective because small α-phase melting peak arises in the melting endotherm.[97] Kang et al compared the structure of iPP incorporated with various nucleating agents by dictating ordered structure in the melt via tuning the final melting temperature.[119] The study of crystallization kinetics of β-nucleated iPP with dual nucleating agents is difficult because of the overlapping crystallization temperature range and different growth rate of the modifications.[16,120]

1.8 Phase Transitions

Phase transformation of the β- to the α-phase via melt recrystallization during heating is well documented.[115] In addition, β- to α- growth transitions (the nuclei of α-phase forms on the growing β-crystal front) has been observed in isotactic polypropylene and is controlled by temperature of crystallization (T_C). Growth transitions occur in low and high temperature ranges. Varga et al. found high temperature growth transition occured at 140 °C and was termed as high T(β to α).[13] Lotz and co-workers observed β to α growth transitions at low temperature range (80-105 °C) which was labelled as low T(α

to β). However, in the presence of strong β-nucleants, the temperature range was found to vary.[130]

1.9 Mechanical properties of α-nucleated iPP

In general, semi-crystalline polymers are hypothesized as solid composite of two phases, amorphous and crystalline. Mechanical performance of the semi-crystalline polymer is determined by combinations of many factors such as crystalline form, lamella dimensions, crystallite size, spherulite size, number of tie molecules, crystallinity, etc.[121] Ghugare et al. showed that the combination of a small addition of the nanoscale filler with 0.2% nucleating agents has been found to give higher Young's modulus and thermal stability.[122] Zhang compared the mechanical properties and crystallization behaviors of iPP nucleated with two types of nucleating agents viz., organic phosphorous (Irgastab NA-11 and ADK NA-21) and sorbitol derivatives (Irgaclear DM and Millad 3988). All the four compounds were equally effective nucleating agents but showed variance in their mechanical and optical properties. Irgastab NA-11 and ADK NA-21 improved the tensile and flexural modulus better than Irgaclear DM and Millad 3988 but their effect on the haze was poorer as compared to Irgaclear DM and Millad.[91] Pukánszky et al. observed the correlation between Young modulus and lamellar thickness which increased with increasing temperature of crystallization.[123] Nagasawa et al. studied the crystallisation of polypropylene containing sodium benzoate, graphite powders, Millad 3988 (1,3:2,4-bis(3,4-dimethylbenzylidene sorbitol)) and NA-11 (sodium 2,2'-methylene bis-(4,6-di-tert-butylphenyl)phosphate). Nucleated polymer showed correlation between Young's modulus with the nucleus density but independent of the type of the nucleator.[124] Zhao et al. studied the crystallization, mechanical, and fracture behaviors of slilane modified alumina-filled polypropylene nanocomposites. They showed Young's modulus and the yield strength of the PP increased by the addition of Al_2O_3 particles and suggested strong interfacial interaction between the nanoparticles and PP matrix.[125] Tensile properties of polypropylene matrix incorporated with $CaCO_3$, coated with silane coupling agents have been studied by DemjÈn et al.[126]

1.10 Mechanical properties of *β*-nucleated iPP

Isotactic polypropylene with *β*-phase shows improved mechanical properties compared to the *α*-form of polypropylene. The iPP with *β*-phase exhibits banded spherulites indicating twist along the growth direction.[11] On the other hand, *α*-spherulites show low deformability and higher rigidity than the *β*-spherulites and contributes to the higher modulus of elasticity, but show slower toughness of *α*-PP.[11] Chen et al. achieved combination of *α*- and the *β*-phase properties by applying the oscillatory shear on to the *β*-nucleated polypropylene during injection molding. The skin and intermediate layer would experience more shear leading to the formation of highly oriented *α*-phase crystals while inner core crystallization would be dominated by the *β*-nucleant. This caused structural hierarchy across the injection molded specimen, consequently exhibited improved mechanical properties.[127]

Chen et al showed that the fracture toughness *β*-phase was superior to *α*-phase polypropylene and correlated to the molecular weight and tie molecules density, lamellae morphology, local hardening due to the transformation of low density *β*-phase to high density *α*-phase.[128] Xiuhong Li et al. found that the PP/ZnO nanocomposites showed lower defects (voids and dislocations) compared to that of pure PP when they analysed structural changes during tensile stretching deformation using small-angle X-ray scattering (SAXS) and wide-angle X-ray scattering (WAXS) techniques. However, defects (voids and dislocations) increased linearly with ZnO content.[129]

1.11 Effect of shear on the pure iPP, *α*- and *β*-nucleated iPP

Development of crystalline structure and morphology of polymers under shear flow attracted attention because final properties strongly depend on the processing where the polymer melt experiences intense shear stress. Leugering and Kirsch showed that the row nuclei formed in orientated polymer melt induced *β*-modification of iPP.[131] Influence of shear stress on the development of *β*-phase was successfully demonstrated by Varga and Karger-Kocsis, who showed the growth of *β*-phase on *α*-row nuclei formed by melt-shearing with fiber pulling.[15] Hsiao et al found that combination of shear and *β*-nucleant (TMB-5, an aryl amide derivative) depressed the *β*-phase content, although both the shear and *β*-nucleant independently induced *β*-polymorph in isotactic

polypropylene.[107] Chen et al. introduced relaxation process after applying a shear flow field but before cooling to crystallize β-nucleated iPP, in order to enhance fraction of β-modification.[132] Schneider and co workers showed β-nucleating ability of NJS (at higher concentration) was retarded on the application of shear while at lower concentration its β-nucleating ability retained.[133] Huo et al. demonstrated that in the presence of high content of β-nucleating agent (a mixture of lanthanum stearate (LaC), and CaCO3), the high shear rate prevented the formation of a high proportion of β-PP. On the other hand, the β-phase fraction increased with increasing shear rate when there was no or low β-nucleant content.[134] Wang and Yang found that the strong shear force applied during the gas-assisted injection molding (GAIM) process greatly influenced the morphology and the formation of β-crystals in the pure PP specimens. Detailed analysis of the molded iPP specimen showed β-phase morphology in the entire cross section.[135] Fu et al. found that the addition of polyhedral oligomeric silsesquioxane (POSS) significantly increased the crystallization rate during shear compared with the rate for the neat polymer. They postulated that molecularly dispersed POSS molecules acted as weak crosslinkers in polymer melt and increased the relaxation time of iPP chains after shear, although they have a limited role in shear-induced crystallization.[136] Jiashu Fan et al. compared the relaxation behaviour of shear induced precursors developed in the pure iPP and iPP nucleated with a series of sobitol-based nucleating agents (NA) with different nucleating abilities. In the case of nucleated iPP, the shear induced precursors relaxed much slower compared to the non-nucleated iPP. The relaxation further decreased with increasing the nucleating efficiency of the NAs.[137] Xu et al. demonstrated that under a relatively weak shear flow (at a rate of 20 s^{-1} for 5 s duration) and a low degree of supercooling, neat iPP showed isotropic structure due to the relaxation of row nuclei. While, antisotropic crystals were observed when shear flow applied to graphene nano sheets (GNs)/iPP nanocomposites, indicating the formation of a network structure assisted by GNSs which hindered the mobility of iPP chains and allowing the survival of oriented row nuclei for a long period of time. So, GNSs not only enhanced the orientation of iPP crystals but also preserved them to induce β-crystals.[138] Rastogi and co-workers found that in the presence of nucleating agent the orientation of polymer chain occurs with the lower shear rate compared to neat iPP.[139]

1.12 References

(1) "http://www.transparencymarketresearch.com/polypropylene-market.html", in Transparency Market Research

(2) https://www.platts.com/IM.Platts.Content/Downloads/PDFs/platts-global-polyolefins-outlook.pdf

(3) D. Papageorgiou, K. Chrissafis, D. Bikiaris, *Polym Rev*, 2015, **55**, 596.

(4) N. Pasquini, Polypropylene Handbook, 2nd edn, Hanser Publications, Munich, 2005, p. 147.

(5) Polypropylene at Fifty, Reliance Industries Ltd., 2010.

(6) G. Natta, P. Corradini, *Il Nuovo Cimento (1955-1965)*, 1960 **15**, 40.

(7) X. Chen, S. Kumar, R. Ozisik, *J. Polym. Sci., Part B: Polym. Phys.*, 2006, **44**, 3453.

(8) F. Auriemma, O. Ballesteros, C. Rosa, P. Corradini, *Macromolecules*, 2000, **33**, 8764.

(9) H. Keith, F. Padden, N. Walter, H. Wyckoff, *J. Appl. Phys.*, 1959, **30**, 1485.

(10) R. A. Campbell, P. Phillips, J. S. Lin, *Polymer*, 1993, **34**, 4809.

(11) F. Padden, H. Keith, *J. Appl. Phys.*, 1959, **30**, 1479.

(12) C. Rosa, G. Guerra, R. Napolitano, V. Petraccone, B. Pirozzi, *Eur. Polym. J.*, 1984, **20**, 937.

(13) J. Varga, *J. Macromol. Sci., Part B: Phys.*, 2002, **41**, 1121.

(14) D. Papageorgiou, K. Chrissafis, D. Bikiaris, *Polym. Rev.*, 2015, **55**, 596.

(15) J. Varga, J. Karger-Kocsis, *J. Polym. Sci., Part B: Polym Phys.*, 1996, **34**, 657.

(16) Y.-H. Chen, Y.-M. Mao, Z.-M. Li, B. Hsiao, *Macromolecules*, 2010, **43**, 6760.

(17) H. Dragaun, H. Hubeny, H. Muschik, *J. Polym. Sci., Phys. Ed.*, 1977, **15**, 1779.

(18) V. Leugering, Kirsch, *Angew. Makromol. Chem.*, 1973, **33**, 17.

(19) A. Lovinger, J. Chua, C. Gryte, *J. Polym. Sci., Phys. Ed.*, 1977, **15**, 641.

(20) T. Jones, J. Aizlewood, Beckett, *Angew. Makromol. Chem.*, 1964, **75**, 134.

(21) E. J. Addink, Beintema, *Polymer*, 1961, **2**, 185.

(22) B. Lotz, S. Graff, J. Wittmann, *J. Polym. Sci., Part B: Polym Phys.*, 1986, **24**, 2017.

(23) D. Libster, A. Aserin, N. Garti, *J. Colloid Interface Sci.*, 2006, **299**, 172.

(24) D. Libster, A. Aserin, N. Garti, *J. Colloid Interf. Sci.*, 2006, **302**, 322.

(25) R. Krache, R. Benavente, J. López-Majada, J. Pereña, M. Cerrada, E.

Pérez, *Macromolecules*, 2007, **40**, 6871.

(26) K. Busse, J. Kressler, R.-D. Maier, J. Scherble, *Macromolecules*, 2000, **33**, 8775.

(27) B. Lotz, *Macromolecules*, 2014, **47**, 7612.

(28) K. M. Bernland, Ph. D Thesis, ETH-Zurich, 2010.

(29) M. Schmidt, J. Wittmann, R. Kress, H.-W. Schmidt, J. Senker, *Chem. Commun.*, 2012, **49**, 267.

(30) C. Mathieu, A. Thierry, J. C. Wittmann, B. Lotz, *Polymer*, 2000, **41**, 7241.

(31) D. Alcazar, J. Ruan, A. Thierry, B. Lotz, *Macromolecules*, 2006, **39**, 2832.

(32) R. H. Ebengou, *J. Polym. Sci., Part B: Polym Phys.*, 1997, **35**, 1333.

(33) T. Smith, D. Masilamani, L. Bui, Y. Khanna, R. Bray, W. Hammond, S. Curran, J. Belles, S. Binder-Castelli, *Macromolecules*, 1994, **27**, 3147.

(34) F. L. Binsbergen, *Polymer*, 1970, 253.

(35) D. Libster, A. Aserin, N. Garti, *Polym. Adv. Technol.*, 2007, **18**, 685.

(36) M. Gahleitner, C. Grein, S. Kheirandish, J. Wolfschwenger, Nucleation of Polypropylene Homo- and Copolymers. Intern. Polym. Proces. 2011, **26**, 2.

(37) A. Menyhárd, M. Gahleitner, J. Varga, K. Bernreitner, P. Jääskeläinen, H. Øysæd, B. Pukánszky, *Eur. Polym. J.*, 2009, **45**, 3138.

(38) H. N. Beck, *J. Appl. Polym. Sci,*. 1967, **11**, 673.

(39) T. Smith, D. Masilamani, L. Bui, R. Brambilla, Y. Khanna, K. Garbriel, *J. Appl.Polym. Sci.*, 1994, **52**, 591.

(40) M. Kristiansen, M. Werner, T. Tervoort, P. Smith, M. Blomenhofer, H.-W. Schmidt, *Macromolecules*, 2003, **36**, 5150.

(41) C. Marco, G. Ellis, M. GÓmez, J. Arribas, *J. Appl. Polym. Sci.*, 2002, **84**, 2440.

(42) M. Blomenhofer, S. Ganzleben, D. Hanft, H.-W. Schmidt, M. Kristiansen, P. Smith, K. Stoll, D. Mäder, K. Hoffmann, *Macromolecules*, 2005, **38**, 3688.

(43) M. Kristiansen, P Smith, H Chanzy, C. Baerlocher, V. Gramlich, L. McCusker, T. Weber, P. Pattison, M. Blomenhofer, H.-W. Schmidt, *Cryst. Growth & Design*, 2009, **9**(6), 2553.

(44) F. Abraham, R. Kress, P. Smith, H.-W. Schmidt, *Macromol. Chem. Phys.*, 2013, **214**, 17.

(45) S. Yoshimoto, T. Ueda, K. Yamanaka, A. Kawaguchi, E. Tobita, T. Haruna,

Polymer, 2001, **42**, 9627.

(46) Y. Shi, Z. Xin, *J. Appl. Polym. Sci.*, 2012, **125**, 2963.

(47) P. Svoboda, C. Zeng, H. Wang, J. Lee, D. Tomasko, *J. Appl. Polym. Sci.*, 2002, **85**, 1562.

(48) A. Pozsgay, T. Fráter, L. Papp, I. Sajó, B. Pukánszky, *J. Macromol. Sci. Part B: Phys.*, 2002, **41**, 1249.

(49) H. Miltner, N. Grossiord, K. Lu, J. Loos, C. Koning, B. Mele, *Macromolecules*, 2008, **41**, 5753.

(50) J. Qian, P. He, K. Nie, *J. Appl. Polym. Sci.*, 2004, **91**, 1013.

(51) S. Jain, H. Goossens, M. Duin, P. Lemstra, *Polymer*, 2005, **46**, 8805.

(52) N. Preschilla, A. Rasheed, S. Sahadevan, A. Biswas, J. Bellare, S. Shyamroy, *J. Macromol. Sci. Part B: Phys.*, 2010, **48**, 1786.

(53) A. Pawlak, J. Morawiec, E. Piorkowska, A. Galeski, *Solid State Phenomena*, 2003, **94**, 335.

(54) S. C. Tjong, S. Bao, e-Polymers, 2007, art no. **139**, 1.

(55) R. Masirek, E. Szkudlarek, E. Piorkowska, M. Slouf, J. Kratochvil, J. Baldrian, *J. Polym. Sci., Part B: Polym Phys.*, 2010, **48**, 469.

(56) J. P. Trotignon, L. Demdoum, J. Verdu, *Composites*, 1992, **23**, 313.

(57) D. E. Medeiros, R Tocchetto, and D. L. Carvalho, I. M. G. Santos, A. G. Souza, *J. Therm. Anal. Cal.*, 2001, **66**, 523.

(58) E. Ferrage, F. Martin, A. Boudet, S. Petit, G. Fourty, F. Jouffret, P. Micoud, P. De Parseval, S. Salvi, C. Bourgerette, J. Ferret, Y. Saint-Gerard, S. Buratto, J. P. Fortune, *J. Mat. Sci.*, 2002, **37**, 1561.

(59) C. Marega, V. Causin, A. Marigo, G. Ferrara, H. Tonnaer, *J. Nanosci. Nanotechnol.*, 2009, **9**, 2704.

(60) M. Avella, S. Cosco, M. L. Lorenzo, E. Pace, M. E. Errico, G. Gentile, *Eur. Polym. J.*, 2006, **42**, 1548.

(61) K. Mitsuishi, S. Ueno, S. Kodama, H. Kawasaki, *J. Appl. Polym. Sci.*, 1991, **43**, 2043.

(62) Y. Lin, H. Chen, C.-M. Chan, J. Wu, *Macromolecules*, 2008, **41**, 9204.

(63) D. Bravet, O. Guiselin, and G. Swei, *J. Appl. Polym. Sci.*, 2010, **116**, 373.

(64) J. Tang, Y. Wang, H. Liu, L. Belfiore, *Polymer*, 2004, **45**, 2081.

(65) B. Grady, F. Pompeo, R. Shambaugh, D. Resasco, *J. Phys.Chem. B*, 2002, **106**, 5852.

(66) A. Bhattacharyya, T. Sreekumar, T. Liu, S. Kumar, L. Ericson, R. Hauge, R. Smalley, *Polymer*, 2003, **44**, 2373.

(67) E. Assouline, A. Lustiger, A. H. Barber, C. A. Cooper, E. Klein, E. Wachtel, H. D. Wagner, *J. Polym. Sci., Part B: Polym Phys.*, 2003, **41**, 520.

(68) S. Reyes-de Vaaben, A. Aguilar, F. Avalos, L. F. Ramos-de Valle, *J. Therm. Anal. Cal.*, 2008, **93**, 947.

(69) J.-Z. Xu, C. Chen, Y. Wang, H. Tang, Z.-M. Li, B. Hsiao, *Macromolecules*, 2011, **44**, 2808.

(70) J. Chen, X. Li, C. Wu, *Polym. J.*, 2007, **39**, 722.

(71) P. Liu, K. White, H. Sugiyama, J. Xi, T. Higuchi, T. Hoshino, R. Ishige, H. Jinnai, A. Takahara, H.-J. Sue, *Macromolecules*, 2013, **46**, 463.

(72) A. Kovalchuk, V. Shevchenko, A. Shchegolikhin, P. Nedorezova, A. Klyamkina, A. Aladyshev, *J. Mat. Sci.*, 2008, **43,** 7132.

(73) H. Kim, A. Abdala, and C. Macosko, *Macromolecules*, 2010, **43**, 6515.

(74) J. Potts, D. Dreyer, C. Bielawski, R. Ruoff, *Polymer*, 2011, **52**, 5.

(75) S. Zhang, M. Minus, L. Zhu, C.-P. Wong, S. Kumar, *Polymer*, 2008, **49**, 1356.

(76) K. Lu, N. Grossiord, C. Koning, H. Miltner, B. van Mele, J. Loos, *Macromolecules*, 2008, **41**, 8081.

(77) J.-I. Lee, S.-B. Yang, H.-T. Jung, *Macromolecules*, 2009, **42**, 8328.

(78) T. A. Shepard, C. R. Delsorbo, R. M. Louth, J. L. Walborn, D. A. Norman, N. G. H. Richard, J. Spontak, *J. Polym. Sci. B: Polym Phys.*, 1997, **35,** 2617.

(79) A. Nogales, G. Mitchell, A. Vaughan, *Macromolecules*, 2003, **36**, 4898.

(80) B. Okesola, V. Vieira, D. Cornwell, N. Whitelaw, D. Smith, *Soft Matter*, 2015, **11**, 4768.

(81) A. Thierry, C. Straupe, B. Lotz and J. C. Wittmann, *Polym. Commun.*, 1990, **31**, 299.

(82) Z. Horváth, B. Gyarmati, A. Menyhárd, P. Doshev, M. Gahleitner, J. Varga, B. Pukánszky, *RSC Adv.*, 2014, **4**, 19737.

(83) M. Kristiansen, M. Werner, T. Tervoort, P. Smith, M. Blomenhofer, H.-W. Schmidt, *Macromolecules*, 2003, **36**, 5150.

(84) K. Bernland, T. Tervoort, P. Smith, *Polymer*, 2009, **50**, 2460.

(85) S. Cantekin, T. de Greef, A. Palmans, *Chem. Soc. Rev.*, 2012, **41**, 6125.

(86) M. Schmidt, J. Wittmann, R. Kress, D. Schneider, S. Steuernagel, H.-W. Schmidt, J. Senker, *Cryst. Growth Des.*, 2012, **12**, 2543.

(87) P. Kristiansen, A. Gress, P. Smith, D. Hanft, H.-W. Schmidt, *Polymer*, 2006, **47**, 249.

(88) G. Zhang, Z. Xin, J. Yu, Q. Gui, S. Wang, *J. Macromol. Sci. Part B: Phys.*, 2003, **42**, 467.

(89) G.-S. Jang, W.-J. Cho, C.-S. Ha, *J. Polym. Sci. Part B: Polym Phys.*, 2001, **39**, 1183.

(90) Y.-F. Zhang, *J. Macromol. Sci. Part B: Phys.*, 2008, **47**, 1188.

(91) M. Guo, Y. Zhang, J. Li, G. Pan, H. Yan, Y. Luo, Y. Liu, *RSC Adv.*, 2014, **4**, 11931.

(92) R. Phillips, J. Månson, *J. Polym. Sci. Part B: Polym. Phys.*, 1997, **35**, 875.

(93) Q. Li, X. Zhang, J. Li, Z. Ouyang, H. Wang, G. Wei, Z. Su, *Polym. Eng. Sci.*, 2014, **54**, 2112.

(94) Y. Quan, H. Li, S. Yan, *Ind. Eng. Chem. Res.*, 2013, **52**, 4772.

(95) *J. Varga, G. W. Ehrenstein, A. K. Schlarb, eXPRESS polym. Let.*, 2008, **2**, 148.

(96) F. Luo, C. Geng, K. Wang, H. Deng, F. Chen, Q. Fu, B. Na, *Macromolecules*, 2009, **42**, 9325.

(97) *A. Menyhárd, J. Varga, G. Molnár. J. Therm. Anal. Calorim.*, 2006, **83**, 625

(98) J. Varga and A. Menyhárd, *Macromolecules*, 2007, **40**, 2422.

(99) N. Mohmeyer, H.-W. Schmidt, P. Kristiansen, and V. Altstädt, *Macromolecules*, 2006, **39**, 5760.

(100) Q. Lu, Q. Dou, *Polym. J.*, 2009, **41**, 254.

(101) J. Varga, K. Stoll, A. Menyhárd, Z. Horváth, *J. Appl. Polym. Sci.*,, 2011, **121**, 1469.

(102) Leugering, V. *Die Makromol. Chem.* **1967**, *109*, 204–216.

(103) Jacoby, P.; Bersted, B.; Kissel, W.; Smith, C. *J. Polym. Sci. Part B: Polym. Phys.* **1986**, *24*, 461–491.

(104) Varga, J; Mudra, I; Ehrenstein, GW. *J. Appl. Polym.Sci.*, **1999** 74, 2357-2368.

(105) X. Li, K. Hu, M. Ji, Y. Huang, G. Zhou, *J. Appl. Polym.Sci.*, 2002, **86**, 633.

(106) M. Dong, Z. Guo, J. Yu, Z. Su, *J. Polym. Sci. Part B: Polym. Phys.*, 2008, **46**, 1725.

(107) Y.-H. Chen, Y.-M. Mao, Z.-M. Li, B. Hsiao, *Macromolecules*, 2010, **43**, 6760.

(108) L. Chvátalová, J. Navrátilová, R. Čermák, M. Raab, M. badal, *Macromolecules*, 2009, **42**, 7413.

(109) A. Zeng, Y. Zheng, S. Qiu, Y. Guo, *J. Appl. Polym. Sci.*, 2011, **121**, 3651.

(110) J. Feng, M. Chen, Z. Huang, Y. Guo, H. Hu, *J. Appl. Polym. Sci.*, 2002, **85**, 1742.

(111) A Janevski, G Bogoeva-Gaceva, V Stefov, *Maced. J. Chem. Chem. Eng.*, **2015** *34, 189.*

(112) A. Lovinger, J. Chua, C. Gryte, *J. Polym. Sci.: Polym. Phys. Ed.*, 1977, **15**, 641.

(113) P. Forgács, B. Tolochko, M. Sheromov, *Polym. Bullet.*, 1981, **6**, 127.

(114) S. Vleeshouwers, *Polymer*, 1997, **38**, 3213.

(115) K. Cho, D. Saheb, J. Choi, H. Yang, *Polymer*, 2002, **43**, 1407.

(116) W. Xu, D. Martin, E. Arruda, *Polymer*, 2005, **46**, 455.

(117) Z. Cai, Y. Zhang, J. Li, F. Xue, Y. Shang, X. He, J. Feng, Z. Wu, S. Jiang, *Polymer*, 2012, **53**, 1593.

(118) Varga, *J. Therm. Anal.*, 1986, **31**, 165.

(119) J. Kang, G. Weng, Z. Chen, J. Chen, Y. Cao, F. Yang, M. Xiang, *RSC Adv.*, 2014, **4**, 29514.

(120) A. Menyhárd, G. Dora, Z. Horváth, G. Faludi, J. Varga, *J. Therm. Anal. Calorim.*, 2011, **108**, 613.

(121) J. Karger-Kocsis, *Polym. Eng. Sci.*, 1996, **36**, 203.

(122) S. Ghugare, P. Govindaiah, C. Avadhani, *Polym. Bull.*, 2009, **63**, 897.

(123) B. Pukánszky, I. Mudra, P. Staniek, *J. Vinyl Addit. Technol.*, 1997, **3**, 53.

(124) S. Nagasawa, A. Fujimori, T. Masuko, M. Iguchi, *Polymer*, 2005, **46**, 5241.

(125) H. Zhao, R. Li, *J. Polym. Sci. Part B: Polym. Phys.*, 2005, **43**, 3652.

(126) Z. Demjén, B. Pukánszky, *Polymer Composites*, 1997, **18**, 741.

(127) Y.-H. Chen, G.-J. Zhong, Y. Wang, Z.-M. Li, L. Li, *Macromolecules*, 2009, **42**, 4343.

(128) H. Chen, J. Karger-Kocsis, J. Wu, J. Varga, *Polymer*, 2002, **43**, 6505.

(129) X. Li, K. Schneider, B. Kretzschmar, M. Stamm, *Macromolecules*, 2008, **41**,

4371.

(130) B. Fillon, A. Thierry, J. Wittmann, B. Lotz, *J. Polym. Sci. Part B: Polym. Phys.*, 1993, **31**, 1407.

(131) V. Leugering G. Kirsch, *Die Angew. Makromol. Chem.*, 1973, **33**, 17.

(132) Y.-H. Chen, D.-F. Fang, J. Lei, L.-B. Li, B. Hsiao, Z.-M. Li, *J. Phys. Chem. B*, 2015, **119**, 5716.

(133) Chen, K. Schneider, B. Kretzschmar, G. Heinrich, *Polymer*, 2014, **55**, 5477.

(134) H. Huo, S. Jiang, L. An, J. Feng, *Macromolecules*, 2004, **37**, 2478.

(135) L. Wang, M.-B. Yang, *RSC Adv.*, 2014, **4**, 25135.

(136) B. Fu, L. Yang, R. Somani, S. Zong, B. Hsiao, S. Phillips, R. Blanski, P. Ruth, *J. Polym. Sci. Part B: Polym. Phys.*, 2001, **39**, 2727.

(137) J. Fan, Q. Zhang, D. Hu, Q. Ren, J. Feng, *Phys. Chem. Chem. Phys.*, 2016, **18**, 8926.

(138) J.-Z. Xu, C. Chen, Y. Wang, H. Tang, Z.-M. Li, B. Hsiao, *Macromolecules*, 2011, **44**, 2808.

(139) N. Patil, C. Invigorito, M. Gahleitner, S. Rastogi, *Polymer* 2013 **54**, 5883.

CHAPTER 2

Scope and objectives

2.1 Introduction

A control on the crystallization of isotactic polypropylene (iPP) is very important as it regulates the processing speed, energy spent for processing; aesthetics of the finished products. The crystallization process occurs in two steps; (i) nucleation, followed by (ii) crystal growth. The nucleation step is slow because the formation of nuclei of critical size is a kinetically controlled process and needs high degree of supercooling. However, this problem could be obviated by dispersing nucleating agents (NAs) into the polymer matrix during the melt processing. NAs reduce the free energy barrier of nucleation by providing a suitable surface to the polymer to adhere and grow into desired morphologies like that of spherulites. Since the nucleation step is skipped, the polymer can crystallize at a higher temperature, which decreases the cycle time along with a concomitant increase in the productivity and associated energy savings.[1,2] From commercial perspective, only very few NAs are successful in efficiently nucleating iPP which include sorbitol derivatives, sodium benzoate, phenylene phosphate derivatives etc. Although NAs fall under the class of additives, they are being used in minute amounts (< 2000 ppm) and their exact mechanism of action is still not well-understood. Furthermore, being added in minute quantities, NAs do not have reinforcing effect.

2.2. Objectives of the present work

2.2.1. The role of the molecular structure of carboxylate-alumoxanes in the enhanced nucleation of polypropylene

The structural diversity of known NAs pose a major problem in finding new nucleating agents based on chemical structures and functionalities. The existing efficient nucleating agents are based on sorbitol, benzenetrisamide and phenylenephosphate platforms.[3-5]

The focus of the present work is to develop nucleating agents having different efficiencies based on carboxylate-alumoxane platform which can be an inexpensive alternative to the existing platforms. Thus, a series of carboxylate-alumoxane was prepared using carboxylic acids having different structures and functionalities. The key aspect is to understand the nucleation mechanism and correlate the role of carboxylate-alumoxane molecular structure on the nucleating efficiency of the iPP.

2.2.2. Enhanced nucleation of polypropylene by metal-organic frameworks (MOFs) based on aluminum dicarboxylates: Influence of structural features

Preparation of carboxylate-alumoxane using dicarboxylic acids give rise to metal organic framework (MOF) structure in which ligation around of aluminum centres similar to that of carboxylate-alumoxane.[6] The physical and chemical properties of aluminum dicarboxylate MOF are different from carboxylate-alumoxanes.

The another objective of the present work is to study the nucleating ability of the various Al-dicarboxylate MOFs. The focus is to study the effect of the minor structural variation in the ligand back bone (saturated to unsaturated dicaboxylate) in the nucleation of iPP. Also, to study the influence of (i) backbone length of the dicarboxylate (varying number of intervening CH_2 groups) and (ii) changing the metal centre to Cr and Zr.

2.2.3. New understanding on regulating the crystallization and morphology of *β*-polymorph of isotactic polypropylene based on carboxylate-alumoxane nucleating agents

Isotactic polypropylene exhibits various polymorphs depending on the experimental conditions. Among various crystalline modifications, the *β*-phase exhibits higher ductility and impact strength compared to the *α*-phase.[7] The iPP can be crystallized in the *β*-phase by *β*-selective nucleating agents.[8,9] The *β*-phase selective nucleating agents are highly limited compared to *α*-nucleants. The lamellar morphology of iPP nucleated with different *α*- and *β*-nucleating agents crystallized at different crystallization temperatures (T_C) under controlled non-isothermal conditions has not been studied so far. With the proper choice of the carboxylic acids, the carboxylate-alumoxane can be made to nucleate iPP in the β phase.

Yet another objective of the present study is to characterize the development of β-phase by carboxylate-alumoxanes derived from p-n-alkylbenzoic acids where the length of the n-alkyl group systematically increased from 2-8 carbon atoms. The β-phase obtained from p-n-alkylbenzoate-alumoxanes is compared with the β-phase obtained from calcium pimelate (CaP), an efficient β-phase selective nucleating agent.. The lamellar morphology of iPP nucleated with different nucleating agents crystallized at different crystallization temperatures (T_C) under controlled non-isothermal conditions

are studied in detail for the first time using WAXS, SAXS and DSC analysis. The morphological difference between the α- and the β-phases are discussed and attributed to the differences in the impact properties and the melting temperature.

22.4. Effect of carboxylate-alumoxane on syndiotactic polystyrene (sPS) crystallization and morphology

Above studies are based on the investigation of iPP nucleation by varying the chemical structure of the carboxylate-alumoxanes. It would be interesting to study the effect of carboxylate-alumoxanes by changing the side group of the iPP. Syndiotactic polystyrene is a polyolefin, analogous to iPP, having pendent phenyl groups along the polymer backbone. Further, the nucleating agents for sPS are rather limited mainly because of its higher processing temperature (*ca.* 300 °C) where most of the nucleating agents degrade. Also, the self-nucleation analysis based on sPS has not been studied so for which is essential to measure the nucleation efficiency of nucleating agents.

Another objective of the present work is to study the effect of carboxylate (PTBBA) - alumoxane nano particles on the crystallization and morphology of syndiotactic polystyrene (sPS). The effect of PTBBA-alumoxane on the crystalline phase of sPS is studied using DSC and WAXS. Also studied in detail is the effect of self nucleation using α- and the β-nuclei and their role in controlling the final crystalline morphology of sPS using DSC and WAXS analysis.

References

1) H. Zweifel, *Plastics Additives Handbook*, 5th ed.; Hanser Publications: Munich, 2001, p 952.
2) https://www.scribd.com/document/189907881/Nucleating-and-Clarifying-Agents
3) T. Smith, D. Masilamani, L. Bui, R. Brambilla, Y. Khanna, K. Garbriel, *J. Appl.Polym. Sci.*, 1994, **52**, 591.
4) M. Blomenhofer, S. Ganzleben, D. Hanft, H.-W. Schmidt, M. Kristiansen, P. Smith, K. Stoll, D. Mäder, K. Hoffmann, *Macromolecules*, 2005, **38**, 3688.
5) S. Yoshimoto, T. Ueda, K. Yamanaka, A. Kawaguchi, E. Tobita, T. Haruna, *Polymer*, 2001, **42**, 9627.

6) E. Alvarez, N. Guillou, C. Martineau, B. Bueken, B. Van de Voorde, C. Le Guillouzer, P. Fabry, F. Nouar, F. Taulelle, D. de Vos, J. Chang, K. Cho, N. Ramsahye, T. Devic, M. Daturi, G. Maurin, C. Serre, *Angew. Chem. Int. Ed. Engl.*, 2015, **54**, 3664.
7) J. Varga, G. W. Ehrenstein, A. K. Schlarb, *Exp. Polym. Lett.*, 2008, **2**, 148.
8) J. Varga, *J. Macromol. Sci.: Part B* 2002, **41**, 1121.
9) D. Papageorgiou, K. Chrissafis, D. Bikiaris, *Polymer Reviews* 2015, **55**, 596.
10) R. Callender, C. Harlan, N. Shapiro, C. Jones, D. Callahan, M. Wiesner, D. MacQueen, R. Cook, A. Barron, *Chem. Mater.*, 1997, **9**, 2418.

CHAPTER 3

Experimental techniques and characterization

3.1 Materials

Aromaticcarboxylic acids, Phenylalkylcarboxylic acids and aliphaticdicarboxylic acids were procured from Sigma-Aldrich. Metal nitrates viz., $Al(NO_3)_3.9H_2O$, $ZrO(NO_3)_2.xH_2O$ and $Cr(NO_3)_3.9H_2O$ were purchased form Vijay chemicals Ltd, India.

Isotactic polypropylene (iPP) homopolymer (stabilized) in the form of powder was kindly supplied by Reliance Industries Ltd., Mumbai. The weight-average molar mass obtained by gel permeation chromatography (GPC) in 1,2,4-trichlorobenzene at 160 °C was found to be Mw = 250 000 with the polydispersity index of Mw/Mn = 4.6.

Syndiotactic polystyrene (sPS) was kindly supplied by Dow Chemicals. The weight-average molecular weight was 275 000, and the melt index was 4.3. Amorphous films of sPS were obtained by rapidly quenching melted samples in an ice-water bath at 0 °C.

3.2 Methods

3.2.1 Preparation of *p*-*t*-butylbenzoate (PTBBA)-alumoxane: $Al(NO_3)_3.9H_2O$ (Al) was taken in a 500 ml jacketed reactor equipped with an overhead stirrer. Subsequently 225 ml of deionized water was added and the solution was heated to 100 °C. It formed a boehmite gel when the solution pH was adjusted to neutral by 5% of freshly prepared ammonia solution while stirring at 1000 rpm. After 30 min 75 ml of isopropyl alcohol containing *p*-*t*-butylbenzoic acid (PTBBA) was added and the reaction mixture was stirred for 2 hrs at 100 °C at 1000 rpm. The white precipitate was separated by centrifugation and washed with methanol. The product was powdered and dried under vacuum at 80 °C for about 12 hrs. The same procedure was followed for the preparation of other carboxylate-alumoxanes based on aromatic and phenylalkylcarboxylic acids and Zirconium-PTBBA complex. The metal nitrate to carboxylic acid molar ratio was maintained at 1:2. $ZrO(NO_3)_2.xH_2O$ salt was used to prepare Zirconium-PTBBA complex.

The PTBBA-alumoxane with various amount of organic (PTBBA) content was prepared by varying the Al/PTBBA molar ratio viz., 3.0, 2.5, 2.0, 1.5, 1.0, 0.7 and 0.5.

3.2.2 Preparation of aluminium succinate (Al-SucA) MOF: $Al(NO_3)_3.9H_2O$ was taken in a 500 ml jacketed reactor equipped with an overhead stirrer. Subsequently, 100 ml of deionized water was added and the solution was heated to 100 °C. It formed a boehmite gel when the pH was adjusted to neutral by 5% of freshly prepared ammonia solution while stirring at 1000 rpm. After 15 min, succinic acid (SucA) was added and the reaction mixture was stirred for 2 hrs at 100 °C at 1000 rpm. The neutral pH was maintained by ammonia solution. The white precipitate was separated by centrifugation and washed with methanol. The product was powdered and dried under vacuum at 80 °C for about 12 hrs. The same procedure was followed for the preparation of other aluminium dicarboxylates, and zirconium suberate compounds. The same procedure was adapted for the preparation of chromium subearte with a slight change in the sequence of addition of suberic acid which was added before the addition of 5% ammonia solution. The metal nitrate to dicarboxylic acid molar ratio was maintained at 1:10. $Cr(NO_3)_3.9H_2O$ and $ZrO(NO_3)_2.xH_2O$ salts were used to prepare Cr-suberate and Zr-suberate compounds respectively.

3.2.3 Preparation of Calcium Pimelate (CaP):

Calcium Pimelate was synthesized in the lab following standard procedure by reacting sodium pimelate with calcium chloride.[1] The sodium pimelate was obtained by reacting pimelic acid with sodium bicarbonate. The sodium pimelate was in the dissolved state in water and precipitated out using calcium chloride. It was filtered and washed with water and ethanol.

3.3 Melt extrusion

The NAs were pre-mixed with iPP powder and extruded at 200 °C using a DSM twin-screw micro extruder (model no. DSM 5). The samples were allowed to mix for 2 min in the barrel at 100 rpm screw speed. Similar procedure was adapted for the melt mixing of sPS with nucleating agents. However, the extrusion was performed at 300°C due to the high melting temperature of sPS compared to iPP. Previously, sPS beads were made in to a powder form using cryo ball mill (Retsch Cryomil).

3.4 Chracterization Techniques

The MALDI−TOF analysis was done on AB SCIEX TOF/TOF 5800 (Applied Biosystem, Framingham, USA) equipped with 337 nm pulsed nitrogen laser used for desorption and ionization. The samples were dispersed in benzyl alcohol and premixed with dithranol matrix before spotting onto the 96-well stainless MALDI plate. The samples were thoroughly dried at room temperature before MALDI analysis.

FT-IR spectra with a resolution of 2 cm^{-1} were collected using Perkin-Elmer spectrometer (model Spectrum GX) with samples in KBr pellets.

Thermo gravimetric analyses (TGA) were performed using PerkinElmer simultaneous thermal analyzer (model STA 6000) under nitrogen atmosphere at a heating rate of 10 °C min^{-1}. The sample size was about 5-8 mg.

TEM images of the NAs were taken using a Transmission Electron Microscope model FEI Technai G2 T20, Japan. The samples were prepared by dispersing NAs in benzylalcohol and drop casted on to 200 mesh carbon coated copper grids.

The dispersion of NAs in the iPP was analysed using TEM. The extruded iPP samples were micro sectioned in to 110 nm thin film using microtome (Leica Ultracut UCT) and were placed on the 200 mesh copper grids. The micro sectioned samples were stained by exposing to RuO_4 vapours for 5 minutes in a fumehood for better contrast of the particles.[2]

The nitrogen gas sorption-desorption experiments (0-1 bar) were performed using a Quantachrome Quadrasorb automatic volumetric instrument. Brunauer–Emmett–Teller (BET) method was used to measure the surface area of the samples.

Differential Scanning Calorimetry analyses were made with DSC TA Q100 in N_2 atmosphere at a purge flow rate of 50 mL/min. About 4-6 mg of sample was heated to 200 °C at 50 °C/min and held for 2 min. Then cooled to room temperature at 10 °C/min

and the crystallization peak was recorded. The crystallization temperature (T_C), was taken as the peak crystallization temperature of the crystallization exotherm. Similar procedure was followed for sPS. In the case of sPS the samples were heated to 300 °C.

The wide-angle X-ray scattering (WAXS) measurements in transmission mode were carried out using a Rigaku Micromax-007HF diffractometer operating at 40 kV and 30 mA. The samples were exposed to the X-ray beam for 3 min and the scattering pattern was imaged by Rigaku R-AXIS IV^{++} area detector. The 2D pattern was converted to 1D pattern by Rigaku 2DP software. The beam size at the sample was about 70 µm. The variable temperature WAXS experiments were performed using a hot stage, which was fabricated specially by Rigaku, Japan. The iPP sample, removed from the DSC, was mounted in the copper holder attached with the hot stage. The sample was kept under vacuum (about $1x10^{-3}$ torr).

SAXS analyses were made using Bruker NanoSTAR (Cu kα radiation) equipped with rotating anode using an operating voltage of 40 kV at a current 20 mA. Scattering data were collected on a multi-wire gas filled Hi-star 2D area detector and were reduced to 1D using the Bruker offline software. SAXS patterns were processed further to get the electron density correlation function following the method given by Hsiao,[3] Strobl,[4] and Santa Cruz et al.[5]

The amount of β-phase content (k_β) in the β-nucleated iPP sample was calculated from the relative peak intensity (H) of the α- and the β-crystalline phases from WAXS pattern as detailed by Turner Jones and coworkers.[6]

$$k_\beta = \frac{H_\beta(300)}{H_\beta(300) + H_{\alpha1}(110) + H_{\alpha2}(040) + H_{\alpha3}(130)}$$

The crystallized sPS samples were used for WAXS analysis and the amount of the α-phase content (P_α) was calculated based on the relative intensities (H) of α-phase peak appears at 2θ=11.7° and the β phase peak appears at 2θ=12.3° from WAXS pattern as detailed by Guerra et al.[7]

$$P_a = \frac{[1.8\mathrm{H}(11.7_\alpha)/\mathrm{H}(12.4_\beta)\,]}{[1 + 1.8\mathrm{H}(11.7_\alpha)/\mathrm{H}(12.4_\beta)\,]} * 100$$

DFT details

All DFT calculations were performed using the Turbomole 6.4 suite of programs.[8] Geometry optimizations were performed using the Perdew, Burke, and Ernzerhof density functional (PBE).[9] The electronic configuration of the atoms was described by a triple-ζ basis set augmented by a polarization function (Turbomole basis set TZVP).[10] The resolutions of identity (RI)[11] along with the multipole accelerated resolution of identity (marij)[12] approximations were employed for an accurate and efficient treatment of the electronic Coulomb term in the density functional calculations. Single point calculations were made with the hybrid B3-LYP functional [13, 14] in order to obtain more reliable energy values for the different molecular structures.

3.5 References

1) X. Li, K. Hu, M. Ji, Y. Huang, G. Zhou, *J. Appl. Polym. Sci.,* 2002, **86**, 633.
2) G. M. Brown, J. H. Butler, *Polymer*, 1997, **38**, 3937.
3) B. Hsiao, R. Verma, *J. Synchrotron Rad.,* 1998, **5**, 23.
4) G. Strobl, M. Schneider, *J. Polym. Sci. Polym. Phys. Ed.,* 1980, **18**, 1343.
5) C. Cruz, N. Stribeck, H. Zachmann, F. Calleja, *Macromolecules,* 1991, **24**, 5980.
6) T. Jones, J. Aizlewood, D. Beckett, *Die Makromol. Chem.,* 1964, **75**, 134.
7) G. Guerra, V. Vitagliano, C. Rosa, V. Petraccone, P. Corradini, *Macromolecules,* 1990, **23**, 1539.
8) Ahlrichs, R.; Bär, M.; Häser, M.; Horn, H.; Kölmel, C. Chem. Phys. Lett. 1989, 162 (3), 165−169.
9) Perdew, J. P.; Burke, K.; Ernzerhof, M. Phys. Rev. Lett. 1996, 77 (18), 3865.
10) Scha¨fer, A.; Horn, H.; Ahlrichs, R. J. Chem. Phys. 1992, 97, 2571–2577.
11) Eichkorn, K.; Treutler, O.; Öhm, H.; Häser, M.; Ahlrichs, R. Chem. Phys. Lett. 1995, 240 (4), 283−289.
12) Sierka, M.; Hogekamp, A.; Ahlrichs, R. J. Chem. Phys. 2003, 118, 9136.
13) Becke, A. D. *J. Chem. Phys.* 1993, *98*, 5648.
14) Lee, C.; Yang, W.; Parr, R. G. *Phys. Rev. B.* 1988, *37*, 785.

CHAPTER 4

The role of the molecular structure of carboxylate-alumoxanes in the enhanced nucleation of polypropylene

This chapter is adapted from "M. Mani, R. Chellaswamy, Y.N. Marathe, V. Pillai, *Chem. Commun.,* **2015**, 51, 10026-10029".

4.1 Introduction

The present chapter focuses on the role of molecular structure on the polymer nucleation i.e., the specific interactions possible between two materials in contact having vastly different molecular structure and properties, especially if one of them is available in a ppm amount. The main material is polypropylene, a semi-crystalline polymer used extensively for making articles in everyday use. The other material is carboxylate-alumoxanes, a well known inorganic-organic hybrid material. The physical and chemical properties of the carboxylate-alumoxanes can be varied by the appropriate selection of carboxylic acids.[1,2] Carboxylate-alumoxanes are more specifically considered to be alumina particles of 5-200 nm in diameter where the surface is covered by many covalently bonded carboxylate groups.[2,3] However, there are many variants like the oxo centred trinuclear aluminium carboxylate[4,5] and the simplest one recently reported by Kalita et al.[6] where carboxylate groups and an oxo ligand bridge the aluminium centres. US6369183 describes the preparation of polymer composite, hybrid polymers and resins based on carboxylate-alumoxane which are chemically bonded to the polymer backbone.[7]

This chapter discusses for the first time that ppm levels of carboxylate-alumoxane can nucleate isotactic polypropylene very efficiently along with a possible mechanistic explanation of the influence of molecular structure on the nucleation efficiency of iPP, using experimental results from a variety of techniques.

4.2 Results and Discussion

The crystallization temperature on cooling from the melt is a measure of the nucleation efficiency of the polymer. The higher T_C indicates higher nucleation efficiency and higher crystallization rate. Furthermore, T_C on cooling depends on cooling rate and all the experiments were done with 10 °C/min, so that the values can be compared. Figure 4.2 shows the dependence of T_C on the concentration of *p-t*-butylbenzoate (PTBBA)-alumoxane, where, higher crystallization temperature undoubtedly, indicates faster crystallization rate. The T_C, obtained using 1,3:2,4-bis(3,4-dimethylbenzylidene) sorbitol (DMDBS), which is an industrial standard NA for iPP, is also shown in Figure 4.1 for comparison. The data clearly shows that PTBBA-

alumoxane is far more efficient than DMDBS as the crystallization temperature of iPP is increased by 10 °C despite being at 3 ppm, while DMDBS shows no major nucleation effect even at 1000 ppm. More significantly, about 400 ppm of PTBBA-alumoxane increases the T_C by 17 °C which is equivalent to the utilization of DMDBS at 2000 ppm. The enhancement on crystallization temperature is observed for different cooling rates and given in Table 4.1. Isothermal crystallization performed at 140 °C also confirms the efficient nucleation of iPP by PTBBA-alumoxane and is shown in Figure 4.2. The T_C values of iPP nucleated with various NAs are given in Table 4.2. The data clearly shows that the additives have an important role on the nucleation efficiency. The x-ray diffraction studies on the nucleated samples indicate that the carboxylate-alumoxanes nucleate iPP in α-phase only like DMDBS and the WAXS patterns are presented in Figure 4.3.

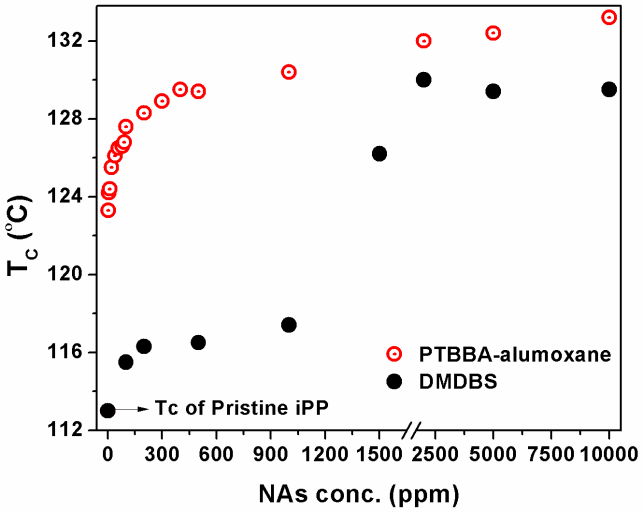

Figure 4.1: The variation of concentration of nucleating agents (NAs) with the crystallization temperature (T_C) of isotactic polypropylene (iPP).

Table 4.1: Crystallization temperature (T_C) of pure iPP and nucleated with 2000 ppm of PTBBA- alumoxane and DMDBS on various cooling rate.

Cooling rate (°C/min)	Crystallization temperature (T_C) of iPP (°C)		
	iPP	PTBBA-alumoxane	DMDBS
5	116.6	134.3	132.6
10	112.6	131.6	130.2
20	108.6	129.0	127.2
30	105.4	126.2	124.8
40	104.0	124.2	123.6

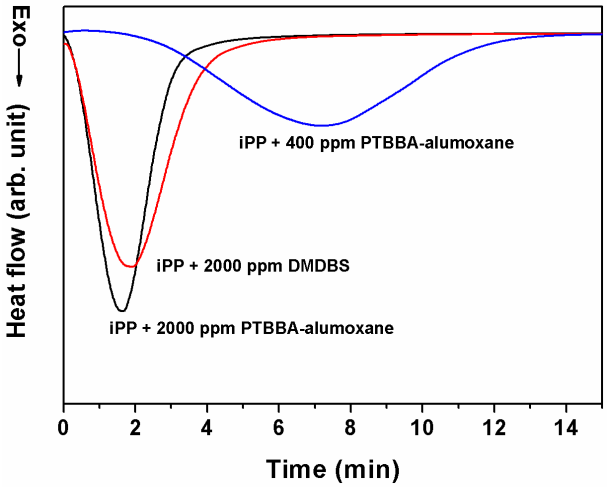

Figure 4.2: DSC curves of isothermally crystallized iPP with PTBBA-alumoxane and DMDBS at 140 °C. Please note that bare iPP and iPP+400ppm DMDBS samples did not nucleate within this experimental time scale.

Table 4.2: A comparison of the crystalline phase transition temperature (TT), peak crystallization temperature (T_C) of nucleated iPP and nucleation efficiency (NE) of various nucleating agents (NAs).

Compound (NAs)	TT (°C)	T_C (°C)[a]	NE (%)[b]
Virgin iPP	-	113.0	0
Self- nucleated iPP	-	140.2	100
PTBBA-alumoxane	390	132.0	68
BA-alumoxane	350	127.0	50
PA-alumoxane	260	119.5	22
PTBBA-galloxane	300	130.5	62
Zr-PTBBA complex	Amorphous	121.4	29
DMDBS	-	130.5	62

[a]Concentration of NAs: 2000 ppm. [b]NE calculated following the method given by Fillon et al.[8] (Annexure-I gives the details of the method).

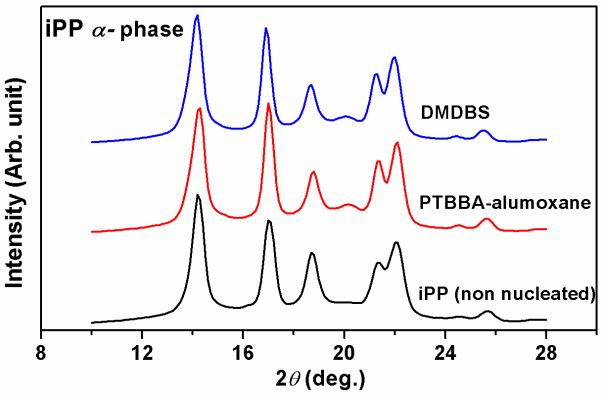

Figure 4.3: The WAXS patterns of iPP (non-nucleated) and nucleated with PTBBA-alumoxane and DMDBS. All the samples have identical processing history. The extruded samples were heated to 210 °C and crystallized on controlled cooling at 10 °C/min.

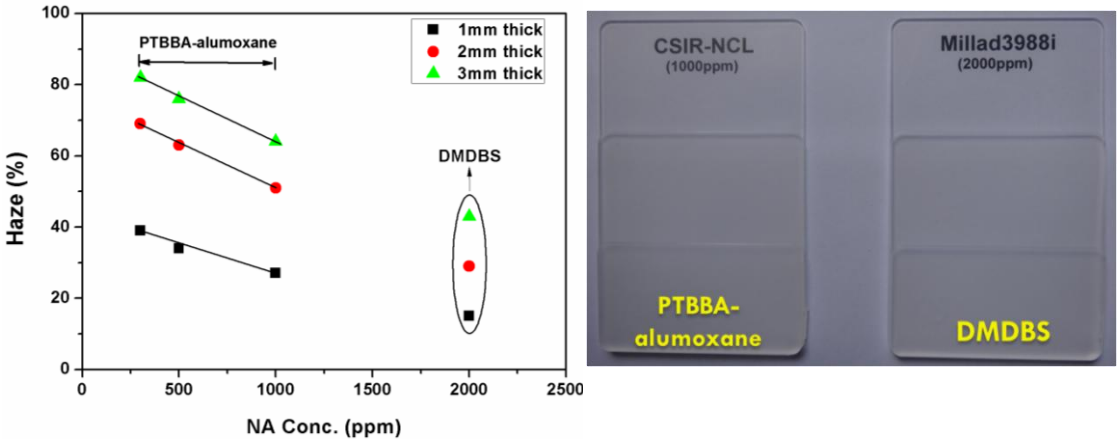

Figure 4.4: (a) The variation of NAs (PTBABA-alumoxane and DMDBS) concentration with the haze of random copolymer (RCP) and (b) Clarified injection molded RCP step chips having thicknesses 1, 2 and 3mm from top.

The clarification effect of PTBBA-alumoxane has been studied in RCP along with effect of an industrial standard clarifying agent DMDBS [Trade name: Millad 3988i]. The samples for the haze measurement are prepared by following the ASTM standard D-1003 and the data is generated by Reliance, Mumbai. The dependence of haze on the concentration of PTBBA-alumoxane is shown in Figure 4.4 along with RCP clarified with DMDBS. 1 mm film thicknesses of DMDBS (2000 ppm) nucleated RCP shows the haze of 15% while for the same film thickness PTBBA-alumoxane (1000 ppm) nucleated sample showed haze value of 27%. Though PTBBA-alumoxane is inferior to DMDBS, the trend shows that the haze value can be reduced with higher PTBBA-concentration. Noticeably, the haze value measured at 1mm film thickness of RCP clarified by PTBBA-alumoxane is equivalent to the 2 mm film thickness of DMDBS clarified RCP.

Barron et al. prepared carboxylate-alumoxanes of general formula $[Al(O)_x(OH)_y(O_2CR)_z]_n$ where $2x + y + z = 3$ from the reaction of carboxylic acids (RCO_2H) with $[Al(O)(OH)]_n$.[2] Boehmite gel reacted with PTBBA to produce PTBBA-alumoxane. The structure of PTBBA-alumoxane is characterized by MALDI-TOF mass spectrometric (MS) analysis which is shown in Figure 4.5 along with FT-IR spectroscopic analysis (Figure 4.11). The MALDI-TOF/MS of PTBBA-alumoxane shows peak at 801 Da and is assigned to the dinuclear aluminium complex (A1 in

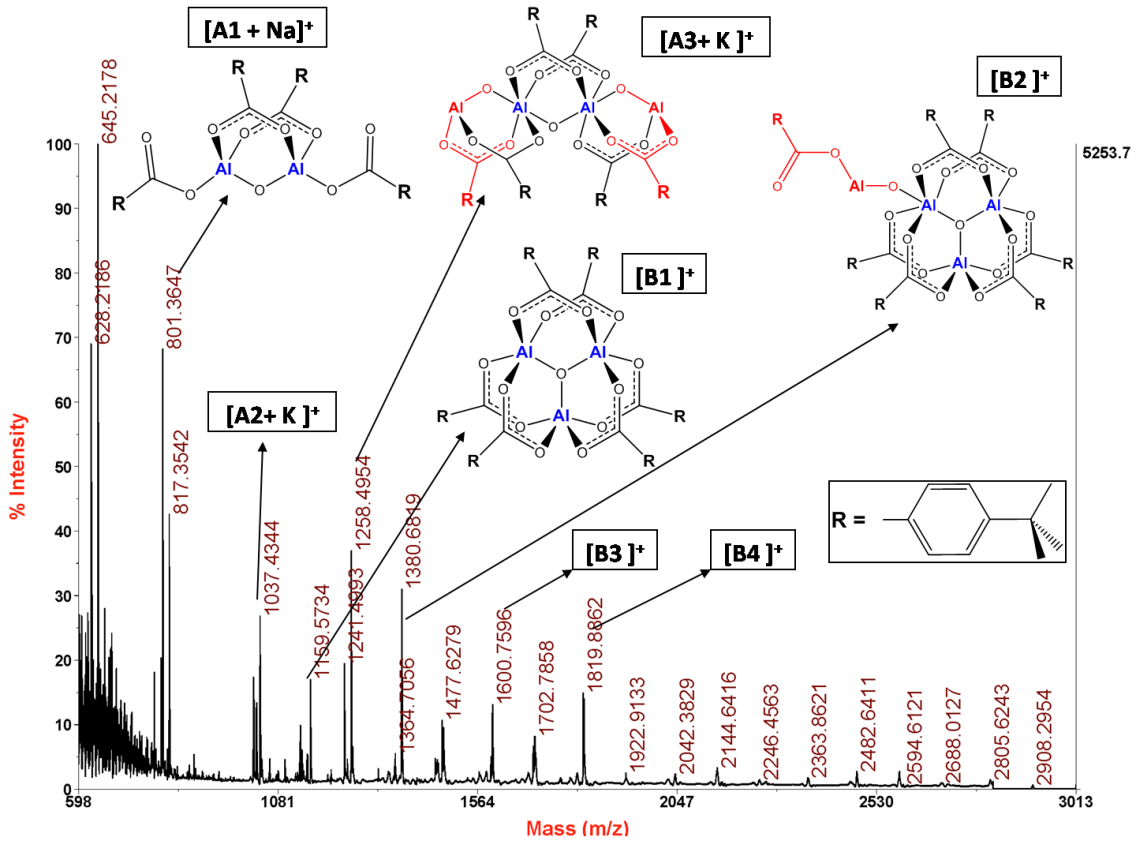

Figure 4.5: MALDI-TOF/MS of PTBBA-alumoxane.

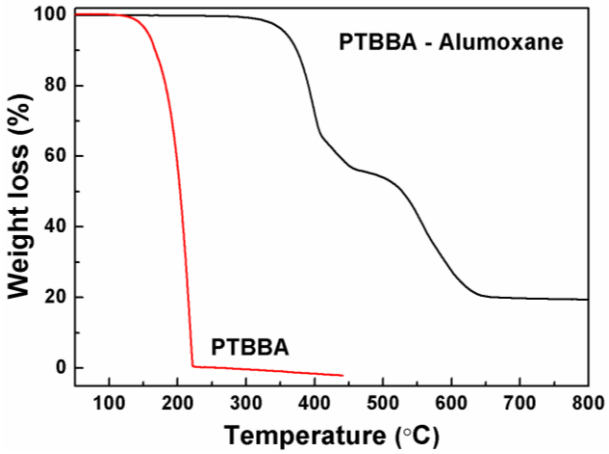

Figure 4.6: Thermogravimetric analysis (TGA) of pure PTBBA and PTBBA-alumoxane.

Figure 4.5) with a molecular formula $[(tBu\text{-}C_6H_4CO_2)Al(\mu\text{-}O)(\mu\text{-}O_2CC_6H_4\text{-}tBu)]_2$ along with that for Na^+ ion. The aluminium centres in the dinuclear complex are bridged by two PTBBA ligands and the oxo ligand to give a bicylic structure similar to the reported complex $[(Me_3Si)_3\text{-}CAl(\mu\text{-}O)(\mu\text{-}Hdtbsa)]_2$ [where Hdtbsa- di-tert-butylsalicylate].[6] The fourth coordination site is occupied by the unidentate PTBBA ligand. PTBBA-alumoxane shows thermal stability above 300 °C (Figure 4.6), much above the iPP

processing temperature, and is attributed to the strong bridging carboxylate and oxo coordination towards Al centers. Energy optimization of the structures using Turbomole 6.4 suite of program shows that the phenyl groups are coplanar with the carboxylate moiety, perhaps to gain enough resonance stabilization energy. Interestingly, this conformation gives a butterfly-like structure (Figure 4.7a) with a dramatic similarity to the v-shaped structure of dibenzylidene sorbitol (DBS). [9,10] Perhaps the butterfly-like structure offers polypropylene segments a shape selective cavity to fit in and involve in a favourable interaction with aromatic cleft (nucleation site), most probably through C-H...π interactions as shown in Figure 4.7d. It is believed that this interaction reduces the free energy barrier to nucleation by modulating the segmental motion of the polymer and subsequent crystallization and growth. Our experimental procedure for the preparation of carboxylate-alumoxanes, interestingly, also produces polynuclear aluminium complexes having butterfly-like structure (Figure 4.5). For example, the formation of oxo-centred trinuclear aluminium complex with bridging carboxylate ligands (B1 in Figure 4.5) is similar to that of $[Al_3(O)(_2OCPh)_6(THF)_3]^+$ reported by Bury et al.[5]

It is also interesting to note that the presence of series of peaks at the regular interval of 220 Da (i.e., 817 Da, 1037 Da, 1258 Da, 1477 Da etc.), indicating that the basic building unit in the higher molecular weight species is O-Al-PTBBA (molecular mass 220 Da). Successive addition of O-Al-PTBBA unit into the dinuclear complex (A1) gives trinuclear (A2), tetranuclear (A3) and pentanuclear (A4) and polynuclear aluminium complexes as shown in Figure 4.5. This is in excellent accordance with the reported coordination polymer of aluminum 1,4-benzenedicarboxylate (BDC), $Al(OH)(C_8H_4O_4)•0.7C_8H_6O_4$.[11,12] Similarly, another series of peaks is observed at 1159 Da, 1380 Da, 1600 Da, 1819 Da etc. corresponding to B1, B2, B3, B4 and like. Notably, these polynuclear complexes are based on oxo-centred trinuclear aluminium core. It seems that water molecules and hydroxyl groups, which would complete the Al coordination sphere, leave the structure during laser ablation process of the MALDI-TOF/MS analysis. Hence the MS analysis gives m/z peaks without such ligands as shown in Figure 4.5.

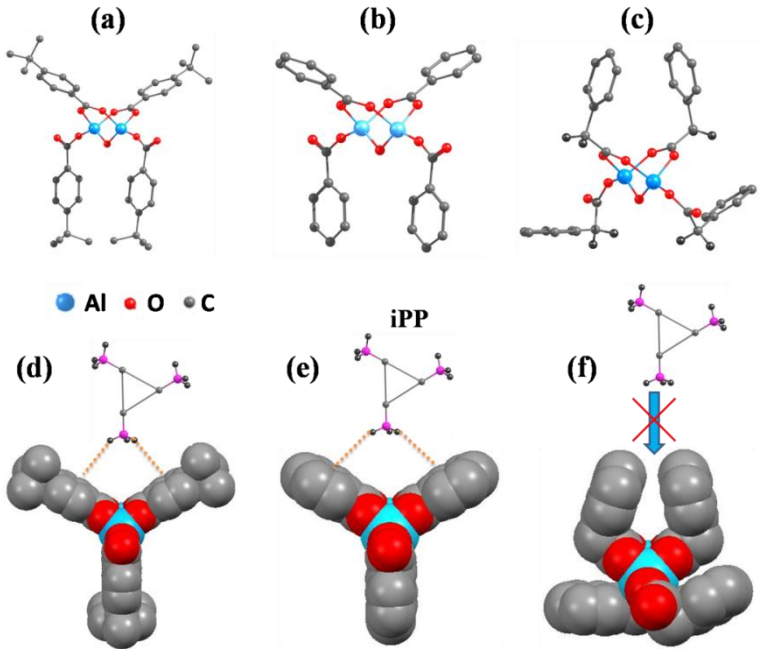

Figure 4.7: Energy optimized structures of (a) PTBBA-alumoxane, (b) BA-alumoxane, (c) PA-alumoxane and the possible interaction of iPP on to the aromatic cleft of (d) PTBBA-alumoxane, (e) BA-alumoxane and (f) PA-alumoxane. H atoms are removed for clarity except methylene hydrogen's in (c).

Apart from PTBBA-alumoxane, the nucleation efficiency of related carboxylate-alumoxanes are also investigated. For example, results using two typical carboxylate-alumoxanes viz. benzoate (BA)-alumoxane and phenylacetate (PA)-alumoxane will be discussed along with the effect due to PTBBA-alumoxane for the impact of molecular structure on nucleation. These compounds were characterized by MALDI-TOF/MS analysis (Figure 4.8 and Figure 4.9) which shows peak correspond to molecular weight of dinuclear aluminium entities with bridging carboxylate and oxo ligand similar to PTBBA-alumoxane. Like PTBBA-alumoxane, the MALDI-TOF/MS of BA-alumoxane (Figure 4.8) shows two series of peaks at the regular interval (i.e., 164 Da, molecular mass of O-Al-BA unit) suggesting that the repeating unit in the other higher molecular weight component is [O-Al-BA]. The first series peaks appear at 577 Da, 741 Da and 905 Da, corresponding to A1, A2 and A3. The second series shows peaks at 823 Da, 987 Da, 1151 Da and 1316 Da corresponding to B1, B2, B3 and B4, which are based on oxo-centered trinuclear aluminium core.

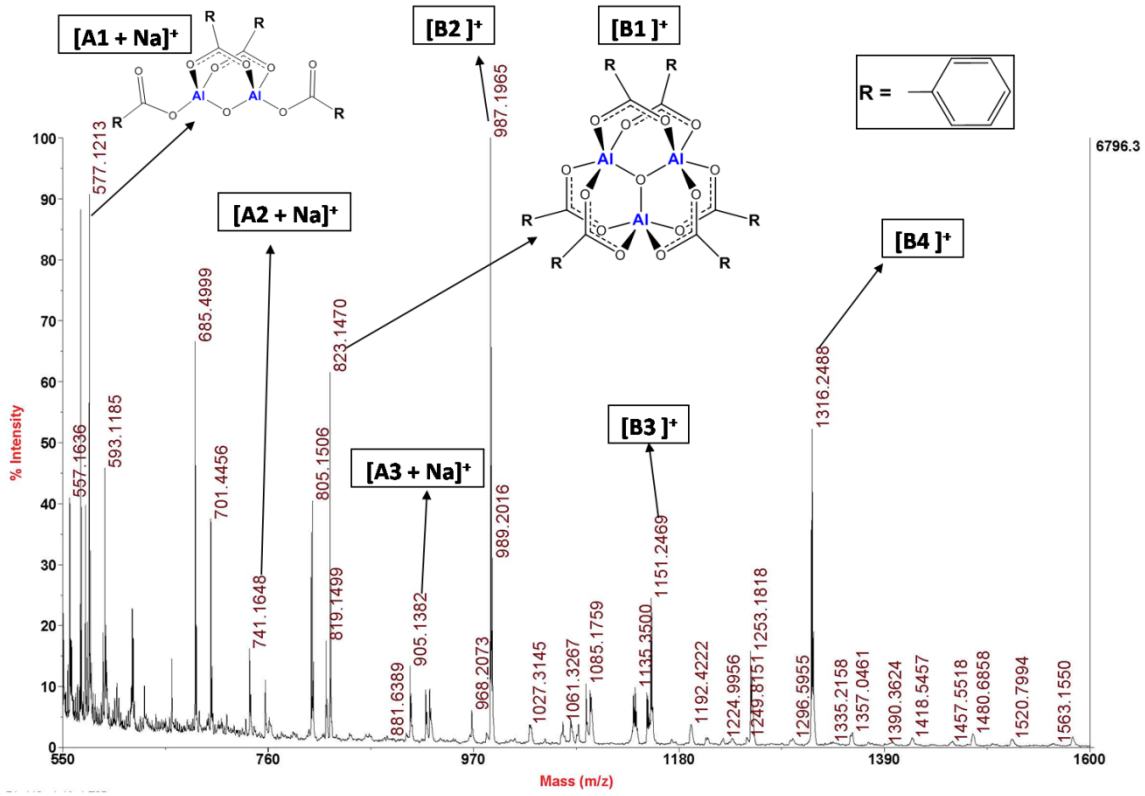

Figure 4.8: MALDI-TOF/MS of BA-alumoxane.

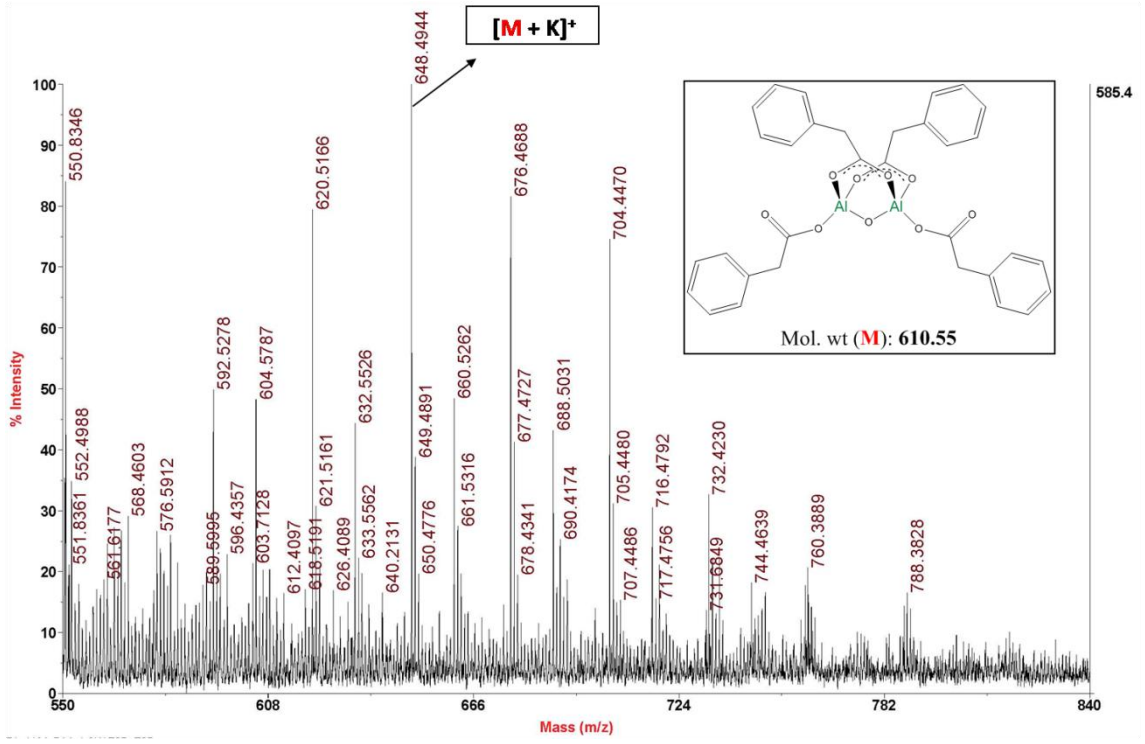

Figure 4.9: MALDI-TOF/MS of PA-alumoxane.

Among these two carboxylate-alumoxanes, BA-alumoxane shows better nucleation efficiency as expected in agreement with the results of the energy optimization. More specifically, BA-alumoxane exhibits a butterfly-like structure (Figure 4.7b), unlike the latter as indicated in Figure 4.7c. However, in the case of PA-alumoxane, the intervening methylene group (sp^3 hybridized carbon) does not support the phenyl group in coplanar with the carboxylate group and hence the phenyl groups close the cleft while taking the stable conformation. This conformation leads to poor interaction of polypropylene with phenyl rings (Figure 4.7f) and consequently to lower nucleation efficiency (Table 4.2).

Further, in order to understand the role of molecular structure on the nucleation efficiency, analogous structure based on gallium is studied, expecting more or less equally efficient nucleation of iPP. Aluminium and gallium are known to form isomorphous structures.[11] The PTBBA-galloxane has been prepared by the same method used for PTBBA-alumoxane except the use of gallium nitrate in place of aluminium nitrate. Powder X-ray patterns of PTBBA-galloxane (Figure 4.10) and PTBBA-alumoxane (Figure 4.10) are indeed, indistinguishable. This indicates that molecular structure and crystalline structure of PTBBA-galloxane and PTBBA-alumoxane are similar. More significantly, a comparison of the nucleation efficiency (Table 4.2) using PTBBA-galloxane shows results similar to that of PTBBA-alumoxane supporting our speculation that the nucleation is due to the interaction of iPP with a butterfly-like structure.

The carboxylate-alumoxanes discussed in this thesis are highly crystalline and show a major peak in the neighbourhood of $2\theta = 6°$. Interestingly, all these samples show a crystalline phase transition on heating as shown in Figure 4.10. The phase transition temperature depends on the sample as shown in Table 4.2. Though, the PTBBA-galloxane and PTBBA-alumoxane have identical structure, a major difference arises in the phase transition temperature. For example, Ga-PTBBA complex transforms at 300 °C while the transformation occurs at 390 °C for PTBBA-alumoxane (Figure 4.10). In fact, the transition is not reversible on cooling although the structure reverts back to the starting form on treating with isopropanol/water at room temperature (Figure 4.10). It

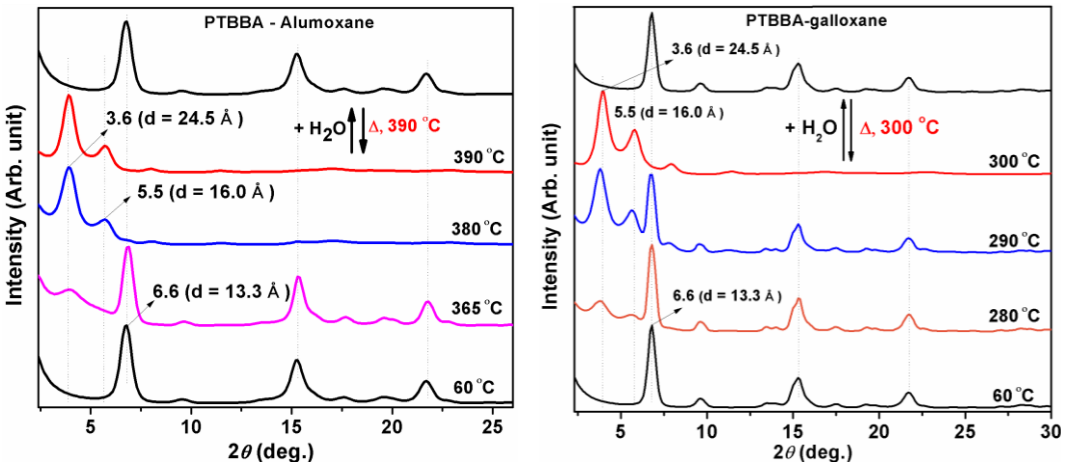

Figure 4.10: Wide Angle X-ray Scattering pattern of PTBBA-alumoxane (left) and PTBBA-galloxane (right) annealed at different temperatures (indicated in graph) and scanned at room temperature.

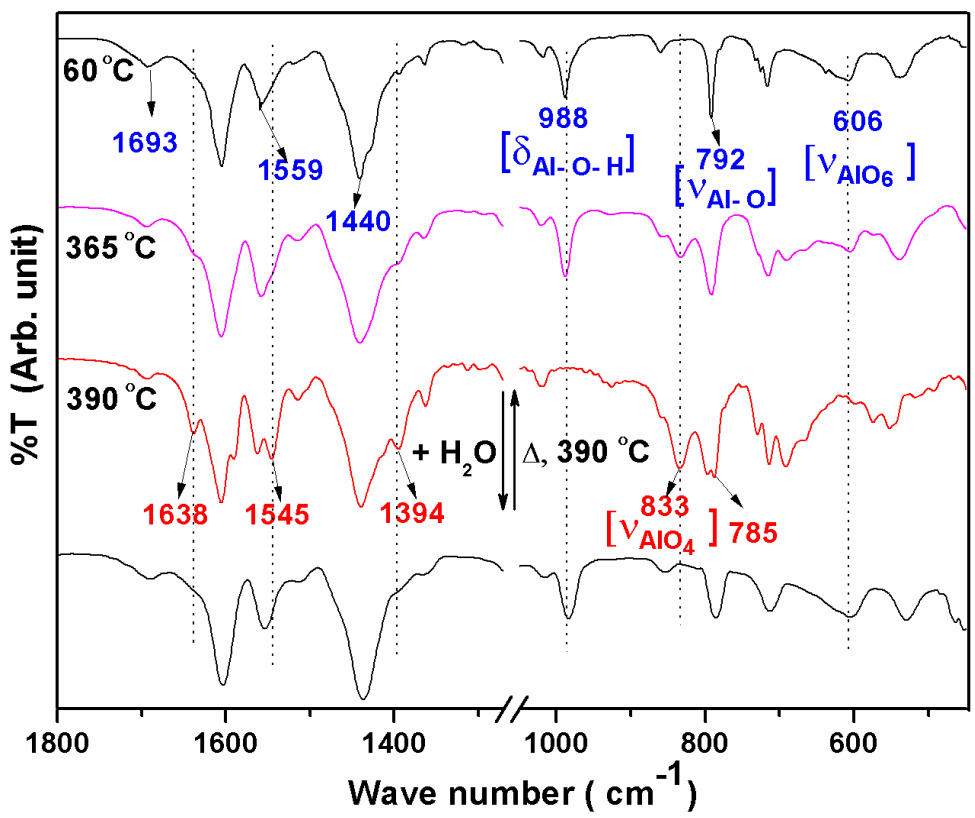

Figure 4.11: FT-IR spectra of PTBBA-alumoxane annealed at different temperatures (indicated in graph) and scanned at room temperature.

seems that water molecules leave the structure during the laser ablation process or during the course of MALDI-TOF/MS analysis facilitating changes from octahedral to

tetrahedral coordination. Hence, the MS analysis apparently gives tetrahedral coordination (A1 in Figure 4.5).

The FT-IR spectrum of PTBBA-alumoxane is shown in Figure 4.11. The asymmetric (ν_{as}) and symmetric (ν_s) COO^- stretching vibrations occur at 1559 cm^{-1} and 1440 cm^{-1} respectively, which are characteristic of bridged bidentate coordination.[2] The peak at 1693 cm^{-1} corresponds to C=O stretching indicating the presence of unidentate PTBBA ligand in the product. The Al-O-H stretching and bending modes are observed at 3696 cm^{-1} and 988 cm^{-1} respectively.[13] As discussed in WAXS data, the compound transforms into another crystalline phase at 390 °C and the corresponding FT-IR spectrum is also shown in Figure 4.11. FT-IR spectrum shows significant molecular level changes in the transformed material. For example, the 606 cm^{-1} peak assigned to AlO_6 is partly masked while couple of new peaks appear at 833 cm^{-1} and 785 cm^{-1} and are assigned to AlO_4 stretching.[13] Concomitantly, Al-O-H stretching and bending peaks at 3696 cm^{-1} and 988 cm^{-1} are vanished indicating dehydroxylation. In addition, another set of new peaks, characteristic of μ-COO- group is observed at 1638 cm^{-1}, 1545 cm^{-1} and 1394 cm^{-1} which are consistent with peak positions of the reported complex $[(Me_3Si)_3\text{-}CAl(\mu\text{-}O)(\mu\text{-}Hdtbsa)]_2$ where the carboxylate group bridges the tetrahedral aluminium centre along with oxo ligand.[6] This spectral change suggests that AlO_6 gets converted into AlO_4 by the removal of coordinated water molecules and hydroxyl groups. This could be the possible reason for the phase transition and is supported by the fact that on treating the transformed material in isopropanol/water the FTIR spectrum reverts back to the original spectrum.

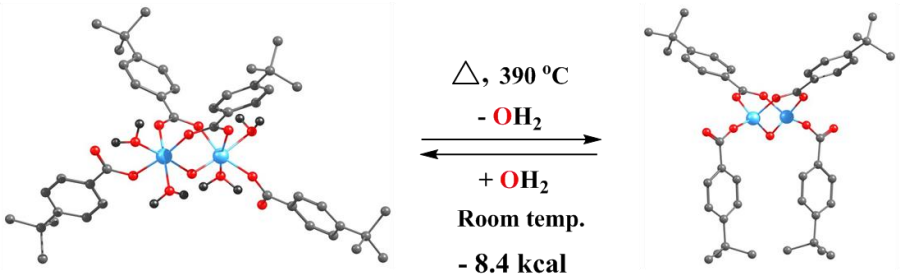

Scheme 4.1: Energy optimized structures of PTBBA-alumoxane with (left) and without water molecules (right). The energy reported in the scheme is the ΔG value.

In order to supplement the octahedral to tetrahedral transition, the energy optimized structures of PTBBA-alumoxane with and without the water molecules are also shown in scheme 4.1. DFT calculations show that PTBBA-alumoxane with surrounding water ligands is energetically more stable than that without water ligands in the coordination sphere. Furthermore, the optimized configurations reveal the butterfly-like structure as present in both the structures. These samples show similar nucleation efficiency even though their crystalline structure is different, indicating that the molecular structure is more important for the nucleation of iPP. This is further supported by the fact that PTBBA-alumoxane sample with low organic content of 38% showed amorphous structure (Figure 4.12a) but it shows a T_C of 126 °C (Figure 4.12b), indicating butterfly-like conformation present in the molecular structure is more important than crystalline structure of the PTBBA-alumoxane. Figure 4.12a shows the X-ray diffraction patterns of PTBBA-alumoxane with different % of organic content. The dependence of T_C on the organic content of PTBBA-alumoxane are shown in Figure 4.12b which indicates T_C increases with increase in organic content of PTBBA-alumoxane.

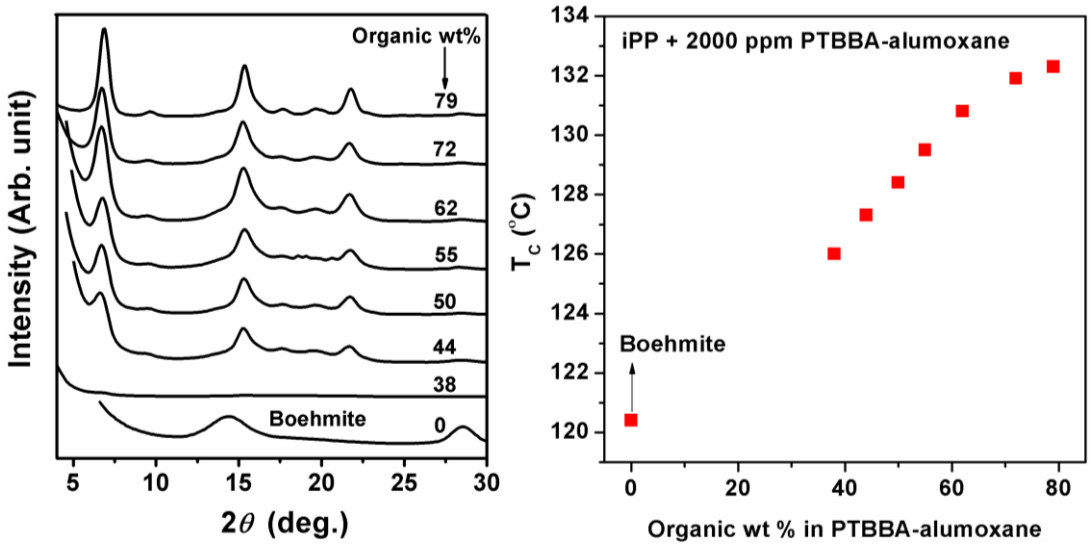

Figure 4.12: (a) The WAXS pattern of PTBBA-alumoxane with various % of organic content (indicated in graph). (b) The variation of organic content of PTBBA-alumoxane on T_C.

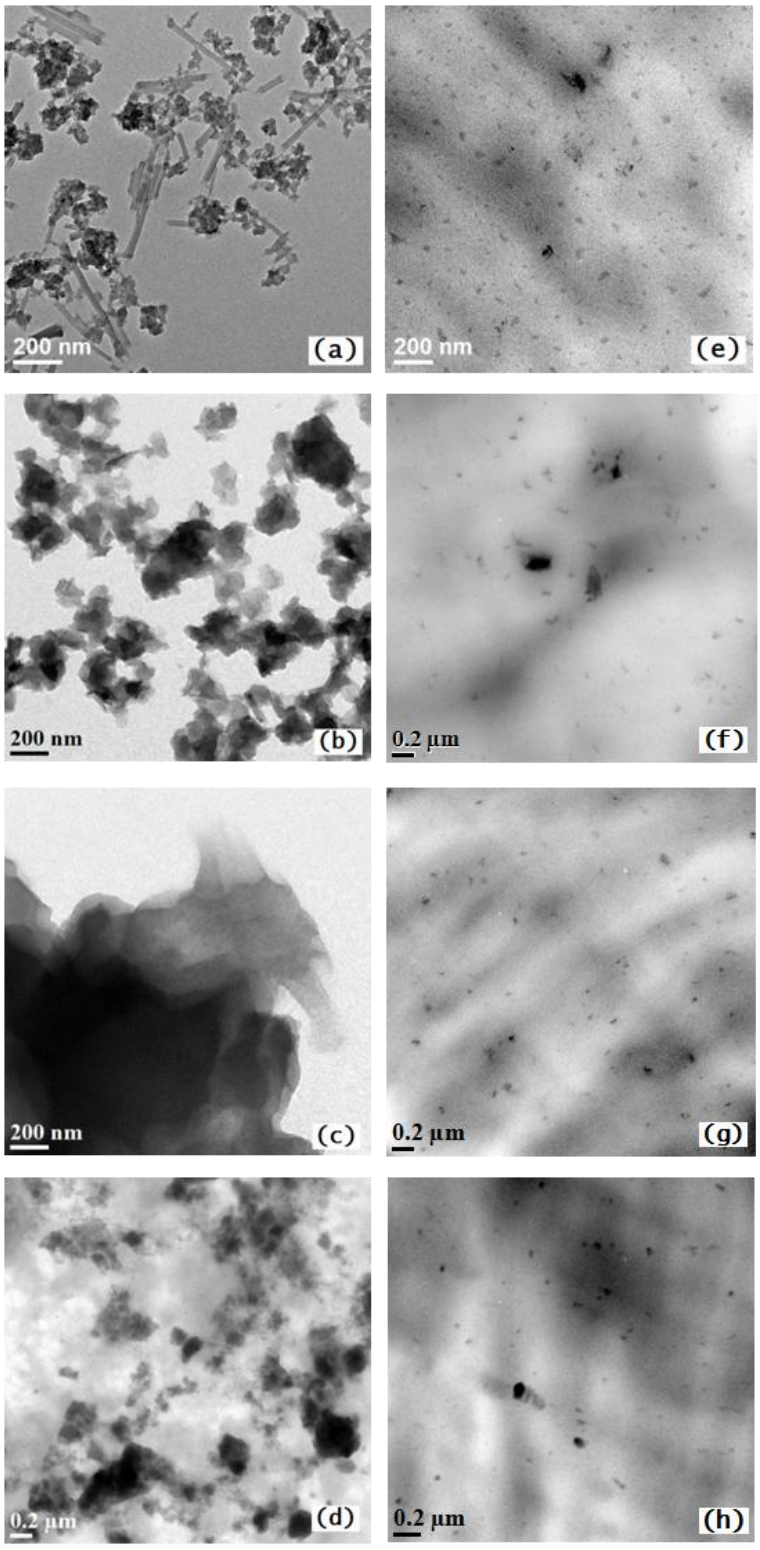

Figure 4.13: TEM images of (left) (a) PTBBA-alumoxane, (b) BA-alumoxane, (c) PA-alumoxane and (d) Zr-PTBBA and their dispersions in the iPP matrix (right) (e), (f), (g) and (h) respectively at 2000 ppm concentration.

Table 4.3: Molecular structure and degradation temperature (T_d) of various carboxylate-alumoxanes. Crystallization temperature (T_C) of iPP nucleated with these carboxylate-alumoxanes (2000 ppm) and their nucleation efficiency (NE).

Carboxylate-alumoxanes							
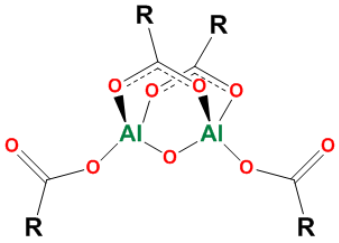							
Butterfly-like structure: Effective nucleation of iPP							
R-substituent	Benzoate (BA)	*p-t*-butylBA	*o*-methylBA	*m*-methylBA	*p*-methylBA	2-naphthoate	1-naphthoate
	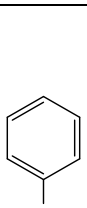	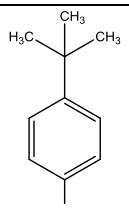	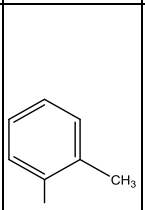	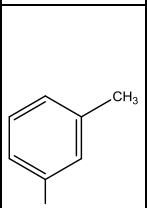	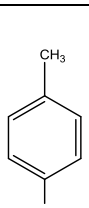	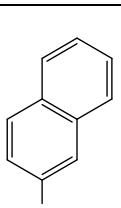	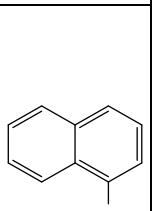
T_d (°C)	272	330	225	229	256	290	310
T_C (°C)	127	132	124	121	125	125	122.7
NE (%)	51	70	40	29	44	44	36
Non-butterfly-like structure: Poor nucleation of iPP							
R-substituent	Phenyl acetate	Cinnamate	Hydro cinnamate	4-Phenyl butyrate	5-Phenyl velerate	6-Phenyl hexanate	1-Naphthyl acetate
	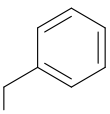	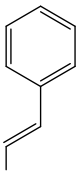	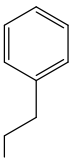	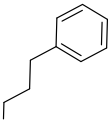	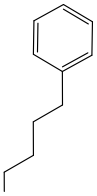	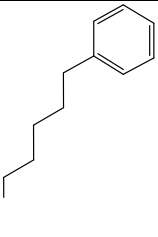	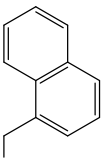
T_d (°C)	270	260	230	240	275	275	300
T_C (°C)	119.5	119.7	120.2	120.2	119.5	118.7	120.6
NE (%)	24	25	26	26	24	21	30

Depending on the structure of the carboxylic acid, alumoxanes inexorably exhibit a nano sheet-like morphology, as also supported by the results of TEM studies (Figure 4.13a and 14b). However, these sheets get fragmented by shearing forces during the melt mixing process in the extruder. Accordingly, a comparison of TEM shows these fragments to be 5 to 25 nm in size dispersed evenly within the iPP matrix. Figure 4.13a and 14b, show the nano sheet morphology of PTBBA-alumoxane and BA-alumoxane respectively and their distribution in iPP matrix after mixing are shown in Figure 4.13e and 14f respectively. (Microtomed iPP samples are stained in RuO_4 vapours using standard procedure for better contrast of the particles).[14]

As discussed earlier, the PTBBA-alumoxane nucleates iPP effectively, whereas PA-alumoxane shows poor nucleation efficiency presumably because of the loss of butterfly configuration mainly due to the methylene group. Nevertheless, PA-alumoxane also shows very good dispersion in iPP matrix (Figure 4.13g), indicating good dispersion alone cannot nucleate iPP effectively. Consequently, carboxylate-alumoxanes were prepared from *p*-*n*-alkylbenzoic acid, where *n*-alkyl group was varied from 1- 8 carbon number in order to see the effect of alkyl chain length on iPP crystallization temperature. As expected intuitively, the nucleation efficiency decreases with increasing the alkyl chain length at para position of BA suggesting that the introduction of alkyl substituent with carbon number above two could mask the nucleation site (aromatic cleft) facilitating the interaction of iPP for inducing crystallization.

The molecular structure and the thermal stability of various carboxylate-alumoxanes are shown in Table 4.3 along with their nucleation efficiency in the iPP. Table 4.3 shows that aromatic carboxylate-alumoxanes exhibits higher nucleation efficiency i.e., above 40 % while phenylalkylcarboxylate-alumoxanes show nucleation efficiency below 30%. This data strongly supports the hypothesis that butterfly-like conformation facilitates the iPP nucleation while non-butterfly-like structure does not. The poor nucleation efficiency of *m*-methybenzoate-alumoxane could be due the variation in the effective interaction of iPP with aromatic cleft due to the *meta* substitution.

We also prepared PTBBA complex based on zirconium as it is larger in size and can have up to eight-coordination.[15,16] In particular, along with monodentate and bridging coordination mode, the carboxylate group can also bind to zirconium through bidentate mode[16] which is restricted in aluminium carboxylates owing to ring strain.[2] Since, it is expected that the ligation of PTBBA and its orientation around zirconium would be different from PTBBA-alumoxane. Surprisingly, Zr-PTBBA complex shows poor nucleation efficiency although the ligand PTBBA is very effective in nucleating iPP when it is coordinated with aluminium. This indicates that the presence of ligand itself is not sufficient for effective nucleation emphasizing the critical role played by the orientational conformation around the metal centre.

4.3 Conclusions

In summary, the critical role played by the molecular conformation of carboxylate-alumoxanes has been correlated well with its nucleating efficiency in iPP using results from a variety of experimental and modeling tools including FT-IR, MALDI-TOF/MS, molecular modeling, WAXS, DSC, TEM and elemental analysis. Apparently, the butterfly structure from bridged bidentate coordination mode and oxo bridging holds the key for controlling the nucleation of this class of polymers. Like sorbitol derivatives and benzenetrisamides, carboxylate-alumoxanes also provide another new platform to develop efficient nucleating agents by choosing appropriate carboxylic acids. The present study also provides more insights into the fundamental aspect of iPP nucleation although a more exhaustive study is needed to understand how iPP-NA interaction induces nucleation in a quantitative manner. Nevertheless, the results undoubtedly provide valuable pathways for controlling nucleation for many industrial processes by tuning the structural conformation of metal complexes with appropriate bridging molecular structures as nucleating agents. Furthermore, the present work demonstrates that vastly improved physical properties can be obtained by suitable choice of materials that can interact in the molecular scale.

4.4 References

(1) R. Callender, C. Harlan, N. Shapiro, C. Jones, D. Callahan, M. Wiesner, D. MacQueen, R. Cook, A. Barron, *Chem. Mater.*, 1997, **9**, 2418.

(2) C. Landry, N. Pappe, M. Mason, A. Apblett, A. Tyler, A. MacInnes, A. Barron, *J.Mat. Chem.*, 1995, **5**, 331.

(3) Derakhshan, L. Rajabi, *Powder Technology*, 2012, **226**, 117.

(4) H. Hatop, M. Ferbinteanu, H. Roesky, F. Cimpoesu, M. Schiefer, H.- G. Schmidt, and M. Noltemeyer, *Inorg. Chem.*, 2002, **41**, 1022.

(5) W. Bury, E. Chwojnowska, I. Justyniak, J. Lewiński, A. Affek, E. Zygadło-Monikowska, J. Bąk, Z. Florjańczyk, *Inorg. Chem.*, 2012, **51**, 737.

(6) L. Kalita, R. Pothiraja, V. Saraf, M. Walawalkar, R. Butcher, R. Murugavel, *J. Organomet. Chem.*, 2011, **696**, 3155.

(7) R. L. Cook, A. R. Barron, K. J. Gleason, D. B. MacQueen, G. L. Sipersky, Y. Koide, C. T. Vogelson, Methods and materials for fabrication of alumoxane polymers U.S. Patent 6369183 Apr. 9, 2002.

(8) B. Fillon, B. Lotz, A. Thierry, J. Wittmann, *J. Polym. Sci. Part B:Polym. Phys.*, 1993, **31**, 1395.

(9) O.Millner, G. Titus, *Chemical Design Automation News* 1990, **5**,10.

(10) T. Smith, D. Masilamani, L. Bui, Y. Khanna, R. Bray, W. Hammond, S. Curran, J. Belles, S. Binder-Castelli, *Macromolecules*, 1994, **27**, 3147.

(11) M. Vougo-Zanda, J. Huang, E. Anokhina, X. Wang, A. J. Jacobson, *Inorg. Chem.*, 2008, **47**, 11535.

(12) E. Alvarez, N. Guillou, C. Martineau, B. Bueken, B. Van de Voorde, C. Le Guillouzer, P. Fabry, F. Nouar, F. Taulelle, D. de Vos, J. Chang, K. Cho, N.Ramsahye, T. Devic, M. Daturi, G. Maurin C. Serre, *Angew. Chem. Int. Ed.Engl.* 2015, **54**, 3664.

(13) G. K. Priya, P. Padmaja, K. G. K. Warrier, A. D. Damodaran, G. J. Aruldhas, *J. Mater. Sci. Lett*., 1997, **16**, 1584.

(14) G. M. Brown, J. H. Butler, *Polymer*, 1997, **38**, 3937.

(15) J. P. Jolivet, *Metal oxide Chemistry and Synthesis*, John Wiley & Sons Ltd, 2000, pp. 84.

(16) R. C. Paul, O. B. Baidya, R. C. Kumar, R. Kapoor, *Aust. J. Chem.*,1976, **29**, 1605.

CHAPTER 5

Enhanced nucleation of polypropylene by metal-organic frameworks (MOFs) based on aluminum dicarboxylates: Influence of structural features

This chapter is adapted from "M. Mani, R. Chellaswamy, Y.N. Marathe, V. Pillai, *RSC Adv.*, **2016**, 6, 1907-1912".

5.1 Introduction

The structural diversity of the known nucleating agents pose major problems in finding new nucleating agents based on chemical structures and functionalities. Nevertheless, the molecular structure of DBS,[1] sodium 2,2'-methylene-bis-(4,6-di-t-butylphenylene)phosph-ate[2] and carboxylate-alumoxanes discussed in the previous chapter shows a butterfly-like or v-shaped conformation and surprisingly all are highly efficient in nucleating iPP. As far as carboxylate-alumoxane is concerned, the butterfly-like structure originated from the bridging coordination of COO^- and oxo ligand towards Al centres,[3] is of critical importance. Recently, it has been reported that the aluminium fumarate (Al-FumA) metal organic framework (MOF) is also built with the similar linkages[4] which also shows a butterfly-like structure. More importantly, this butterfly structure forms a linear channel on the surface and runs along the a-axis.

For the first time, MOFs based on aluminium dicarboxylates as effective nucleating agents for iPP along with possible mechanistic explanation for the nucleation is discussed in this chapter. Also, showed is that a minor structural variation (unsaturated to saturated ligand backbone) has profound influence in the nucleation of iPP. Further, the effect of framework structure in nucleation by changing, (i) the backbone length of the dicarboxylic acid (varying number of intervening CH_2 groups) and (ii) the metal centre (Al, Cr and Zr) with the same dicarboxylate linker are also discussed in order to provide better insights into the selection of generic nucleating agents.

5.1 Results and Discussion

The nucleation efficiency (NE) of aluminium dicarboxylates on iPP along with crystallization temperature (T_C) are given in Table 5.1. The T_C is measured on cooling the polymer melt at 10 °C min^{-1}. It is to be mentioned that the higher T_C indicates higher nucleation efficiency and higher crystallization rate. The nucleation efficiency[5] studies (Annexure-I gives the details of the method) show that all aluminium dicarboxylates MOFs are effective nucleating agents and

Table 5.1 A comparison of the peak crystallization temperature (T_C) of nucleated iPP and nucleation efficiency (NE) of various nucleating agents (NAs).

S. No	Compound (NAs)[a]	-$(CH_2)_n$-	T_C (°C)	NE (%)[b]
1.	Pristine iPP	-	113.0	0
2.	Self-nucleated iPP	-	140.2	100
3.	DMDBS	-	130.5	64
4.	Al-Fumarate (unsaturated)	2	118.0	18
5.	Al-Succinate (saturated)	2	128.6	57
6.	Al-Glutarate (Al-GluA)	3	129.6	61
7.	Al-Adipate (Al-AdiA)	4	127.0	51
8.	Al-Pimelate (Al-PimA)	5	124.5	42
9.	Al-Suberate (Al-SubA)	6	130.0	63
10.	Al-Azelate (Al-AzeA)	7	118.5	20
11.	Al-Sebacate (Al-SebA)	8	125.7	47
12.	Al-Dodecanedioate (Al-DDA)	10	127.5	53
13.	Cr-Suberate (Cr-SubA)	6	120.6	28
14.	Zr-Suberate (Zr-SubA)	6	119.6	24

n - Number of intervening CH_2 groups in the dicarboxylate linker; [a] Concentration of NAs: 2000 ppm; [b] NE calculated following the method given by Fillon et al.[5]

increase the T_C by *ca*. 12 to 17 °C which is obviously higher than that of unnucleated iPP.

The dependence of crystallization temperature (T_C) on the concentration of aluminium suberate (Al-SubA) is shown in Figure 5.1 along with similar data for the standard nucleating agent DMDBS for comparison. Figure 5.1 clearly shows that the 2000 ppm of Al-SubA is as efficient as DMDBS at equal concentration. Interestingly, Al-SubA is efficient even at 3 ppm level and increases T_C by *ca.* 10 °C higher than unnucleated iPP. On the other hand, DMDBS shows nucleation effect for concentrations only above 1000 ppm. In fact, Figure 5.1 appears to be similar to the figure of dependence of crystallization temperature on the concentration of *p*-*t*-butylbenzoate (PTBBA)-alumoxane published elsewhere.[1] The higher nucleation efficiency of Al-SubA at extremely low concentration indicates that Al-dicarboxylates are highly dispersive in the iPP matrix during

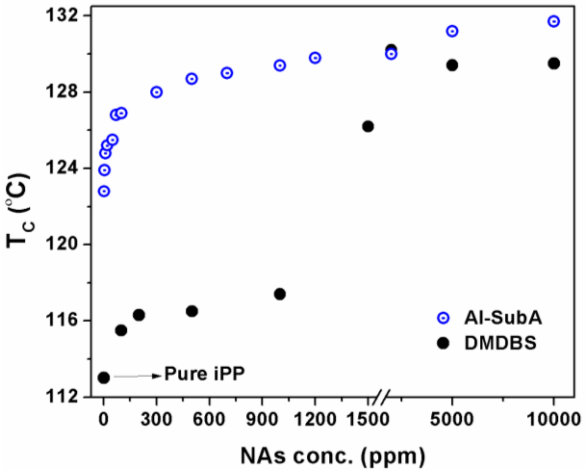

Figure 5.1: Variation of concentration of nucleating agents (NAs) with the crystallization temperature (T_C) of isotactic polypropylene (iPP).

the melt mixing process in the extruder. The Al-dicarboxylates reported here nucleates iPP in the α-phase and is independent of the length of the dicarboxylates. It is worth pointing out that the calcium dicarboxylates can nucleate iPP either in the α-phase or in the β phase.[6]

The structure of Al-dicarboxylate derived from Al-Fumarate (Al-FumA) has been solved recently and shown to be a MOF.[4] Fumaric and succinic acids have the same number of intervening carbon atoms but with and without unsaturated C=C double bond and the respective molecular structures are shown in Figure 5.2. Hence, it is expected that the succinic acid would form a similar MOF structure with aluminium as that of Al-FumA. The WAXS patterns of the Al-FumA and Al-SucA are shown in Figure 5.3a. The x-ray pattern of Al-SucA is comparable with that of Al-FumA with a systematic shift in the peak positions towards the larger 2θ values. For instance, the d spacing of 011 plane in Al-FumA is 8.4 Å while the same distance in Al-SucA is measured to be 7.6 Å and both the compounds show 022 plane at $d_{[011]}/2$ distance. The decrease in the d spacing is expected as succinate is more flexible due to C-C single bond as compared to the rigid fumarate.[4] The flexibility is further confirmed by TGA

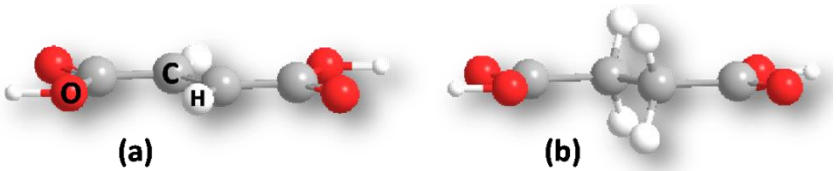

Figure 5.2. The molecular structures of fumaric acid (a) and succinic acid (b).

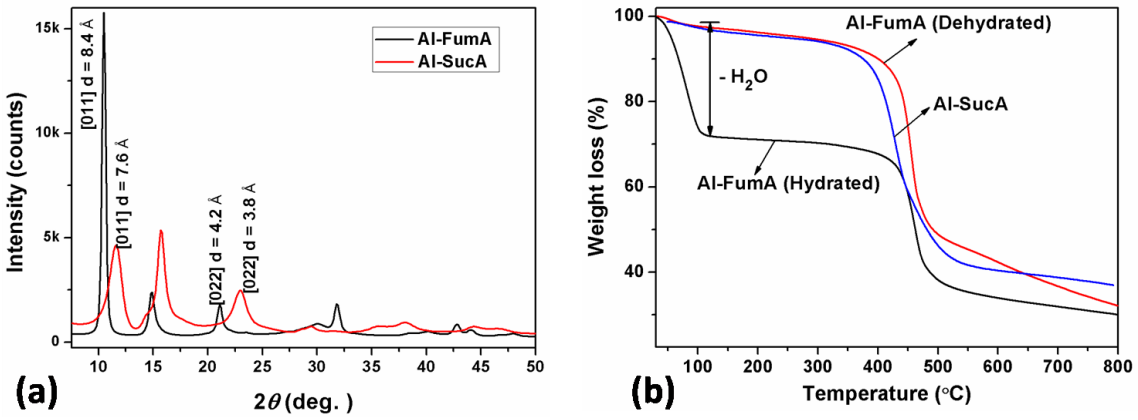

Figure 5.3: (a) WAXS patterns and (b) TGA thermograms of Al-FumA and Al-SucA.

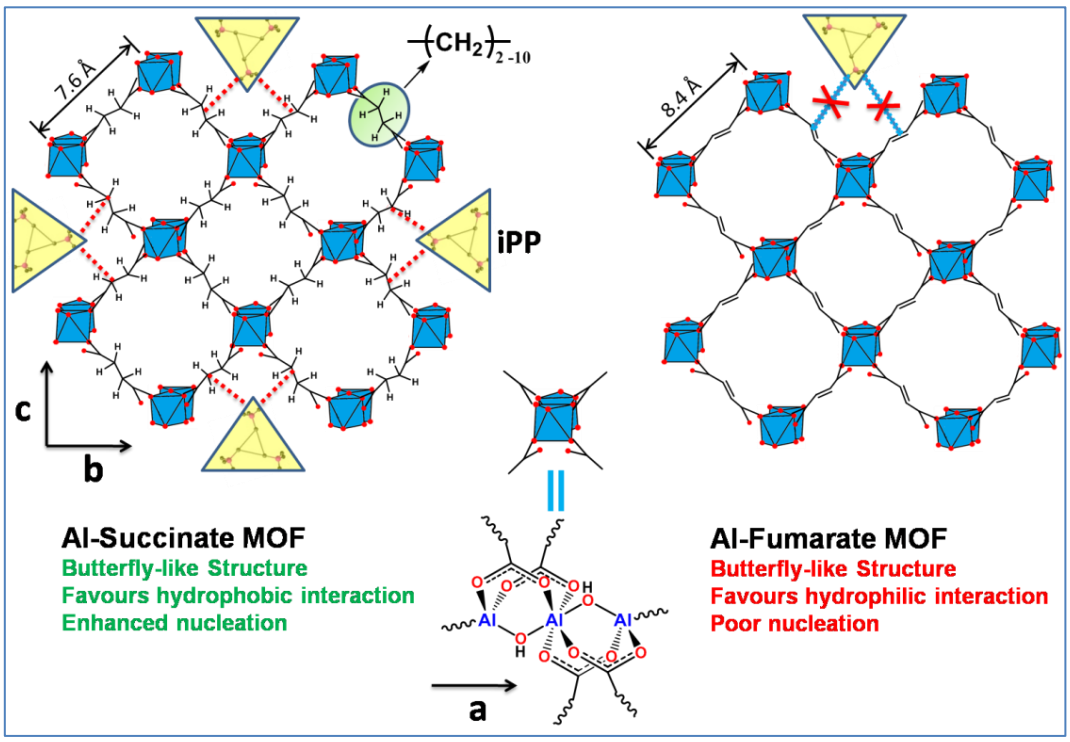

Figure 5.4: A schematic representation of Al-SucA and Al-FumA (MOFs) structures with possible interaction of iPP with the channel wall of the butterfly-like structure.

(Figure 5.3b) which shows that Al-SucA degrades at a lower temperature than dehydrated Al- FumA. In addition, FTIR spectrum of Al-SucA shows asymmetric (ν_{as}) COO^- stretching vibrations at 1610 cm^{-1} and symmetric (ν_s) COO^- vibrations at 1457 cm^{-1}, which are characteristics of bridging coordination.[4,7] The bridging

hydroxyl group vibrations ν(μ_2-OH), typical for corner-sharing $AlO_4(OH)_2$ octahedra is observed at 3693 cm^{-1}.[4,8] Hence, it can be concluded that the Al-SucA possess metal organic framework (MOF) structure very similar to Al-FumA in which trans-corner sharing octahedral $AlO_4(OH)_2$ chains are connected by succinate linkers as shown in Figure 5.4. Furthermore, nitrogen sorption-desorption isotherm studies show BET surface area to be *ca*. 144 m^2/g and 300 m^2/g for Al-SucA and Al-FumA respectively. Lower surface area of Al-SucA indicates less porosity than the Al-FumA. This can be explained on the basis of the incorporation of protruding hydrogen atoms of the succinate linker (sp^3 hybridized methylene groups) towards the pore walls.

The MOFs based on Al-dicarboxylates show butterfly-like structures due to their coordination linkages around Al centre, as shown in Figure 5.4 and is similar to carboxylate-alumoxanes structure discussed in the chapter 4. More specifically, the Al-dicarboxylate MOF structures can form a linear channel on the surface along the a-axis in 3D structure as clearly seen in the Al-FumA MOF structure.[4] By analogy, it can be concluded that all the dicarboxylates based on aluminium do have a MOF structure. This is also supported by the WAXS patterns (Figure 5.5a) which indicates that all Al-dicarboxylate MOFs are highly crystalline and show a sharp peak in the range of (2θ) 5° - 12°, arising from the reflection of 011 plane representing dicarboxylate direction.[4] The $d_{[011]}$ spacing increases with increasing number of intervening methylene groups as shown in Figure 5.5b; with observable odd-even effect.

Interestingly, Al-dicarboxylate MOFs like carboxylate-alumoxanes, act as an efficient nucleating agents for iPP. As with carboxylate-alumoxanes, the interaction of iPP molecular segment with the butterfly-like structure may be responsible for the efficient nucleation of Al-dicarboxylate MOFs as shown in Figure 4. Nevertheless, the Al-dicarboxylate MOFs and carboxylate-alumoxanes differ from each other due to the mode of interaction with iPP. For instance, carboxylate-alumoxane provides aromatic cleft for the iPP interaction while the

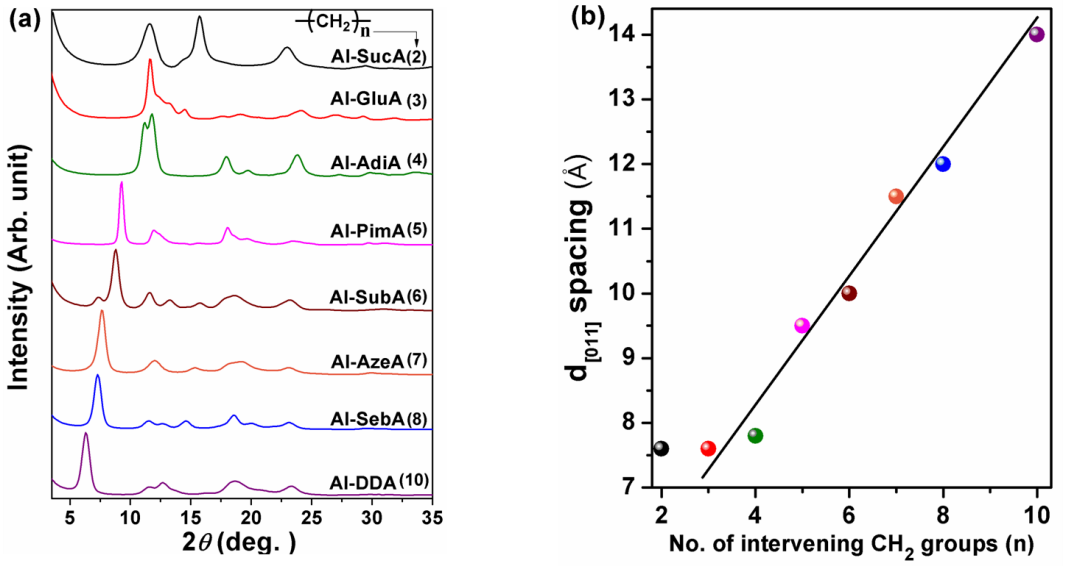

Figure 5.5: (a) WAXS patterns of Al-dicarboxylate based MOFs in which the number of intervening CH_2 groups (n) in the dicarboxylate linker are varied from 2-8 &10. (b) The variation of number of CH_2 groups (n) with $d_{[011]}$ spacings.

higher nucleation efficiency of Al-dicarboxylate MOFs is attributed to the interaction of iPP helical chain with alkyl group of the butterfly-like channel. The repeat distance along the channel, which is along the a-axis is 6.8 Å[4] and is very close to the 6.5 Å of the iPP 3_1 helical chain length suggesting lattice matching between nucleating agent and iPP crystal. However, the Al-FumA and Al-AzeA are exceptions and do not nucleate iPP even though the butterfly-like channel is present along the a-direction and no change in the a-axis repeat unit. It is interesting to compare the structure and nucleation behaviour of Al-FumA (unsaturated Al- dicarboxylate) and Al-SucA (saturated Al-dicarboxylate). While both Al-FumA and Al-SucA have very similar structures, the difference in the nucleation behaviour may be explained due to the difference in the interaction with iPP. More specifically, the Al-FumA is hydrophilic in nature as evident from TGA and is shown in Figure 5.3b and 5.7b. Hydrated Al-FumA shows a weight loss due to absorbed water molecules which is in agreement with the literature,[4] whereas Al-SucA and the higher analogous saturated Al-dicarboxylates does not absorb water molecules even after prolonged treatment with water as seen from Figure 5.3b is indicating the hydrophobicity of these materials. Further, it may be noted that the cavity in the structures of higher analogous saturated Al-

dicarboxylates will be larger than that of the cavity of Al-FumA. In the case of Al-FumA, the hydrophilicity arises due to bridged hydroxyl and carboxylate oxygens which interact with water molecules through hydrogen bonding as reported by Alvarez et al.[4] The hydrophilic sites are open because of the backbone structure of fumarate where the H atoms (sp^2 hybridized CH groups) are coplanar with C=C double bond and hence do not hinder the water molecules interacting with them. However, in the case of Al-SucA, the hydrophilic sites are shielded by the protruding hydrogens of the succinate linker (sp^3 hybridized CH_2 groups) and impart hydrophobic character to the channel wall. Hence, it can be concluded that the subtle change in the structure of ligand backbone (fumarate to succinate) brings remarkable variation in the hydrophilic/hydrophobic character of the channel determined by the butterfly-like structure and subsequent interactions to effect nucleation characteristics of iPP. Therefore, poor nucleation of Al-FumA is due to hydrophilic nature, perhaps caused by the repulsive interactions with hydrophobic iPP while enhanced nucleation of Al-SucA is due to hydrophobic channel which can facilitate attractive interaction with hydrophobic iPP. This suggests that the butterfly structure is prerequisite but favourable interaction is also essential for the effective nucleation of iPP.

Nucleation efficiency studies (Table 5.1) show that all Al-dicarboxylates are effective nucleating agents although they have different $d_{[011]}$ spacing (Figure 5.5b). This indicates that the increase in the intervening methylene groups simply increases the length of the wing of the butterfly-like cavity (Figure 5.4) while the a-axis remain unaltered and hence does not affect the nucleation efficiency considerably. It is worth pointing out that the common feature of efficient nucleating agents presented in the thesis and published in literature[1,2] necessitate a butterfly-like or v-shaped conformation of the single unit and the linear channel arising out of it on the surface in 3D structure. These channels with favourable attraction can align iPP molecular segment in the channel to initiate the nucleation process.

As mentioned earlier, the Al-azelate shows poor nucleation although the x-ray pattern indicates that the structure of Al-AzeA is analogous to other Al-dicarboxylates. At present there is no explanation for its poor nucleation behaviour although it may be speculated that the azelate ligand can bend and coordinate with the same octahedral alumina chain sporadically and this possibility is restricted in other dicarboxylates due to chain length. Hence, it can be expected that sporadic bending of azelate chains could mask the butterfly-like cavity consequently leading to poor interaction and poor nucleation of iPP. Al-dicarboxylates with 9 and higher odd number intervening methylene groups may exhibit similar behavior but needs to be verified experimentally.

High nucleation efficiency of Al-dicarboxylates is accomplished by the presence of butterfly-like structure which arises mainly due to the carboxylate and hydroxyl bridging coordination towards Al centres. The chelation binding is restricted in alumina owing to the ring strain.[7] Hence, it is possible to alter the butterfly-like structure by choosing the metal centre like chromium (Cr), zirconium (Zr) etc. which can coordinate with carboxylate group via a chelation

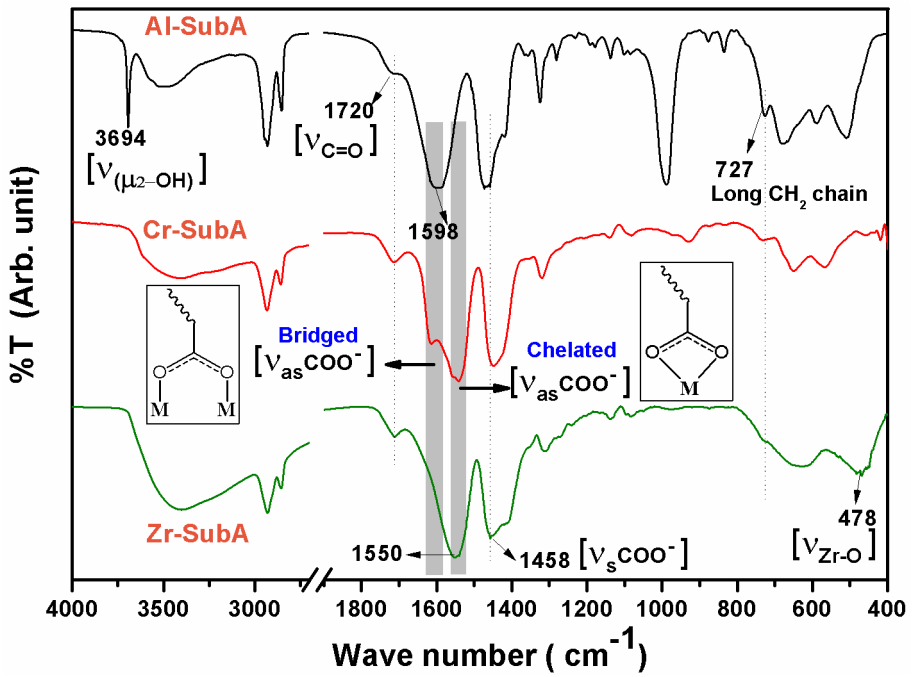

Figure 5.6: A comparison of the FT-IR spectra of Al-SubA, Cr-SubA and Zr-SubA.

mode along with bridging and unidentate binding.[9,10] Further, the Zr can accommodate up to eight ligands in its coordination sphere due to larger size.[11] To clarify the above aspect, the MOFs based on Al-Suberate (Al-SubA), Cr-Suberate (Cr-SubA) and Zr-suberate (Zr-SubA) were prepared followed by an analysis of their nucleation properties. The nature of coordination mode of carboxylate towards metal centre can be identified by FTIR spectroscopy.[12,13] A comparison of the FTIR spectra of Al-SubA, Cr-SubA and Zr-SubA is shown in Figure 5.6, which reveals the symmetric (ν_s) COO^- stretching at the same position in all the above three compounds. However, the position of the asymmetric (ν_{as}) COO^- stretching changes with respect to its associated metal centre. As discussed earlier, the COO^- group is bound to Al centre via a bridging coordination. However, the COO^- group in the Zr-SubA is involved in chelation binding mode as characterized by a lower Δ value of 92 cm^{-1} (ν_{as}- ν_s of COO^-) as compared to a Δ value of 140 cm^{-1} for bridging carboxylate with aluminium. This chelation binding is further confirmed by the presence of peak a at 478 cm^{-1} corresponding to Zr-O stretching in the chelated metal carboxylate ring.[10] On the other hand, the Cr-SubA complex shows both bridging and chelated COO^- coordination as revealed by the presence of two peaks (1613 cm^{-1} and 1541 cm^{-1}) for asymmetric (ν_{as}) COO^- stretching vibrations. The difference in the ligation of carboxylate group towards Zr and Cr strongly suggests that the orientation of suberate ligands around them would be different from that of Al-SubA and consequently, forming a different MOF structure.

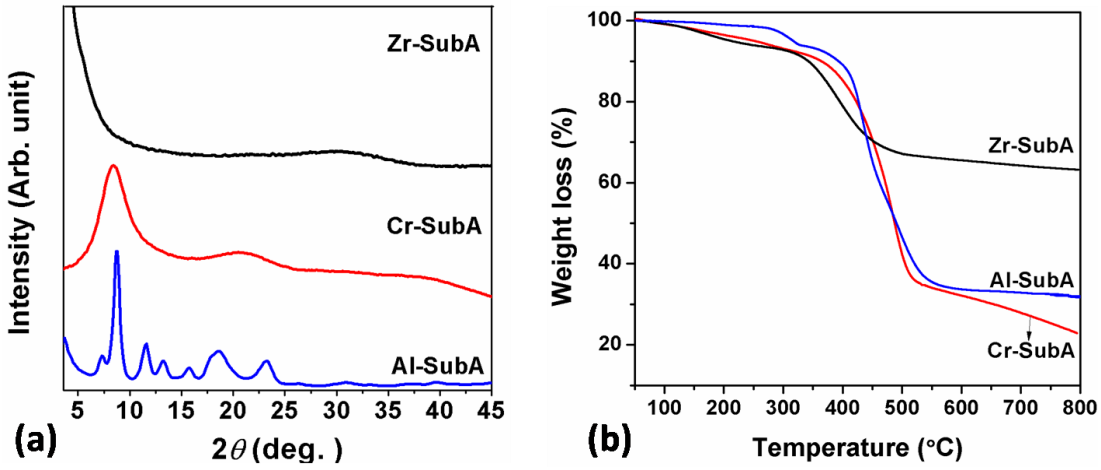

Figure 5.7: (a) WAXS and (b) TGA thermograms of Al, Cr and Zr suberates.

WAXS pattern of Al-SubA and Cr-SubA shown in Figure 5.7a indicates that both Al-SubA and Cr-SubA have similar crystalline order and the difference in the diffraction profiles suggest that their framework structures are different. Zr-SubA does not show any diffraction peaks indicating amorphous nature of MOF. TGA (Figure 5.7b) shows all the three MOFs to have thermal stability above 300 °C, much above the iPP processing temperature. Surprisingly, Zr-SubA and Cr-SubA show poor nucleation efficiency although the suberate is very efficient in nucleating iPP when it forms MOF structure in combination with aluminium. This indicates that the suberate alone is not responsible for the effective nucleation of iPP emphasizing the critical role played by the orientational conformation of the ligand around the metal centre for the iPP nucleation, which is in complete agreement with the studies based on carboxylate-alumoxanes.

5.3 Conclusions

The present study reveals that the nucleating agent should provide a channel (formed by the butterfly-like structure in the present as well as in the most of the other NAs) that can facilitate favourable interactions with iPP for enhanced nucleation. The variation of the alkyl chain length between the alumina chains in the MOF does not alter the nucleation efficiency considerably, suggesting that the butterfly-like structure present in the metal organic framework holds the key for controlling nucleation. Further, the poor nucleation of Cr-SubA and Zr-SubA as compared to Al-SubA corroborates the critical role played by the orientational conformation of the dicarboxylate in the nucleation of iPP. Although, more exhaustive study is needed to understand the mechanism of nucleation in a quantitative manner, the present work undoubtedly provides valuable pathways for developing new nucleating agents based on the MOFs with the proper selection and orientation of the organic linkers around the metal centre. This study also demonstrates that physical properties of the materials can be enhanced multi fold if the interaction occurs in the molecular scale.

5.4 References

1) T. Smith, D. Masilamani, L. Bui, Y. Khanna, R. Bray, W. Hammond, S. Curran, J. Belles, S. Binder-Castelli, *Macromolecules*, 1994, **27**, 3147.
2) G. Zhang, Z. Xin, J. Yu, Q. Gui, S. Wang, *J. Macromol. Sci. Part B: Phys.*, 2003, **42**, B42, (3 & 4) 467.
3) L. Kalita, R. Pothiraja, V. Saraf, M.Walawalkar, R. Butcher, R. Murugavel, *J. Organomet. Chem.*, 2011, **696**, 3155.
4) E. Alvarez, N. Guillou, C. Martineau, B. Bueken, B. Van de Voorde, C. Le Guillouzer, P. Fabry, F. Nouar, F. Taulelle, D. de Vos, J. Chang, K. Cho, N. Ramsahye, T. Devic, M. Daturi, G. Maurin, C. Serre, *Angew. Chem. Int. Ed. Engl.*, 2015, **54**, 3664.
5) B. Fillon, B. Lotz, A. Thierry, J. Wittmann, *J. Polym. Sci. Part B: Polym. Phys.*, 1993, **31**, 1395.
6) X. Li, K. Hu, M. Ji, Y. Huang, G. Zhou, *J. Appl. Polym. Sci.*, 2002, **86**, 633.
7) C. Landry, N. Pappe, M. Mason, A. Apblett, A. Tyler, A. MacInnes, A. R. Barron, *J. Mater. Chem.*, 1995, **5**, 331.
8) M. Vougo-Zanda, J. Huang, E. Anokhina, X. Wang, A. Jacobson, *J. Inorg. Chem.*, 2008, **47**, 11535.
9) M. Murrie, S. Parsons, R. Winpenny, *Chem. Commun.*, 1999, 285.
10) R. C. Paul, O. B. Baidya, R. C. Kumar, R. Kapoor, *Aust. J. Chem.*, 1976, **29**, 1605.
11) J. P. Jolivet, *Metal oxide Chemistry and Synthesis*, John Wiley & Sons Ltd, 2000 pp. 84.
12) X. H. Guan, G. H. Chen, C. Shang, *J. Environ. Sci.*, 2007, **19**, 438.
13) P. Persson, M. Karlsson, L. O. Öhman, *Geochim. Cosmochim. Acta*, 1998, **62** (23/24) 3657.

CHAPTER 6

New understanding on regulating the crystallization and morphology of β-polymorph of isotactic polypropylene based on carboxylate-alumoxane nucleating agents

This chapter is adapted from "M. Mani, R. Chellaswamy, Y.N. Marathe, V. Pillai, *Macromolecules*, **2016**, 49, 2197−2205".

6.1 Introduction

In the preceding chapters, family of nucleating agents based on carboxylate-alumoxanes is shown to be an efficient nucleator for iPP. The key molecular structural feature of the carboxylate-alumoxane is bicyclic ring structure having aluminum centers linked with oxo and aromatic carboxylate groups. This chapter shows that when the normal alkyl chain is attached to the *para* position of the aromatic carboxylate modifies the nucleation behavior and depending on the crystallization conditions it nucleates iPP predominantly in the *β*-phase. Further, we studied the morphological differences between the *α*- and the *β*- phases based on WAXS, SAXS and DSC studies. Another highlight of the work is the observance of two distinct crystallization temperature ranges under non isothermal crystallization for both crystalline modifications. Also, we show for the first time the dependence of *β*-crystal lamellae thickness on the crystalline transition of the *β*-phase in to the *α*-phase during melting.

6.2 Results and Discussion

The molecular structure of *p*-*n*-alkylbezoate (*pn*ABA)-alumoxanes, where n-alkyl group varies from 1-8 carbon atoms, is shown in Figure 6.1a as derived from the MALDI-TOF mass spectrometry analysis. For example, the MALDI-TOF/MS spectrum of *p*-methylbenzoate-alumoxane shows a peak at 633 Da, which is assigned to the dinuclear aluminum complex (A in Figure 6.2) with the molecular formula $[(Me\text{-}C_6H_4CO_2)Al(\mu\text{-}O)(\mu\text{-}O_2CC_6H_4\text{-}Me)]_2$ along with that for Na^+ ion. In addition, the spectrum also shows the formation of oxo-centered trinuclear aluminum complex with bridging carboxylate ligands (B in Figure 6.2). These structures are in excellent accordance with the structures discussed elsewhere in the thesis and in published literature.[1,2] Hence, it may be concluded that the *p*-*n*-alkyl substituted benzoate-alumoxanes reported here would have a similar structure like that of *p*-methybenzoate-alumoxanes. The X-ray patterns (Figure 6.1b) indicate these samples to be crystalline and having a major peak in the (2θ) range of 4° - 8.5°. Interestingly, this peak shifts systematically to lower angle with increasing the alkyl chain length at the para position of the benzoate in the carboxylate-alumoxane as expected from geometric considerations.

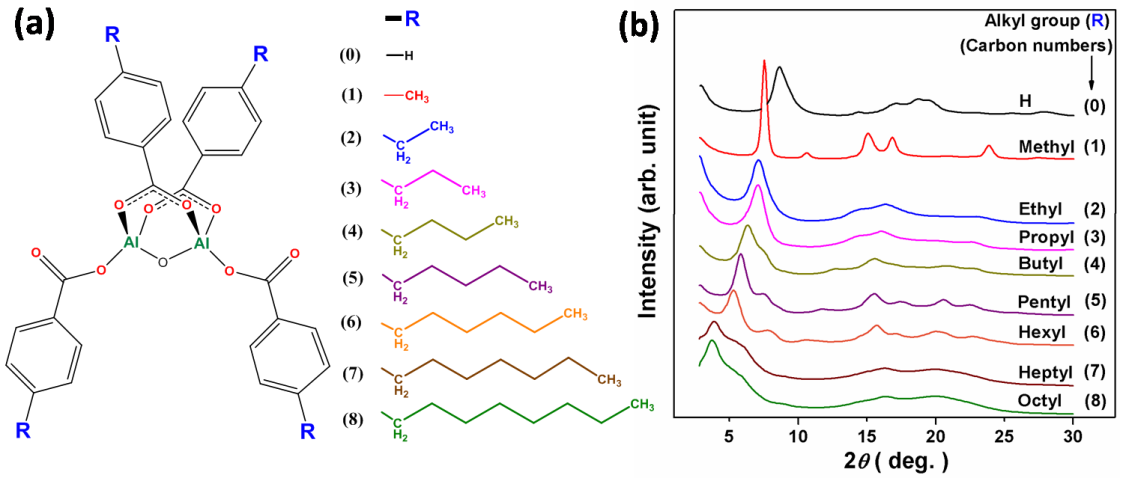

Figure 6.1: (a) Molecular structure of *p-n*-alkylbenzoate-alumoxanes, where the carbon atom in the alkyl group (-R) varies from 0-8 and (b) the corresponding WAXS patterns.

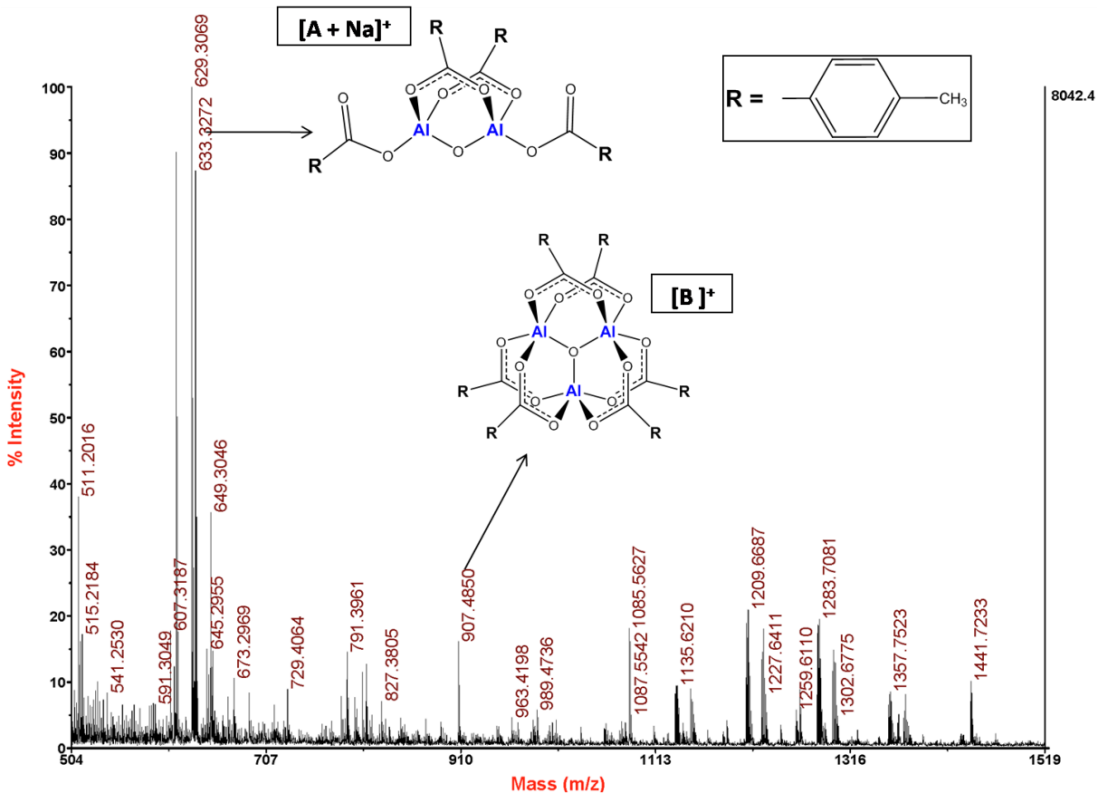

Figure 6.2. MALDI-TOF/MS of p-methylbenzoate-alumoxane.

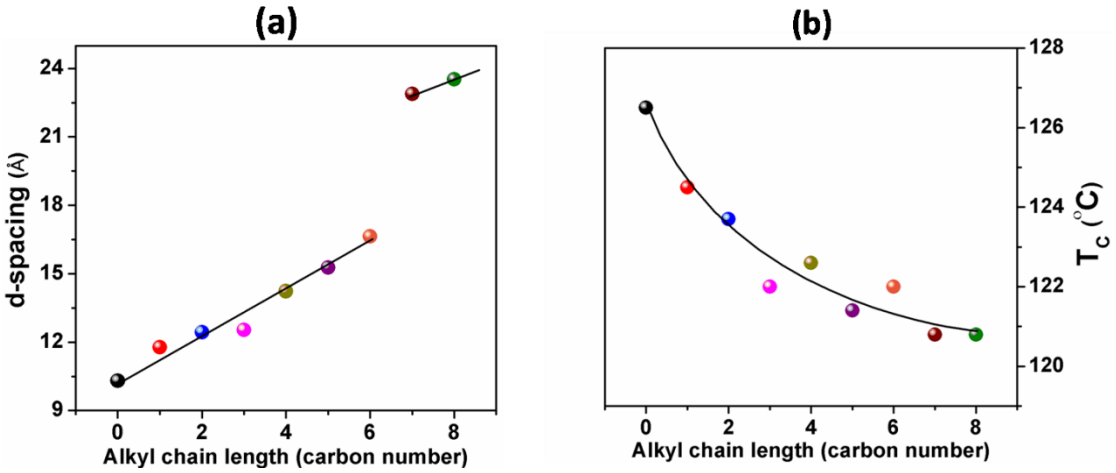

Figure 6.3: (a) Variation of d-spacing of *p*-*n*-alkylbenzoate-alumoxanes with respect to the alkyl chain length and (b) dependence of crystallization temperature (T_C) of the iPP on the alkyl chain length. The color code is described in Figure 6.1a.

The dependence of d-spacing with alkyl chain length is shown in Figure 6.3a, where a linear increase in d-spacing is revealed along with an increase in the alkyl chain length up to six carbon atoms followed by a jump for higher alkyl chain lengths. The nucleation efficiency studies on *pn*ABA-alumoxanes show that the increasing alkyl chain length decreases the nucleation efficiency as shown in Figure 6.3b. The nucleation effects of carboxylate-alumoxanes are attributed to the interaction of iPP with the aromatic cleft of butterfly-like structure as discussed in the chapter 3. Hence, the decreasing trend in the nucleation efficiency suggests the masking effect of alkyl group towards the aromatic cleft (nucleation site).

The DSC melting endotherms of the extruded iPP nucleated with the *p*-*n*-alkylbenzoate-alumoxanes samples having alkyl chain length two or above consistently show a melting peak at *ca.* 155 °C, corresponding to the *β*-phase, in addition to the melting peak of the *α*-phase at *ca.* 165 °C. The WAXS patterns of these samples also reveal the presence of significant amount of *β*-crystalline modification and warrant a systematic study on the *β*-crystalline modification exhibited by iPP nucleated with above *pn*ABA-alumoxanes. It is also worth comparing the *β*-phase obtained by the standard *β*-nucleating agent, calcium pimelate, to understand the formation, morphology and the characteristics of *β*-phase.

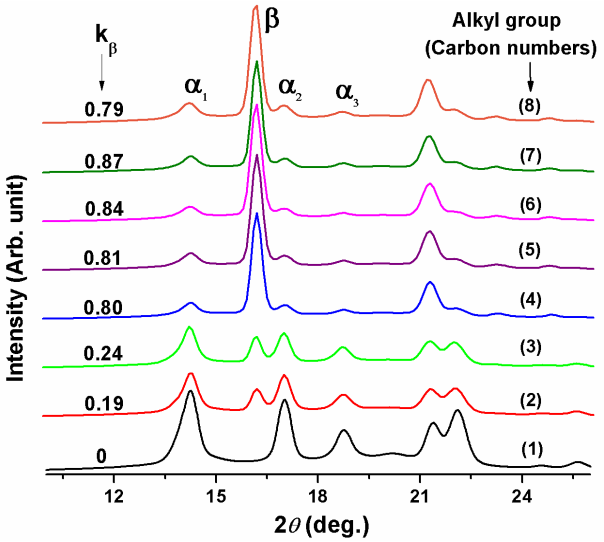

Figure 6.4: WAXS patterns of iPP nucleated with *p*-*n*-alkylbenzoate-alumoxanes having normal alkyl group with varying carbon atoms as indicated in the figure.

Figure 6.4 shows a comparison of the WAXS patterns of *pn*ABA-alumoxanes nucleated iPP crystallized under controlled conditions viz., heating the sample to 210 °C at 50 °C/min and then cooled at 50 °C/min after holding the melt for 2 min at 210 °C. The crystallized iPP samples show peaks corresponding to the α- and the β-crystalline modifications. The iPP nucleated with *pn*ABA-alumoxanes with alkyl chain length of 4 carbons and above show *ca.* 80% β-phase and is independent of alkyl chain length. However, the amount of β-content strongly depends on the concentration of the nucleating agent, end melting temperature, melt holding time and the cooling rate. Detailed investigations on the β-phase have been made with *p*-*n*-Hexylbezoate (HexBA)- alumoxane and accordingly, Figure 6.5 shows the dependence of the amount of crystalline modification on the concentration of HexBA-alumoxane. The amount of the β-modification increases rapidly and reaches a maximum value at 0.2 wt% and further increase in the concentration of nucleating agent the β-content decreases. This shows that the HexBA-alumoxane acts a dual nucleating agent. It nucleates iPP in the β-phase at lower concentration range from 0.1 to 1 wt%, with maximum β-phase at *ca.* 0.2 wt%. Outside this concentration range the α-phase dominates the crystallization. Quinacridone also shows very low levels of β-phase when the concentration is low and it increases with increase in the content of quinacridone.[3]

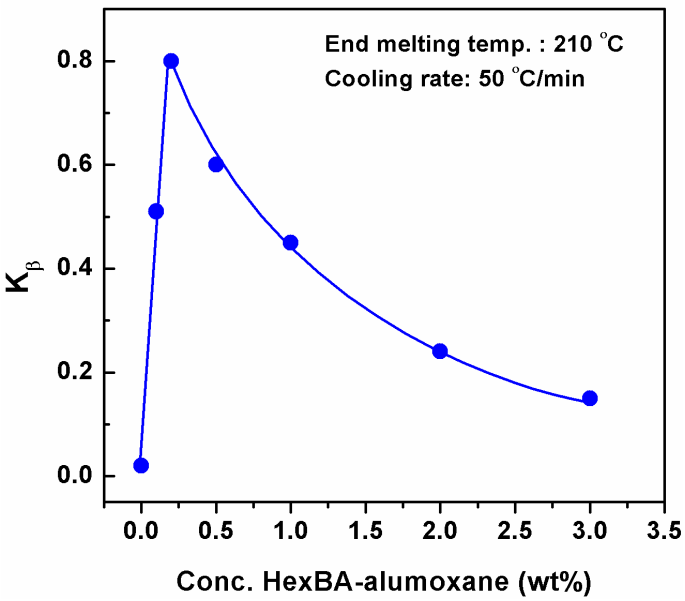

Figure 6.5: The variation of the β-content with the concentration of HexBA-alumoxane.

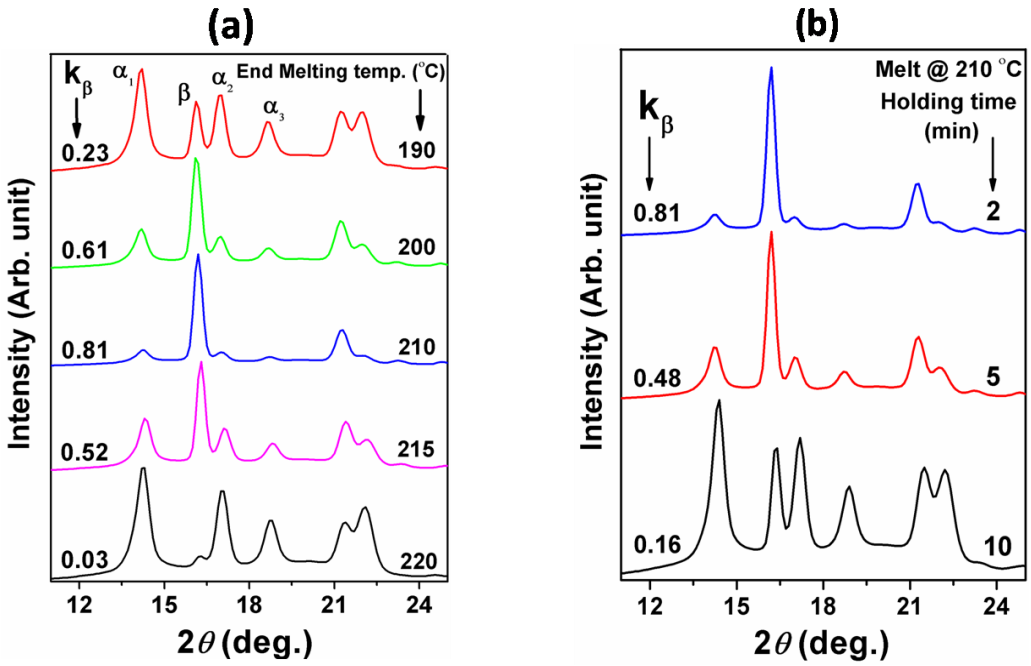

Figure 6.6: A comparison of the WAXS patterns of iPP nucleated with HexBA-alumoxane crystallized at a cooling rate of 50 °C/min (a) from various end melting temperature and (b) melt hold at 210 °C with varying holding time.

Figures 6.6a and 6.6b show the X-ray diffraction pattern for HexBA-alumoxane nucleated iPP samples held at different temperatures for 2 min and at various time intervals at 210 °C respectively. It is clearly seen that the *β*-content is maximum for the case at 210 °C while below 190 °C the samples crystallized predominantly in the *α*-phase. Although the holding temperature of 210 °C gives the maximum amount of *β*-phase, higher holding times at 210 °C decreases the *β*-phase and for 10 min holding time give *ca.* 15% the *β*-phase.

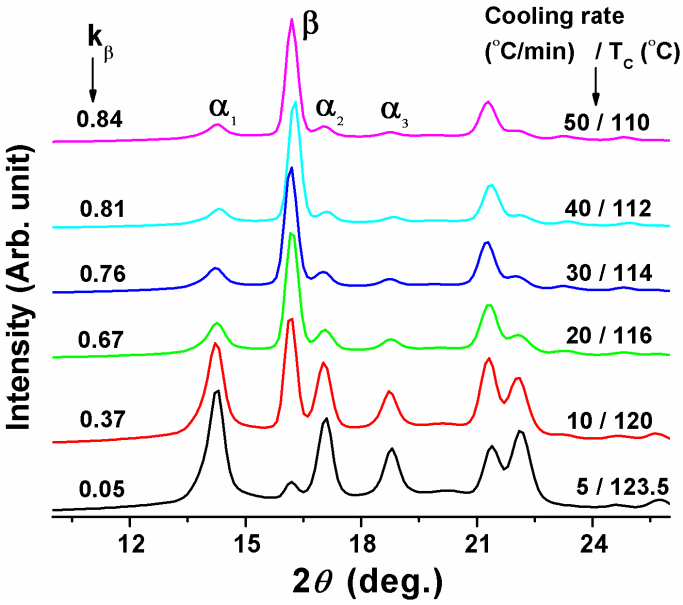

Figure 6.7. WAXS patterns of iPP nucleated with HexBA-alumoxane crystallized at various cooling rates (indicated in the figure) from 210 °C.

Figure 6.7 shows x-ray patterns obtained from the HexBA-alumoxane nucleated iPP samples crystallized with varying cooling rates from 210 °C, showing the strong dependency of *β*-phase on cooling rate. Faster cooling rates give higher content of *β*-phase and 50 °C/min, the fastest cooling rate achievable under controlled conditions, show *ca.* 80%. However, these data is at variance with the sample nucleated with calcium pimelate (CaP). The samples nucleated with CaP always show a very high degree of *β*-content (*ca.*95%) irrespective of the end melting temperature and cooling rate. These results can be explained with the dual efficiency of the nucleating agent based on *pn*ABA-alumoxanes. The results indicate clearly that the *pn*ABA-alumoxanes is not selective exclusively to the *β*-modification, because the *β*-content is moderate

Table 6.1: Crystallization temperature (T_C) of iPP (non-nucleated) and nucleated with 2000 ppm of various nucleating agents (NAs) on various cooling rates.

Compound (NAs)	**CaP**	**HexBA-alumoxane**	**Pure iPP**	**BA-alumoxane**	**DMDBS**	**PTBBA-alumoxane**
Cooling rate (°C)	Crystallization temperature (T_C) (°C)					
50	111	110	105.5	116	121	122
35	114		107.5	-	-	-
20	118.5	116	111	126.5	-	128
10	122.5	120	115	-	130	131.5
5	125	123.5	-	-	-	134
2	128	127	-	132.5	134	137
1	130	129	-	-	-	140

only compared to that in the presence of CaP. Accordingly, the *pn*ABA-alumoxanes always results in the formation of α-nuclei also. At slow cooling rate the crystallization begins at high temperature, where the growth rate of the α- and the β-phase iPP is comparable. In this case the β-phase content is smaller. At faster cooling rate the formation of nuclei is below 140 °C, thus the formation of the α-phase iPP is suppressed and the β-content increases. Table 6.1 gives the various cooling rates and the corresponding crystallization temperatures for CaP and HexBA-alumoxanes nucleated iPP samples respectively.

It is difficult to predict the specific nature of interaction between the *pn*ABA-alumoxanes and iPP melt, but the interaction leads to the formation of β-phase. However, on heating to 210 °C and holding for longer time periods or heating above 210 °C and subsequent cooling gives only the α-phase. This effect can be clearly seen in the dependence of T_C on end melting temperature and is shown in Figure 6.8. A similar result has been reported by Varga and Menyhárd,[4] for NJS and the end melting temperature controls the nucleation efficiency and relative fractions of phases.

As mentioned earlier, WAXS analyses show that the CaP nucleated iPP always crystallizes into the β-phase irrespective of the cooling rates. Nevertheless, these samples exhibit significant variation in melting endotherm on subsequent heating to melt as shown in Figure 6.9a. More importantly, the samples crystallized at higher

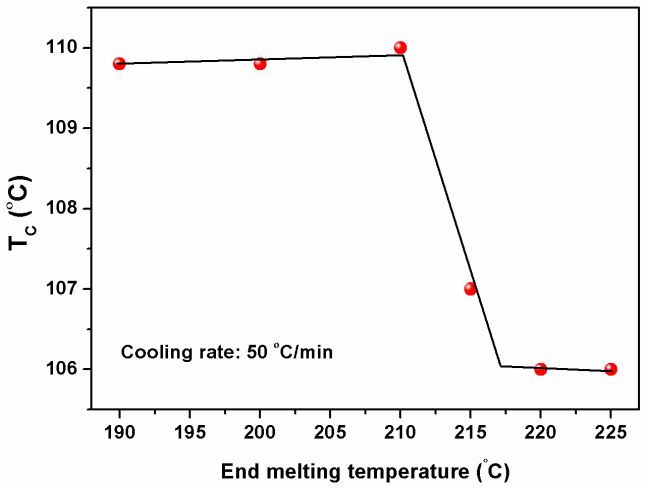

Figure 6.8: Variation of end melting temperature with the peak crystallization temperature (T_C) of iPP nucleated with 0.2 wt% of HexBA-alumoxane.

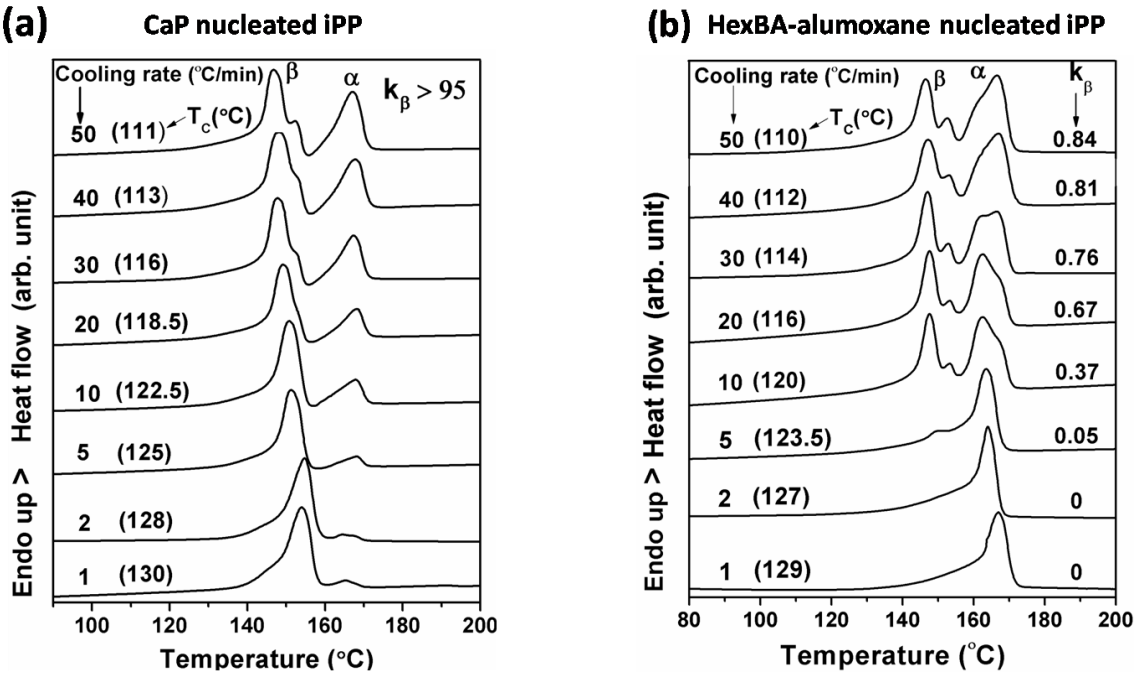

Figure 6.9. A comparison of the DSC melting endotherms of (a) CaP and (b) HexBA-alumoxane nucleated iPP crystallized at various cooling rates as indicated in the figure. The heating rate is 10 °C/min. The amount of the *β*-phase content measured from the WAXS patterns at room temperature before heating to melt is indicated in the graphs.

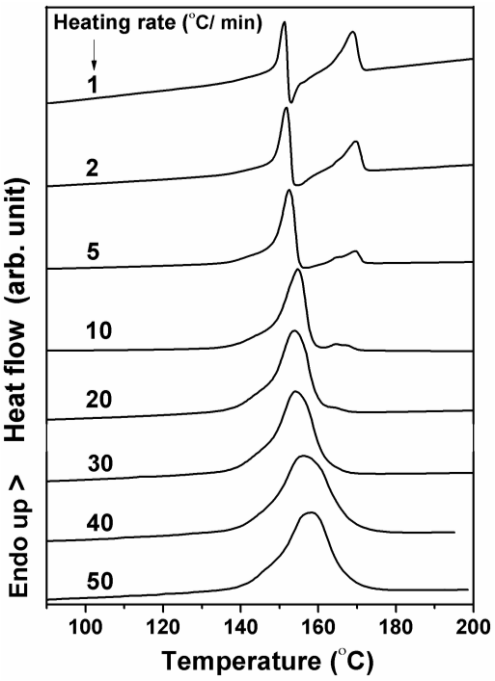

Figure 6.10. DSC melting endotherm of CaP nucleated iPP sample crystallized at cooling rate of 2 °C min^{-1}. The heating rates are as indicated in the Figure.

temperatures do not show the β- to the α- melt recrystallization during the melting of the β-phase. However, samples crystallized at lower temperatures show significant amount of the β- to the α- melt recrystallization with an increasing amount of recrystallized α-phase. However, it may be noted that the sample crystallized at 128 °C show the β- to the α- melt recrystallization on heating at low heating rates 2 °C/min as shown in Figure 6.10. It appears that the morphology of the β-phase depends strongly on the crystallization temperature and plays an important role in the β- to the α- melt recrystallization. The situation is very different for iPP samples nucleated with HexBA-alumoxane because the amount of β-phase depends on the crystallization conditions. Figure 6.9b shows the DSC heating thermograms of the samples crystallized on various cooling rates at a heating rate of 10 °C/min.

It is interesting to note that the CaP and HexBA-alumoxane nucleated samples that are crystallized at cooling at 50 °C/min show very similar melting endotherms, implying identical morphology in these samples. This is further confirmed by HTWAXS studies made on these samples. The WAXS patterns obtained during heating of these samples

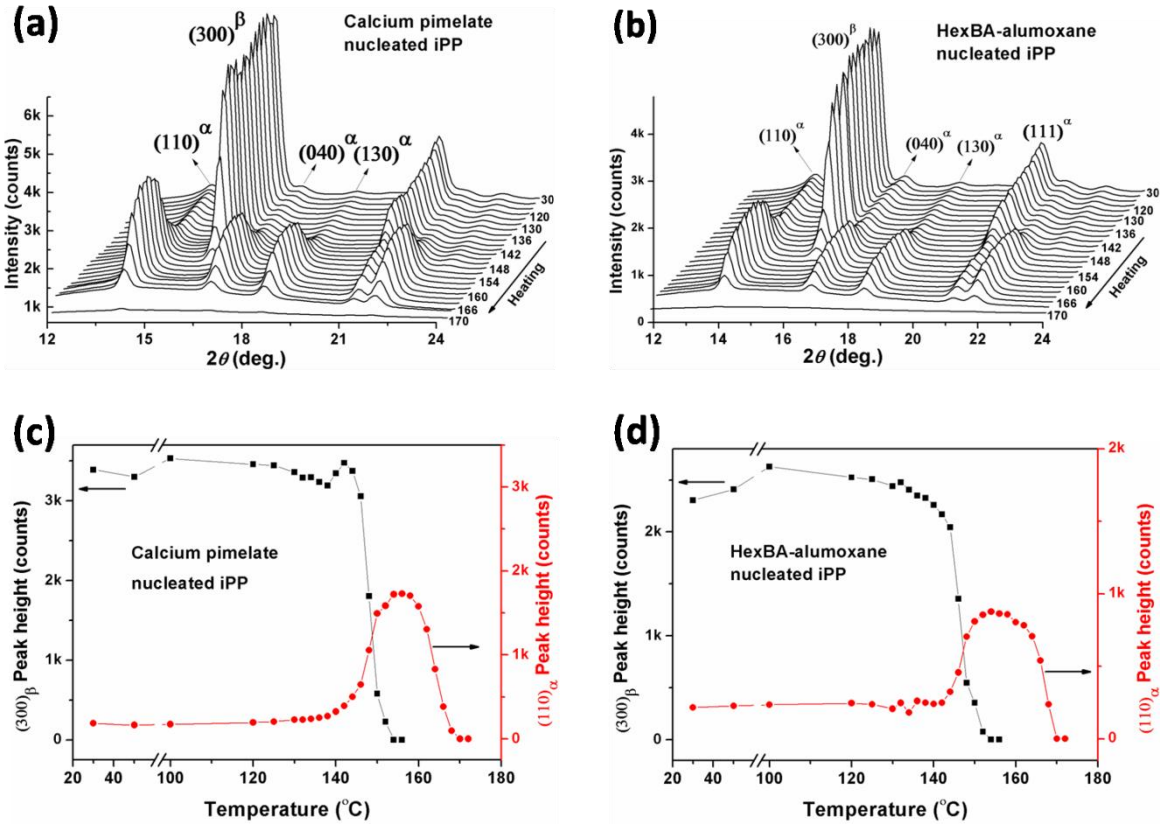

Figure 6.11: Behavior of WAXS patterns of (a) CaP and (b) HexBA-alumoxanes nucleated iPP on heating from room temperature to melting. The samples have been previously crystallized on cooling at 50 °C/min from 210 °C. The variation of height of the α- and the β-crystalline peak of iPP nucleated with (c) CaP and (d) HexBA-alumoxane on heating.

and the data extracted out from the patterns are shown in Figure 6.11. HTWAXS confirms the β- to the α-phase transition occurs via a melt recrystallization process as discussed by Lovinger et al.[5]

The lamellar morphology of the α- and the β-phases of iPP crystallized at wide temperature range has been evaluated using the SAXS analysis. To this end, the iPP samples have been nucleated with various types of α-nucleating agents having different nucleating efficiency, such as BA-alumoxane, PTBBA-alumoxane and DMDBS[6] and melt crystallized using DSC under varying cooling rates ranging from 1 °C/min to 50 °C/min (Table 6.1). For example, PTBBA-alumoxane, the most efficient nucleating agent crystallizes the sample at 140 °C when cooled at 1 °C/min. On the other hand,

non-nucleated sample crystallizes at 105 °C when cooled at 50 °C/min. Similarly, the *β*-phase samples obtained with CaP is melt crystallized at various cooling rates. The data points are limited for *β*-nucleation because only CaP is used to nucleate iPP. The samples are removed from DSC at room temperature and subjected to WAXS and SAXS experiments. Lorentz corrected SAXS patterns of the *α*- and the *β*- phase iPP samples crystallized at various temperatures are shown in Figures 6.12a and 6.12b. In general, the patterns show well defined first order peak at low q values and a discernible second order peak suggesting well defined lamellar structure. The SAXS patterns shows distinct differences between the *α*- and the *β*- phases. The first order peak position

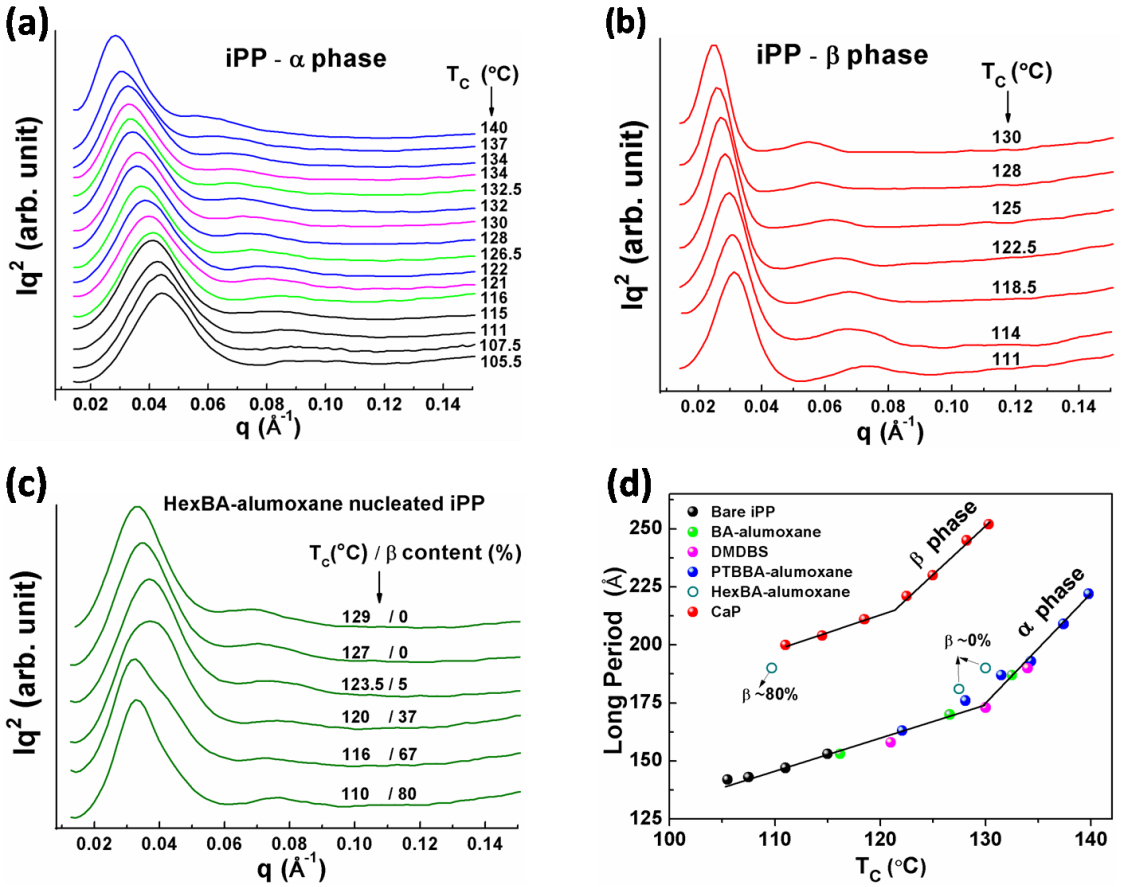

Figure 6.12. Lorentz corrected SAXS patterns of (a) *α*-phase of iPP nucleated with *α*-nucleating agents as indicated in Figure 6.12d, (b) *β*-phase of iPP nucleated with CaP and (c) HexBA-alumoxanes nucleated iPP samples crystallized under non-isothermal conditions. (d) The dependence of long period on crystallization temperature (T_C) for the *α*- and *β*- phases.

occurs at lower *q* value for the *β*-phase compared to the *α*-phase. Also, the second order peak is more well developed in the *β*- phase compared to the *α*-phase. The first and second order peaks shows considerable broadening in the case of the *α*-phase. This may be due the structural complication arising out of the cross-hatching phenomena, well documented in the case of the *α*-phase.[7,8] Nevertheless, the observance of well defined first and second order peaks in SAXS pattern indicates an overriding lamellar structure present in the *α*-phase and may be called apparent lamellar structure. Figure 6.12c shows the SAXS pattern of HexBA-alumoxane nucleated sample crystallized at various cooling rates and the peak appears to be more asymmetric compared to the *α*- and the *β*-nucleated samples. It may be recalled that HexBA-alumoxane nucleated sample gives both the *α*- and *β*-phases for lower cooling rates.

The SAXS profile of both the *α*- and the *β*-phase samples show that the peak position systematically shifts to lower q values with increasing T_C. The dependence of long period on the crystallization temperature (T_C) is shown in Figure 612d where the long period for both *α*- and *β*- phase linearly increases with increasing T_C. Most important point is that at a given crystallization temperature the *β*-phase shows significantly higher long period compared to that of the *α*- phase indicating substantial difference in the semi-crystalline morphologies. Also, these data clearly shows that nucleating agents control the nucleation but the temperature of crystallization controls the lamellar morphology. Another key observation is that the slope of the straight line changes at *ca.* 130 °C for *α*-phase and at *ca.* 121 °C for *β*-phase indicating the crystallization temperatures fall into two temperature ranges; low temperature (LT) range and high temperature (HT) range.

To understand the morphological differences between the *α*- and the *β*-phases, contributions of crystal lamellae thickness (*lc*) and amorphous layer thickness (*la*) to the long period have been calculated using a one-dimensional correlation analysis.[9-11] It must be kept in mind that in the case of the *α*-phase these values are apparent values only because the lamellar morphology developed during the crystallization is modified by the cross-hatching of the lamellae.[10]

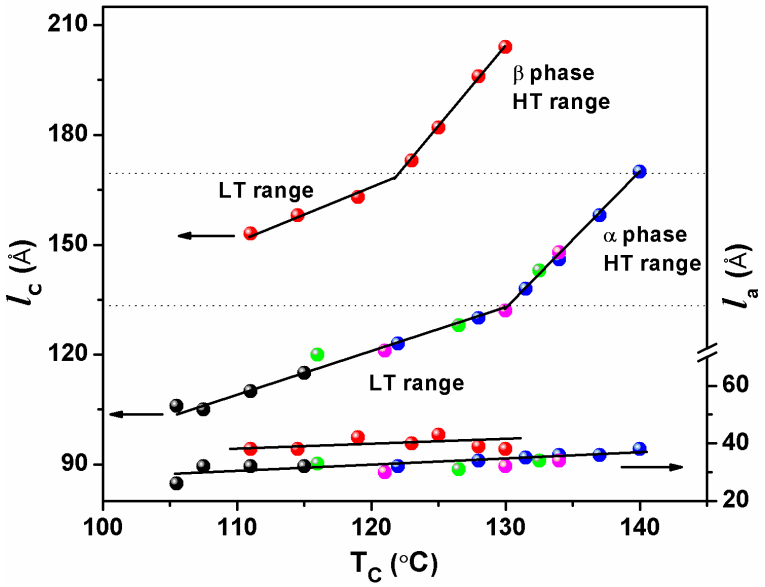

Figure 6.13: Variation of the crystal lamellar thickness (*lc*) and amorphous layer thickness (*la*) of the *α*- and the *β*- phases of iPP with the crystallization temperature (T_C). The color code is described in Figure 6.9d.

The dependence of crystal and amorphous phase thickness on the crystallization temperature is shown in Figure 6.13 revealing that the crystal lamellae thickness increases linearly with increasing the crystallization temperature. The *β*-phase crystal lamella is always larger than the *α*-phase and the difference between these increases with increasing crystallization temperature. However, the amorphous layer thickness shows a marginal increase over the temperature for both the *α*- and the *β*- phases. Another noticeable point is that the linear crystallinity calculated using long period and crystal lamellar thickness is very similar for the *α*- and the *β*- phases (Table 6.2). In Figure 6.13, the slope of the line in the graph changes at *ca.* 130 °C for the *α*- phase and at *ca.* 121 °C for the *β*-phase. The change in the slope is *ca.* 3 for both the phases. It is tempting to correlate the present data to the well known regime crystallization behavior of the polypropylene.[12,13] Regime crystallization behavior is always studied under isothermal crystallization mode and the regime changeover temperature is reported to be *ca.*137 °C for the *α*- phase.[9,12-14] Regime crystallization is also found for the *β*-phase and is *ca.*135 °C.[15] However, in the present case the crystallization has been performed under non isothermal mode and most of the cases the peak crystallization temperature is below 137 °C.

Table 6.2: Crystallization temperature (T_C), Long period (LP) from correlation function, crystal lamellae thickness (l_c), amorphous layer thickness (l_a), linear crystallinity (x_{cl}) and enthalpy of crystallization (ΔH_C) of the α- and the β- phases of iPP crystallized under controlled cooling rates (Table 6.1).

S. No.	T_C (°C)	LP (Å)	l_c (Å)	l_a (Å)	x_{CL} (%)	ΔH_C (J g^{-1})
***α*-phase**						
1.	105.5	132	106	26	80	95
2.	107.5	137	105	32	76	92
3.	111	142	110	32	77	97
4.	115	146	115	32	78	96
5.	116	153	120	33	78	82
6.	121	151	121	30	80	95
7.	122	155	123	32	79	100
8.	126.5	159	128	31	80	94
9.	128	164	130	34	79	100
10.	130	164	132	32	80	97
11.	132	173	138	35	79	100
12.	132.5	177	143	34	80	96
13.	134	182	146	36	80	98
14.	134	182	148	34	81	100
15.	137	194	158	36	81	99
16.	140	208	170	38	81	100
***β*-phase**						
1.	111	190	153	38	78	93
2.	114	196	158	38	78	87
3.	118.5	204	163	42	78	85
4.	122.5	213	173	40	78	87
5.	125	225	182	43	79	87
6.	128	235	196	39	79	91
7.	130	243	202	41	80	90

A careful inspection of the Figure 6.12d shows that the long period of the α-phase crystallized at HT range is equal to the long period of the β-phase crystallized in the LT range. Similar conclusion can be arrived based on the behavior of crystal lamellae thickness with crystallization temperature (Figure 6.13). Alternatively it may be said that the lamellar morphology of the β-phase crystallized in the LT is equivalent to the apparent lamellar morphology of the α-phase crystallized at HT range. Figure 6.14 schematically depicts the morphology in macro scale for the α- and the β- phases at high and low temperature ranges. However, in micro scale there could be variation in morphology within the crystal and amorphous lamellae between the α- and the β-phases. The difference in the micro morphology arises from the density difference between the α- and the β-crystals.[16] The amorphous phase also shows difference between the α- and the β- phases; the amorphous phase in the β-phase shows higher mobility than the α-phase.[17]

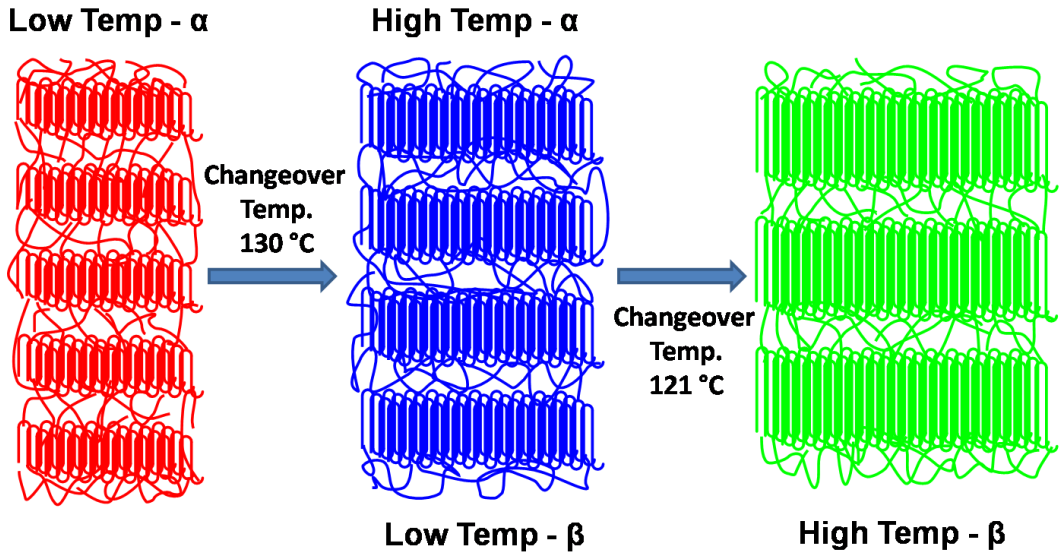

Figure 6.14: The macro scale morphology of the α- and the β-phases of iPP at different crystallization ranges. These cartoons are based on WAXS and SAXS data. In the case of α-phase, the cartoon depicted shows apparent morphology. The morphology developed during the primary crystallization will be modified by the cross hatching of the crystal lamellae during the secondary crystallization. Cross hatching is not reported for the β-phase.

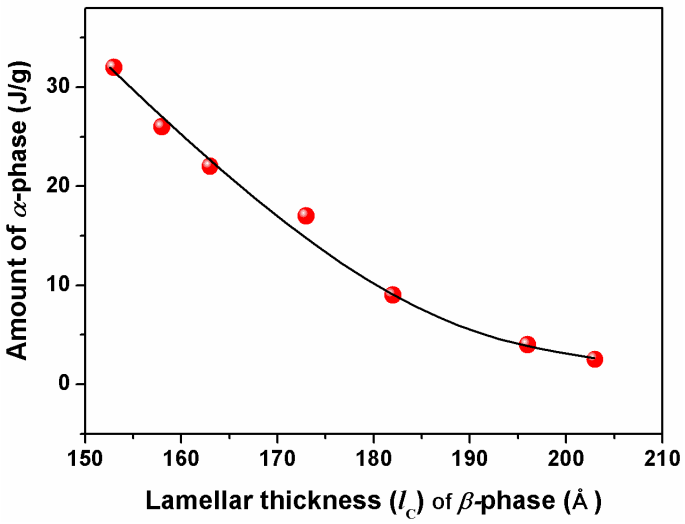

Figure 6.15: The variation of lamellar thickness of β-phase with the amount of α-phase formed via melt recrystallization upon heating at 10 °C/min. The values in the y-axis are the ΔHf of the recrystallized α-phase measured from the Figure 6.9a.

In an earlier section, Figure 6.9a showed the melting and recrystallization of the β-phase during heating. The data clearly show that the recrystallization of the β-phase into the α- phase depends on the crystallization temperature at which the β-phase is formed. Figure 6.15 shows the amount of material transformed into the α-phase during melt-recrystallization process with lamellar thickness of the β-phase. The amount of material transformed decreases with increasing lamellar thickness indicating the crystalline transition of the β- phase into α-phase during melting depends on the lamellar thickness. Even though literature references[18] indirectly attributed this effect, this is the first experimental data to prove it.

6.3 Conclusions

Alkyl substituted benzoate-alumoxanes act as dual nucleating agent and nucleates iPP into predominantly in the β-phase under specific conditions. Further, the selectivity of the β-phase nucleation can be controlled by melting and crystallization conditions. On the other hand, the CaP nucleated iPP always crystallizes in the β-phase irrespective of the crystallization conditions. At a given crystallization temperature the β-phase shows a significantly higher long period compared to that of α-phase indicating substantial difference in the semi-crystalline morphologies. Both the α- and the β-phases show two

distinct crystallization temperature ranges when crystallized under non-isothermal mode. Further, this study reveals the *β*-phase lamellar morphology controls the *β*- to the *α*- phase transition and the amount of material transforms correlates well with the lamellar thickness of the *β*-phase. This study also proves that the morphology of the *α*-phase or the *β*-phase mainly depends on the T_C and not on the nature of the nucleating agents. The improved impact strength shown by the *β*-phase may be traced to macro and micro morphological differences between the *α*- and the *β*- phases. Also, the difference in morphology leads to lower melting temperature of the *β*-phase compared to that of *α*-phase even though the crystal lamellae thickness of the *β*-phase is always higher than that of the *α*-phase crystal lamellae. The higher mobility of the amorphous phase[17] in the *β*-phase may give rise to higher fold surface interfacial energy and consequently lower melting temperature.

6.4 References

1) L. Kalita, R. Pothiraja, V. Saraf, M. Walawalkar, R. Butcher, R. Murugavel, *J. Organomet. Chem.* 2011, **696**, 3155.
2) W. Bury, E. Chwojnowska, I. Justyniak, J. Lewiński, A. Affek, E. Zygadło-Monikowska, J. Bąk, and Z. Florjańczyk, *Inorg. Chem.,* 2012, **51**, 737.
3) P. Jacoby, B. Bersted, W. Kissel, C. Smith, *J. Polym. Sci. Part B: Polym. Phys.*, 1986, **24**, 461.
4) J. Varga, A. Menyhárd, *Macromolecules,* 2007, **40**, 2422.
5) A. Lovinger, J. Chua, C. Gryte, *J. Polym. Sci.: Polym. Phys. Ed.,* 1977, **15**, 641.
6) M. Kristiansen, M. Werner, T. Tervoort, P. Smith, M. Blomenhofer, H.-W. Schmidt, *Macromolecule,s* 2003, **36**, 5150.
7) J. Janimak, S. Cheng, P. Giusti, E. Hsieh, *Macromolecules,* 1991, **24**, 2253.
8) T. Albrecht, G. Strobl, *Macromolecules,* 1995, **28**, 5267.
9) B. Hsiao, R. Verma, *J. Synchrotron Rad.,* 1998, **5**, 23.
10) G. Strobl, M. Schneider, *J. Polym. Sci. Polym. Phys. Ed.,* 1980, **18**, 1343.
11) C. Cruz, N. Stribeck, H. Zachmann, F. Calleja, *Macromolecules,* 1991, **24**, 5980.
12) E. Clark, J. Hoffman, *Macromolecules,* 1984, **17**, 878.

13) A. Celli, E. Zanotto, I. Avramov, *J. Macromol. Sci., Part B*, 2003, **42**, 387.

14) S. Cheng, J. Janimak, A. Zhang, HN. Cheng, *Macromolecules*, 1990, **23**, 298.

15) G. Shi, X. Zhang, Z. Qiu, *Die Makromol. Chem.*, 1992, **193**, 583.

16) J. Karger-Kocsis, *Poly. Eng. & Sci.*, 1996, **36**, 203.

17) O. Policianová, J. Hodan, J. Brus, J. Kotek, *Polymer* 2015, **60**, 107.

18) A. Celli, A. Fichera, C. Marega, A. Marigo, G. Paganetto, R. Zannetti, *Eur. Polym. J.* 1993, **29**, 1037.

CHAPTER 7

Effect of carboxylate-alumoxane on syndiotactic polystyrene (sPS) crystallization and morphology

7.1 Introduction

Syndiotactic polystyrene (sPS) is an engineering thermoplastic and the chemical structure is analogues to iPP. The major difference is the methyl pendent group is replaced by phenyl group. It is of interest to study the nucleating efficiency of carboxylate-alumoxane in nucleating sPS. The sPS exhibits various polymorphic forms depending on the crystallization conditions.[1-3] Polymer chain takes all trans-planar-zigzag (T4) conformation when crystallized from the melt and depending on the thermal conditions sPS crystallizes in the α- and the β-phases.[4] While solvent crystallized sPS shows T_2G_2 helical conformation and depending on the solvent type, it crystallizes in the γ, δ and ε forms.[5] Controlling the polymorphs by melt crystallization process attracts much attention because melt processing is the most favoured industrial process.

The sPS crystallizes well below the melting temperature, i.e., at larger undercooling ($\Delta T=T_m^0-T_C$). The final lamellar morphology and the metastability of the specific polymorphic composition of the polymer are determined by ΔT.[6,7] NAs have been effectively used in isotactic polypropylene (iPP) to speed up the processing by reducing the cycle time.[8] Unlike iPP, the nucleating agents for sPS are rather limited mainly because of its higher processing temperature (*ca.* 300 °C) where most of the nucleating agents degrade. In this context, thermally stable carbon based materials, layered double hydroxides and silicates have been explored as a filler materials and their nucleation effect has been discussed.[9-13] Papageorgiou et al. studied the influence of nano-fillers viz., multi-wall carbon nanotubes, silver nanoparticles, nanodiamonds and copper-nanofibers on the crystallization and mechanical properties of sPS. Among these nano-fillers multi-walled carbon nanotubes (MWCNTs) was the most efficient nucleating agent and crystallized sPS predominantly in the β-phase.[14] An organic modification to the additive enhances the dispersibility and alters the subsequent nucleation characteristics. For example, the SWNTs attached with polystyrene has been shown to improve the nucleation efficiency compared to that of the unmodified SWNTs .[15] Further, organically modified clays altered the crystallization characteristics of sPS compared to that of the unmodified clay.[9] Similarly, organo modified layered silicates and double hydroxides has been shown to accelerate the overall nonisothermal crystallization process of sPS.[16] In most of the above said cases the amount of additives

added is *ca.* 2-3% and the focus is on the nanocomposite properties. Highly efficient nucleating agents based on carboxylate-alumoxanes and aluminium dicarboxylate MOF have been developed for iPP and discussed in detail in the preceding chapters. These are coordination complexes in which aluminum centers are bridged by carboxylate groups along with oxo/hydroxo ligands. Carboxylate-alumoxane based on *p*-*t*-butylbenzoic acid showed thermal stability above 300 °C and are suitable candidate for sPS nucleation. In the present chapter the carboxylate-alumoxane as an efficient nucleating agent for sPS along with possible mechanistic explanation for the nucleation is presented. Further, the self-nucleation studies based on pure α- and the β-phases were conducted in order to measure the nucleation efficiency of PTBBA-alumoxane. The self-nucleating ability of the α- and the β-nuclei along with their role in controlling the final crystalline morphology of sPS were also studied using DSC and WAXS analysis.

7.2 Results and Discussion

The crystallization behaviour of sPS without nucleating agents is studied using DSC and discussed first. The DSC thermogram of amorphous sPS on heating to melt and subsequent cooling from the melt at 10 °C/min is shown in Figure 7.1. The amorphous sPS shows three thermal events on heating from RT to 300 °C. The glass transition temperature of the sPS is seen at 98 °C and then the cold crystallization at 148 °C. On further heating, the crystallized fraction melts at 265 °C. On cooling from 300 °C, the sample shows the melt crystallization at 231°C and the T_g at 93 °C.

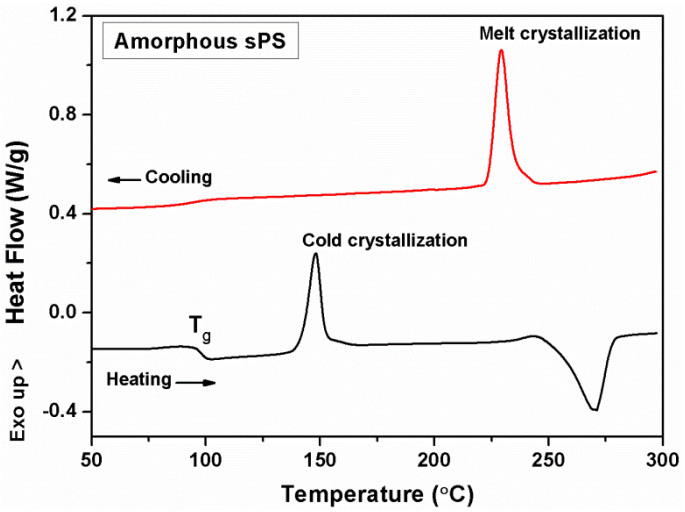

Figure 7.1: DSC thermogram of amorphous sPS on heating and subsequent cooling.

On the addition of *p*-*t*-butylbenzoate (PTBBA)-alumoxane, the crystallization behaviour of the sPS is modified. sPS samples were quenched at low temperature (0 °C) in the presence of PTBBA-alumoxane at different concentrations and the corresponding DSC heating and cooling thermogram is shown in Figure 7.2a and b respectively. Figure 7.2a shows that the cold crystallization peak shifted to lower temperature on the addition of PTBBA-alumoxane compared to pure sPS while melt crystallization peak shifted to higher temperature (Figure 7.2b). In addition, both the cold and the melt crystallization peak shows systematic change with increasing the PTBBA-alumoxane concentration. The large decrease in the cold T_C and the increase in the melt T_C clearly indicate that the PTBBA-alumoxane acts as an efficient nucleating agent for sPS. The dependence of cold T_C and the melt T_C on the concentration of PTBBA-alumoxane is shown in Figure 7.3. PTBBA-alumoxane at *ca.* 1 wt% concentration increases the melt T_C of *ca.* 19 °C higher than pure sPS and above this concentration it shows only marginal increase in the T_C. It is to be noted that the cold crystallization temperature follows similar trend, but in the opposite direction with the PTBBA-alumoxane concentration. The glass transition temperature retains at the same position indicating PTBBA-alumoxane has no influence on the glass transition temperature although it modifies the cold crystallization temperature.

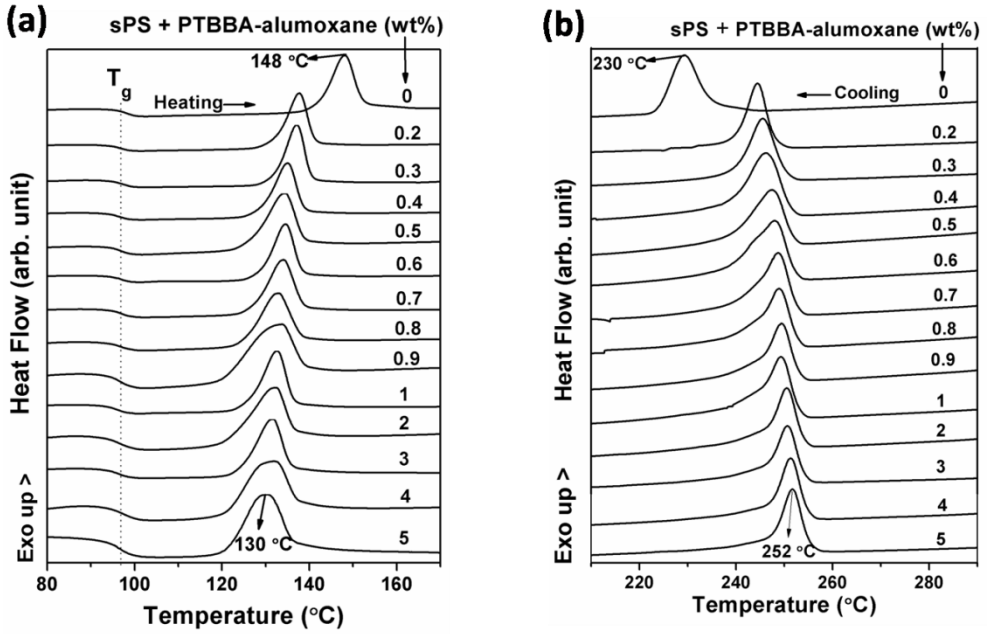

Figure 7.2: DSC heating (a) and cooling (b) thermograms of amorphous sPS incorporated with various concentration of PTBBA-alumoxane.

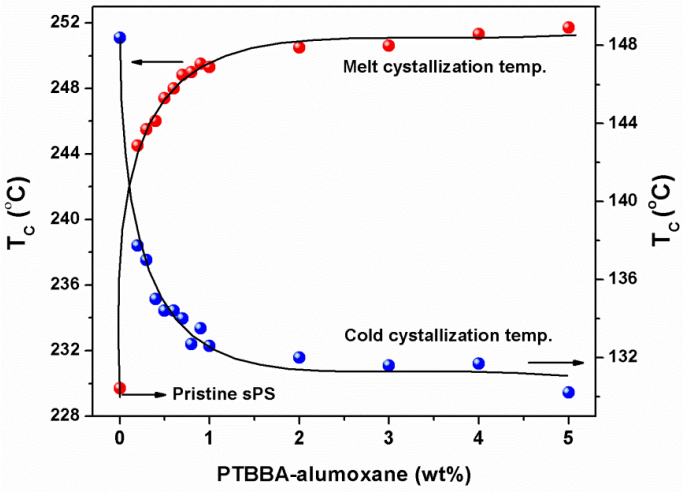

Figure 7.3: Variations of PTBBA-alumoxane concentration with the crystallization temperature (T_C) of sPS.

The carboxylate-alumoxane and its structural correlation to the nucleation efficiency of isotactic polypropylene (iPP) have been discussed in chapter 3. The key molecular structure of the carboxylate-alumoxane is a bicyclic ring structure consists of aluminium centers bridged by two carboxylate groups and the oxo ligand. The carboxylate-alumoxane core with aromatic moiety attached to carboxylate ligands gives butterfly-like conformation and has been speculated to interact with iPP and induce the crystallization. As with iPP, the strong nucleation ability of PTBBA-alumoxane suggests that the butterfly-like conformation facilitating effective interaction with the sPS probably through edge-to-face phenyl-phenyl interactions and/or C-H....π interactions.

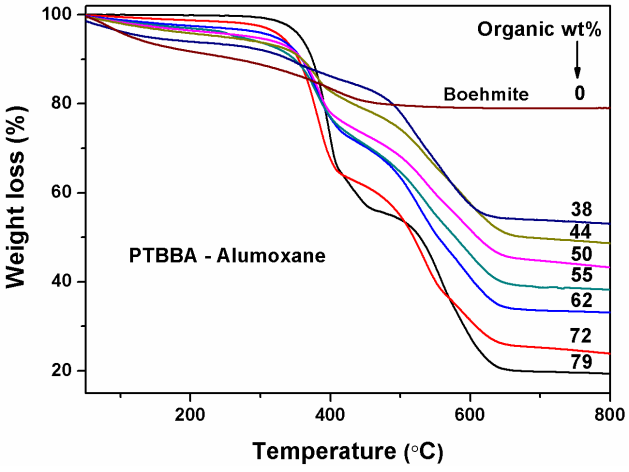

Figure 7.4: Thermogravimetric analysis (TGA) of PTBBA-alumoxane having various amount of organic content.

In order to study the effect of organic (PTBBA) content in the PTBBA-alumoxane on the sPS nucleation, the PTBBA-alumoxane having various amount of PTBBA content was prepared by varying the Al/PTBBA molar ratio during the preparation of PTBBA-alumoxane. The amount of organic (PTBBA) content in the PTBBA-alumoxane was measured from the thermogravimetric analysis (Figure 7.4). The organic content increases with increasing PTBBA molar content as evident from the systematic increase weight loss in the TGA. The dependence of PTBBA content in the alumoxane on T_C is shown in Figure 7.5 and indicates that both the cold and melt crystallization temperature show more or less linear dependency with the amount of PTBBA content in the alumoxane.

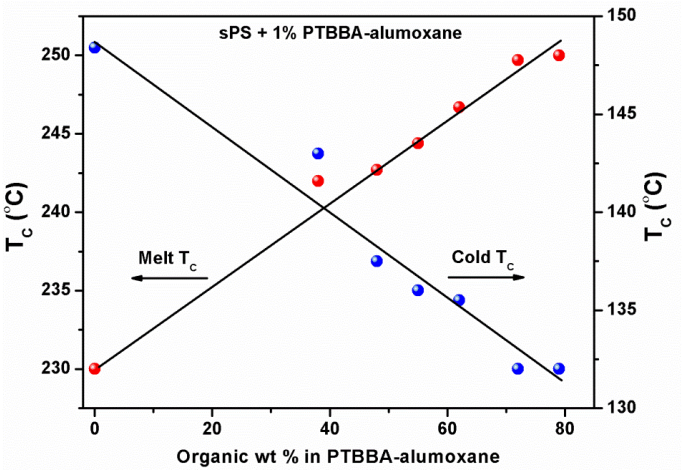

Figure 7.5: Variations of melt and cold crystallization temperature (T_C) with organic wt% in the PTBBA-alumoxane.

To re-establish the role of the orientational conformation of the PTBBA around the metal centre on the sPS nucleation, studies have been made with zirconium PTBBA complex where the orientation of PTBBA would be different from that of PTBBA-alumoxane due to difference in the ligation of carboxylate group. Nnucleation efficiency studies show that Zr-PTBBA complex does not nucleate sPS although PTBBA is very effective in nucleating sPS when it is coordinated aluminium. This suggests that PTBBA alone is not responsible for the effective nucleation of sPS but the aromatic cleft from the butterfly-like conformation plays a vital role in facilitating the interaction and subsequent nucleation of sPS. These results are in agreement with the iPP crystallization results discussed in the previous chapters.

The nucleation effect of aluminium succinate MOF has also been studied, which shows butterfly-like structure as that of PTBBA-alumoxane due similar coordination linkages around aluminium centres in the framework structure. In addition, 3D-structure of Al-succinate MOF shows a linear channel on the surface along a-axis. Due to highly interconnected structure with strong bridging carboxylate and hydroxo coordination towards Al centres, these MOF shows higher thermal stability (>300 °C) above the processing temperature of sPS. Nucleation efficiency studies show that aluminium succinate MOFs does not nucleate sPS although it has been shown to nucleate iPP very efficiently. The poor nucleation ability is attributed to the poor interaction between alkyl groups of the butterfly channel and the sPS due to the polarity difference. This suggests that the butterfly structure is not only a prerequisite but favourable interaction is also essential for the effective nucleation of sPS.

The crystalline morphology of sPS nucleated with various concentrations of PTBBA-alumoxane is studied using WAXS analysis. The nucleated sPS samples are melt crystallized from 300 °C at 10 °C/min cooling rate using DSC. Subsequently, the samples are removed from the DSC pan at room temperature and subjected to WAXS analysis. The WAXS pattern of sPS nucleated with various concentrations of PTBBA-alumoxane along with the pure sPS processed under identical conditions are shown in Figure 7.6a. The WAXS pattern of the pure sPS shows peaks corresponding to β-phase

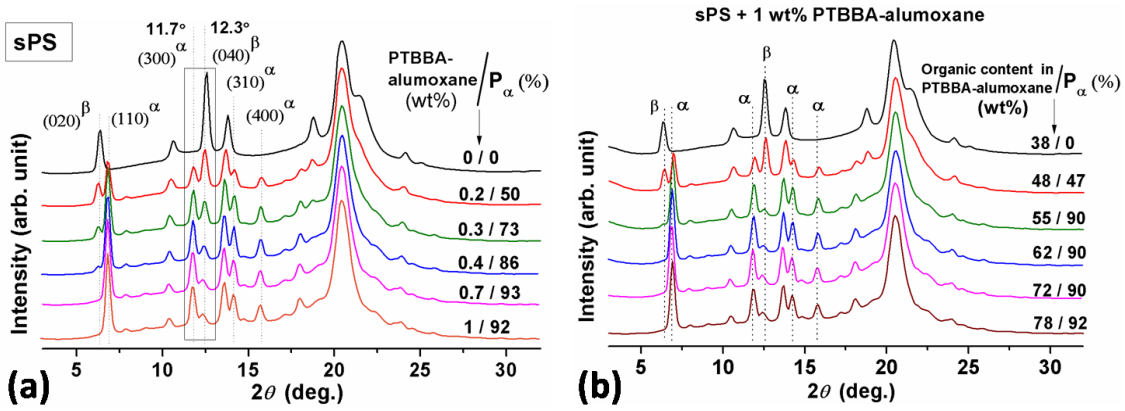

Figure 7.6: (a) WAXS patterns of sPS containing various concentrations of PTBBA-alumoxane and (b) sPS containing 1 wt% of PTBBA-alumoxane having different amount of organic content. The nucleated samples are non-isothermally crystallized from the melt 310 °C at 10 °C/min.

only while sPS nucleated with PTBBA-alumoxane shows peaks corresponding to both the α- and the β-phases. Noticeably, with increasing the PTBBA-alumoxane concentrations, the intensity of α-phase peaks increases and concomitantly the intensity of β-phase peaks decreases. The variation of the α-phase content with various concentrations of PTBBA-alumoxane is also shown in Figure 7.6a which clearly shows that the amount of α-phase increases with increasing PTBBA-alumoxane concentration. For instance, 0.2%, 0.3% and 0.4% concentrations show 50%, 72% and 86% of the α-phase content respectively. Further increasing the PTBBA-alumoxane concentration the α-phase reaches a maximum value of 92% at 1% concentration and then remains unchanged. This indicates that the PTBBA-alumoxane nucleates sPS specifically in the α-phase.

Similarly, the influence of PTBBA-alumoxane having various % of organic content on the crystalline phase of sPS was studied using WAXS analysis and is shown in Figure 7.6b. The PTBBA-alumoxane with 38% organic content shows the β-phase as that of pure sPS. However, with increasing organic wt% in the PTBBA-alumoxane, the β-phase peak intensity decreases with concomitant increase in the α-phase peak intensity. This suggests that the PTBBA moiety in the alumoxane is responsible for the observed α-phase in the nucleated sPS.

In order to establish the nucleation efficiency of PTBBA-alumoxane, self-nucleation experiments are performed following the method outlined by Fillon et al. In this experiment, the pure sPS sample is non-isothermally crystallized from different end melting temperatures (T_{max}). The T_{max} becomes self-seeding temperature (T_S) when it is just above the melting temperature of the polymer. The self-nucleation studies are done on sPS starting with the pure α- and the β-phases because these phases may have different self-nucleation characteristics. The first set of self-nucleation studies are carried out with pure β-phase obtained by melt crystallization of sPS on cooling from 310 °C at 10 °C/min. In Figure 7.7a, the top curve shows the melting endotherm of the β-phase. The sample is again recrystallized on cooling after reaching a temperature Tmax. In these experiments the maximum Tmax is 310 ^{o}C, the minimum Tmax temperature is 268.5 ^{o}C, which very close to the peak melting temperature of the β-phase. The heat of crystallization (ΔH_C) remains nearly constant in this temperature

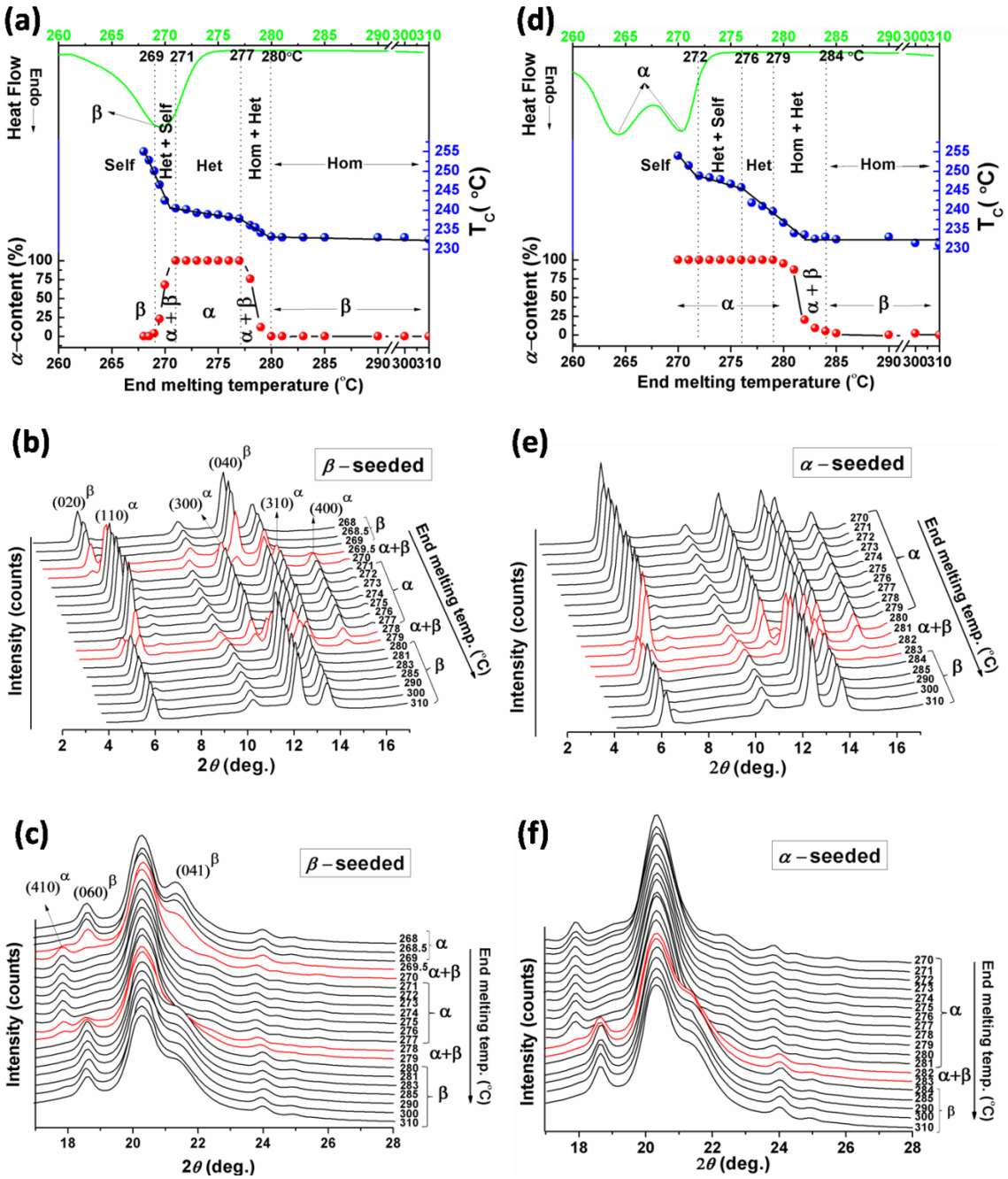

Figure 7.7: (a) top, DSC melting endotherm of β-phase; middle and bottom, The variation of T_C and the α-content with the end melting temperature (T_{max}) respectively. (b) and (c) The behaviour of WAXS pattern of β-sPS after non-isothermal crystallization from different T_{max}. (d) top, DSC melting endotherm of α-phase; middle and bottom, The dependence of T_C and the α-content on T_{max} respectively. (e) and (f) WAXS pattern of α-sPS after non-isothermal crystallization from different T_{max}. Please note that the 2θ=20.3° peak intensity is normalized to equal intensity which appears for both the α-and the β-phases.

range showing that the *β*-phase melted fully. However, when the Tmax is lower than 268.5 ^{o}C partial melting of the *β*-phase happens and subsequently lower heat of crystallization results on crystallization during cooling. The dependence of crystallization temperature (T_C) on T_{max} is shown in the middle part of Figure 7.7a. The variation of T_C with the T_{max} clearly shows different Tmax temperature ranges based on the changes in T_C and may be due to different nucleation mechanisms. More importantly, the crystalline phase of the crystallized samples highly depends on the Tmax range. In the temperature range 280 to 310 °C the T_C remains constant at *ca.* 233 ^{o}C. The constant T_C indicates that the homogeneous nucleation controls the crystallization. This would mean that when the melt temperature is above 280 ^{o}C, all the crystallites are fully melted and no remnants of the crystals are left in the melt which can act as heterogeneous nucleating site on further crystallization. In this Tmax range the samples crystallized predominantly in the *β*-phase. The bottom curve in the Figure 7.7a shows the variation *α*-content with Tmax. It can be seen in the figure the amount of *α*-phase is very close to zero and the *β*-phase is dominating in this Tmax range. When the Tmax is lowered below 280 ^{o}C the T_C increases rapidly with decreasing Tmax. Also, the *β*-phase starts to decrease and concomitantly the *α*-phase increases. The increase in the T_C value shows that the mode of crystallization changes from homogenous to heterogeneous nucleation. Obviously the remnants are left when the crystallites melt and they provide heterogeneous nucleation sites for crystallization. At Tmax is *ca.* 277 ^{o}C, the samples fully crystallizes in the *α*-phases, even though the crystalline remnants are in the *β*-phase, they induce crystallization in the *α*-phase. A further decrease in the Tmax up to 271 ^{o}C shows marginal increases in Tc and sample crystallizes in the *α*-phase only. Hence, in the temperature range 277 to 271 ^{o}C the sample is heterogeneously nucleated. In the Tmax region below 271 ^{o}C, the Tc again increases rapidly and again the phase reverses to *β*-phase. Since the Tmax overlaps with the final stage of the melting, apart from the remanants of the crystallites, the melt will be having strong memory of the *β*-phase. Hence, the sample quickly recrystallizes into *β*-phase. The phase reversal with varying Tmax is very clearly seen in the WAXS pattern shown Figure 7.7b. The diffraction peaks at (2*θ*) 6.2^{o}, 12.3^{o}, 18.6^{o}, 20.2^{o}, and 21.3^{o} are characteristics of the *β*-phase. The characteristic peaks for *α*-phase appear at (2*θ*) 6.7^{o}, 11.7^{o}, 14.0^{o}, 15.6^{o} and 20.3^{o}. The x-ray pattern shows that the sPS crystallizes in the *β*-

phase when the T_{max} is above 280 °C. Below 280 °C, the *β*-phase peaks intensity decreases with concomitant increase in the *α*-phase which reaches to 100% when the T_{max} range between 277 – 271 °C. Further decrease in the T_{max} again reverse in to *β*-phase as evident from the decreasing the *α*-phase peaks intensity with the concomitant appearance of the *β*-phase.

The second set of self-nucleation studies are carried out with pure *α*-phase obtained by melt crystallizing the *β*-sPS from Tmax 275 °C at 10 °C/min as shown in the above studies. The melting endotherm of *α*-phase shows double melting and is shown in Figure 7.7d (top curve). The results are very similar to the *β*-seeded sample discussed in the preceding section. Nevertheless, there are significant variations also. In this case the phase reversal, *β*- to *α*-phase occurs at 284 °C and the sample always crystallises in the *α*-phase on further lowering Tmax. Also, the Tc values are significantly higher than the *β*-seeded sample for Tmax below 284°C. This data clearly show that the remnants of the *α*-crystallites helps the sample to nucleate faster compared to the *β*-remnants samples.

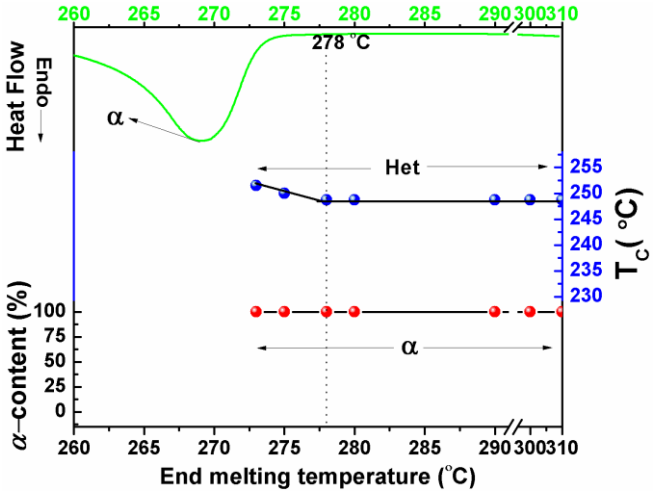

Figure 7.8: (a) top, DSC melting endotherm of *α*-phase nucleated by PTBBA-alumoxane; middle, The variation of T_C with the end melting temperature (T_{max}); bottom, The dependence of *α*-content on T_{max}.

In contrast to pure *α*- or *β*-phase sPS, the PTBBA-alumoxane nucleated *α*-sPS sample shows single melting endotherm as shown in top part of Figure 7.8. Also, nucleated sample always crystallizes at higher T_C independent of Tmax and increases slightly when the Tmax is 275 °C. Similarly, the nucleated sample always crystallizes in the *α*-

phase irrespective of the Tmax. This indicates that the PTBBA-alumoxane fully controls the crystallization process. As a nucleating agent it is more effective than the self seeds of sPS crystallites. Further, PTBBA-alumoxane shows the nucleation efficiency above 90% in sPS and is 70% in the iPP. The higher nucleation efficiency with sPS suggests that the PTBBA-alumoxane shows better interaction with sPS compare to that of iPP. Thus, the present study strongly suggests that interaction between the NAs polymer is crucial for an efficient nucleation.

7.3 References

(1) G. Guerra, V. Vitagliano, C. Rosa, V. Petraccone, P. Corradini, *Macromolecules*, 1990, **23**, 1539.

(2) C. Rosa, O. Ballesteros, M. Gennaro, F. Auriemma, *Polymer*, 2003, **44**, 1861.

(3) A. Sorrentino, R. Pantani, G. Titomanlio, *J. Polym. Sci. Part B: Polym. Phys.*, 2010, **48**, 1757.

(4) E. M. Woo, Y. S. Sun, C.-P. Yang, *Prog. Polym. Sci.*, 2001, **26**, 945.

(5) B. Gowd, K. Tashiro, Ramesh, *Prog. Polym. Sci.*, 2009, **34**, 280.

(6) Wunderlich, B. *Macromolecular Physics, Crystal Melting*; Academic Press: New York, 1980; Vol. III.

(7) R.-M. Ho, C.-P. Lin, H.-Y. Tsai, E.-M. Woo, *Macromolecules*, 2000, **33**, 6517.

(8) H. Zweifel, *Plastics Additives Handbook*, 5th ed.; Hanser Publications: Munich, 2001, p 952.

(9) C. Tseng, H. Lee, F. Chang, *J. Polym. Sci. Part B: Polym. Phys.*, 2001, **39**, 2097.

(10) C. Tseng, S. Wu, J. Wu, F. Chang, *J. Appl. Polym. Sci.*, 2002, **86**, 2492.

(11) A. Sorrentino, L. Vertuccio, V. Vittoria, *Express Polym. Lett.*, 2010, **4**, 339.

(12) S. Kumar, T. Rath, R. N. Mahaling, C. K. Das, *Compos. Part A: Appl. Sci. Manuf.*, 2007, **38**, 1304.

(13) C.-L. Huang, C. Wang, *Eur. Polym. J.*, 2011, **47**, 2087.

(14) G. Z. Papageorgiou, D. S. Achilias, N. P. Nianias, P. Trikalitis, D. N. Bikiaris *Thermochim. Acta*, 2013, **565**, 82.

(15) H. Xiong, Y. Gao, H. M. Li, *Express Polym. Lett.*, 2007, **1**, 416.

(16) F.-A. He, L.-M. Zhang, F. Yang, L.-S. Chen, Q. Wu, *J. Polym. Res.*, 2006, **13**, 483.

CHAPTER 8

Summary and Conclusions

8.1 Summary

The key findings and conclusions of the present thesis are summarized below:-

Carboxylate-alumoxanes synthesized and used as nucleating agent for iPP. The structures of the NAs are characterized using MALDI–TOF mass spectrometry (MS) and FT-IR spectroscopy analyses. The key molecular feature of carboxylate-alumoxanes is the bicyclic ring structure having aluminum centers linked with two carboxylate groups and the oxo ligand. The carboxylate-alumoxane with butterfly-like conformation correlates well with the nucleation characteristics of iPP and, for the first time, the impact of a thermally induced, crystalline transition of carboxylate-alumoxanes, which alters neither the structural conformation nor the nucleation efficiency of the transformed material, is demonstrated. Further, the butterfly-like structure has been subtly disturbed by appropriately choosing carboxylic acid in order to confirm its profound influence in the nucleation of iPP. The structure of *p*-*t*-butylbenzoate (PTBBA)-galloxane is isomorphic with PTBBA-alumoxane and exhibits similar crystalline transition behaviour and nucleation efficiency as that of PTBBA-alumoxane supporting the butterfly-like structure in controlling nucleation of iPP.

Preparation of carboxylate-alumoxane using dicarboxylic acids give rise to metal organic framework (MOF) which exhibit a unique butterfly-like structure similar to that of carboxylate-alumoxanes due to the similar ligation around Al centers and correlates well with the nucleation characteristics of iPP. A subtle change in the structure of ligand backbone (fumarate/ succinate) does not alter the framework, nevertheless impacts the hydrophilic/hydrophobic character of the network and its subsequent nucleation characteristics. This suggests that nucleating agent should facilitate favourable interaction with hydrophobic iPP for efficient nucleation. Further, a systematic variation of the alkyl chain length in the Al-dicarboxylate does not change the nucleation efficiency considerably, even though it increases the distance between the octahedral alumina chains in the metal-organic framework, suggesting that the butterfly-like structure present in the framework is a key aspect for nucleation. Further, the significance of the orientational conformation of the dicarboxylate around the metal centre for the nucleation is confirmed by the poor nucleation efficiency of chromium

and zirconium suberates MOF where the orientation of suberate would be different from that of aluminium suberate due to difference in the ligation of carboxylate group.

Isotactic polypropylene exhibits various polymorphs depending on the experimental conditions. Among various crystalline modifications, the *β*-phase attracts attention as much as that of the *α*-phase. The *β*-phase exhibits higher ductility and impact strength compared to the *α*-phase. The iPP can be crystallized in the *β*-phase by *β*-selective nucleating agents. Carboxylate-alumoxane derived from *p*-*n*-alkylbenzoic acids, where length of the *n*-alkyl group varies from 2-8 carbon atoms, exhibits dual nucleating ability and nucleates isotactic polypropylene (iPP) into predominantly in the *β*-phase under specific conditions. The selectivity of the *β*-phase nucleation depends on the concentration of the nucleating agent, end melting temperature and cooling rate. The *β*-phase obtained from *p*-*n*-alkylbenzoate-alumoxanes is compared with the *β*-phase obtained from calcium pimelate (CaP), an efficient *β*-phase selective nucleating agent, using the results from DSC, WAXS and SAXS analysis. The lamellar morphology of iPP nucleated with different nucleating agents crystallized at different crystallization temperatures (T_C) under controlled non-isothermal conditions are evaluated using SAXS analysis. The long period increases with increasing crystallization temperature and the long period of the *β*-phase is always larger than that of the *α*-phase for a given crystallization temperature. Furthermore, the variation of long period with crystallization temperature clearly brings out two crystallization temperature ranges; the low temperature range and the high temperature range. The one-dimensional correlation analysis of the *β*-phase shows that the thickness of the crystal lamellae (*l*c) increases with T_C and exhibits the low and high crystallization temperature ranges. The morphological difference between the *α*- and the *β*-phases are discussed and attributed to the differences in the impact properties and the melting temperature.

The influence of carboxylate-alumoxane nano particles on the crystallization and morphology of syndiotactic polystyrene (sPS) has been studied to understand the efficacy of these particles in the nucleation of sPS. Syndiotactic polystyrene is a polyolefin, analogous to iPP, having pendent phenyl groups along the polymer backbone. Nucleation efficiency studies show that the PTBBA-alumoxane is a highly efficient nucleating agent for sPS and nucleates predominantly in the *α*-phase as revealed by WAXS analysis. The poor nucleating ability of zirconium PTBBA complex

signifies the critical role of the orientational conformation of PTBBA around metal centre in the nucleation of sPS. Aluminium succinate MOF shows coordination linkages around aluminium similar to PTBBA-alumoxane and shows higher thermal stability above 300 °C but exhibits poor nucleation efficiency. This is attributed to poor interaction of sPS with alkyl groups of MOF due to difference in the polarity. The self nucleating ability of the α- and the β-crystals was evaluated by self-seeding experiments. For both the α- and the β-seeded sPS, the T_C increase with decreasing T_{max} as expected. However, α-seeded sPS always crystallizes at higher temperature compared to β-seeded sPS for a given T_{max}. Also, the dependence of T_C on T_{max} shows different temperature ranges which is attributed due to homogeneous, heterogeneous and self nucleation mechanisms. Further, crystalline morphology of the sPS non-isothermally crystallized from different T_{max} are analysed using WAXS analysis. Interestingly, the α-phase is formed from the β-seeded sPS when the T_{max} range is between 277 to 271 °C. This suggests that either the β-nuclei acts itself as heterogeneous α-nucleator or the β-nuclei transforms in to α nuclei and subsequently crystallizes in to the α-phase at this temperature range. The self-nucleation studies based on pure α- and the β-crystals suggest that under non isothermal conditions, the end melting temperature controls the final crystalline form not the crystallization temperature.

The present results thus provides valuable pathways for developing new nucleating agents based on carboxylate-alumoxanes and Al-dicarboxylate MOFs with appropriate selection and orientation of the organic linkers around the metal centre.

8.2 Conclusions

The major conclusions arising out of the present work are given below.

Carboxylate-alumoxanes act as efficient nucleating agents for isotactic polypropylene (iPP). The molecular conformation of carboxylate-alumoxanes has been correlated well with the nucleation efficiency in iPP. Apparently, the butterfly-like structure from the bridging carboxylate coordination along with oxo bridging holds the key for controlling the nucleation of this class of polymers. Like sorbitol derivatives, benzenetrisamides and organic phosphates, carboxylate-alumoxane also provide alternate platform to

develop efficient nucleating agents by choosing appropriate carboxylic acids.

Metal organic framework (MOFs) based on aluminium dicarboxylate also provide an efficient nucleating site for the iPP nucleation. Nucleating ability is attributed due to the interaction of iPP with butterfly-like structure of MOF similar to the carboxylate-alumoxane. The variation of the alkyl chain length between the octahedral alumina chains in the MOF does not alter the nucleation efficiency considerably, suggesting that the butterfly-like structure present in the MOFs holds the key for controlling the nucleation. The butterfly-like conformation remains unaltered by minor structural variation in the ligand back bone (fumarate/succinate) despite changing the hydrophilic/hydrophobic interaction and subsequent nucleation characteristics. This suggests that the butterfly structure is not only a prerequisite but favourable interaction is also essential for the efficient nucleation. Further, the poor nucleation of Cr-SubA and Zr-SubA as compared to Al-SubA signifies the critical role played by the orientational conformation of the ligand around the metal centre in facilitating the interaction and the subsequent nucleation of iPP.

Alkyl substituted benzoate-alumoxanes act as dual nucleating agent and nucleates iPP into predominantly in the β-phase under specific processing conditions. Further, the selectivity of the β-phase nucleation can be controlled by melting and crystallization conditions. On the other hand, the CaP nucleated iPP always crystallizes in the β-phase irrespective of the crystallization conditions. Structure and morphology point of view, at a given crystallization temperature the β-phase shows a significantly higher long period compared to that of α-phase indicating substantial difference in the semi-crystalline morphologies between the two phases. Both the α- and the β-phases show two distinct crystallization temperature ranges when crystallized under non-isothermal mode. Further, the present study reveals that the β-phase lamellar morphology controls the β- to the α-phase transition on heating and the amount of material transforms correlates well with the lamellar thickness of the β-phase. Further, the morphology of the α-phase or the β-phase mainly depends on the T_C and not on the nature of the nucleating agents. The improved impact strength shown by the β-phase may be traced to macro and micro morphological differences between the α- and the β-phases. Also, the difference in morphology leads to lower melting temperature of the β-phase compared to that of α-

phase even though the crystal lamellae thickness of the β-phase is always higher than that of the α-phase crystal lamellae. The higher mobility of the amorphous phase[17] in the β-phase may give rise to higher fold surface interfacial energy and consequently lower melting temperature.

Carboxylate (PTBBA)-alumoxane is an efficient nucleating agent for syndiotactic polystyrene (sPS) as well. The chemical structure of sPS is analogues to iPP in which the methyl group is replaced by phenyl group. PTBBA-alumoxane exhibits higher nucleation efficiency in sPS compared to iPP and is attributed due to the better interaction with sPS than iPP. Interestingly, PTBBA-alumoxane promotes the α-phase crystallization of sPS as evident from WAXS analysis. Self nucleation studies based on the α- and the β-polymorphs of the sPS revealed that the final crystalline form is controlled by the nature of nucleation viz., homogeneous, heterogeneous and self nucleation which in turn controlled by end melting temperature (T_{max}). The α-seeds exhibit higher nucleation ability compared to that of β-seeds for a given T_{max} in the heterogeneous nucleation temperature range. Homogeneous nucleation gives β-phase while heterogeneous nucleation gives α-phase independent of starting crystalline phase. Self nucleation yields same crystalline form as that of the starting crystalline phase due strong melt memory. The formation of α-phase from the β-seeds is an interesting observation and needs further detailed studies to understand this effect. The Al-succinate MOF and zirconium PTBBA complex do not nucleate sPS due to the poor interaction with alkyl channel of the MOF.

The results presented in the thesis suggest that the interaction between the nucleating agent and the polymer controls the nucleation efficiency. Thus the additive should facilitate the favourable interaction with polymer in order to be an efficient nucleating agent. The higher nucleation efficiency of PTBBA-alumoxane with sPS compared to that of with iPP indicates that the stronger the interaction higher the nucleation efficiency. The conclusion arrived in this thesis is that interaction between the polymer and additive is prerequisite for nucleation and if there is a lattice matching, then efficieny become better.

Although, more exhaustive study is needed to understand the mechanism of nucleation in a quantitative manner, the present work undoubtedly provides valuable

pathways for developing new nucleating agents based on the carboxylate-alumoxane and MOFs with the proper selection and orientation of the carboxylate around the metal centre. This study also demonstrates that physical properties of the materials can be enhanced multi fold if the interaction occurs in the molecular scale.

8.3 Future Perspectives

- The effect of carboxylate-alumoxane and Al-MOF with varying chemical structure of carboxylate on the crystallization of PET, PLLA and other semi-crystalline polymer can be studied. In other words, the molecular structure of carboxylate-alumoxane and Al-MOF can be modified according to the nature of the polymer by appropriate selection of carboxylic acid for better impact on the polymer properties.

- The nucleation ability of additives that are structurally similar to carboxylate-alumoxanes and MOFs can be studied.

- In the present work the additives are added in minute amounts to study the nucleating behaviour of the polymer and the additives physical properties do not impact the physical properties of the crystallized polymer. Therefore, it is interesting to add significantly higher amounts of the nucleating agents and study the reinforcing effect of these additives.

Annexure

Nucleation Efficiency

Nucleation effect of additives is determined by the peak crystallization temperature of nucleated iPP in comparison with pure polymer measured at constant cooling rate. An efficient nucleating agent increases the iPP crystallization temperature compared without the additive. Nucleation efficiency is calculated based on the self-nucleation experiments introduced by Fillon et al.[1] In the self-nucleation method, the polymer is partially melted in such a way that the enthalpy of crystallization remains constant. The partial melting temperature (T_S) is chosen between the peak melting temperature and the onset melting temperature. The partial melting leaves crystalline fragments which acts as extremely efficient nucleator due to best epitaxial match and hence crystallize the polymer at maximum achievable crystallization temperature (T_C max). This temperature along with homogeneously achieved crystallization temperature (T_C min) provides a window where the external nucleating agents operate and accordingly nucleation efficiency is calculated. DSC cooling endotherm of pure iPP melt crystallized from different T_S is shown in Figure 1. The dependence of T_C on the T_S is shown in Figure 2 which shows that the T_C increases with decreasing the T_S and shows the maximum T_C (T_C max) of 140.2 °C. Homogeneous nucleation shows the minimum T_C (T_C min) which is 113 °C. The crystallization temperature of the nucleated polymer is T_C NA. Thus, the nucleation efficiency (NE) of the additive can be calculated as,

$$\mathrm{NE} = 100\,\frac{\mathrm{Tc\ NA} - \mathrm{Tc\ min}}{\mathrm{Tc\ max} - \mathrm{Tc\ min}}$$

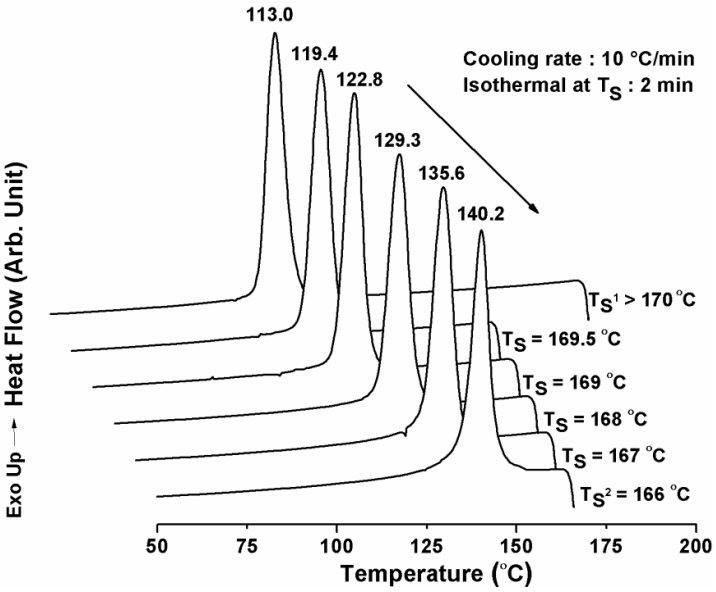

Figure 1. DSC cooling endotherm of pure iPP melt crystallized from different self-nucleation temperatures (T_S).

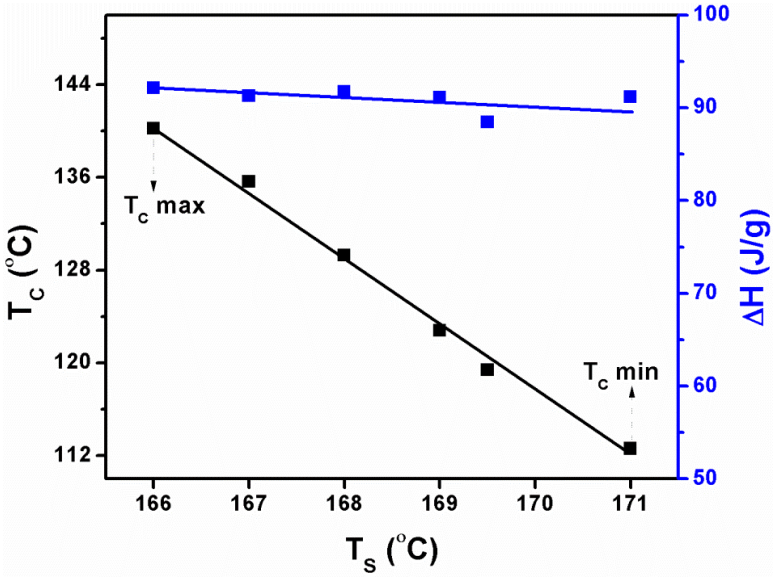

Figure 2. Variation of self-nucleation temperature (T_S) with the crystallization temperature (T_C) of iPP

References

(1) B. Fillon, B. Lotz, A. Thierry, J. Wittmann, *J. Polym. Sci. Part B:Polym. Phys.*, 1993, **31**, 1395.

Details of the Correlation function

In order to measure the morphological variables, specifically the lamellar thickness and the intervening amorphous phase thickness, the SAXS profiles were processed following the method given by Hsiao and Verma.[1] As recorded SAXS profile of the *β*-phase iPP sample crystallized at 130 °C is shown in Figure 1a. The data points of direct beam intensity at low q region were removed and then the intensity is extrapolated to zero at q=0. The Lorentz corrected profile after the extrapolation is shown in Figure 1b. The larger q region was corrected by applying Porod's law with the assumption of finite interface between the crystal and amorphous phases. The representative corrected SAXS profile is given in Figure 1c. Then, the fast Fourier transformation (FFT) was performed on the corrected SAXS data to get the correlation function γ(r) (Figure 1d).

$$\gamma(r) = \frac{1}{Q}\left[\int_0^\infty q^2 I(q)\cos(qr)dq\right]$$

The long period, crystal and amorphous lamellae thicknesses were extracted from the correlation curve according to the method given by Strobl and Schneider.[2]

The value of the first maximum in the correlation function is measured as long period (L). The lamellar thicknesses of the two phases from the long period are calculated using the following equations.[3]

$$\frac{1-x_1}{x_1} = cy \text{ --------(i)}$$

$$x_2=(1-x_1)L \text{ ----------(ii)}$$

The x_1 and x_2 represents larger and lower fractions of the two phases respectively and y is obtained from the correlation function at its first minimum. For example, the *β*-phase of iPP crystallized at 130 °C show y=0.201 (Figure 1d), c is the normalization constant, cγ1(0)=1 and long period (L) is 243Å.

Hence,

$$\frac{1-x_1}{x_1} = 1 * 0.201$$

$$x_1 = \frac{1}{1.201}$$

x_1= 0.83

and

$l_1 = x_1 L$

$l_1 = 0.83 * 243 Å$

$l_1 = 202 Å$

$l_2 = (1-x_1)L$

$l_2 = 41 Å$

Since the isotactic polypropylene is a semi-crystalline polymer, generally having crystallinity *ca.*60-70 %, the larger fraction (x_1) can be considered as thickness of crystal lamellae (l_c) and and x_2 is the contribution from amorphous phase (l_a) present in inter lamellar region.

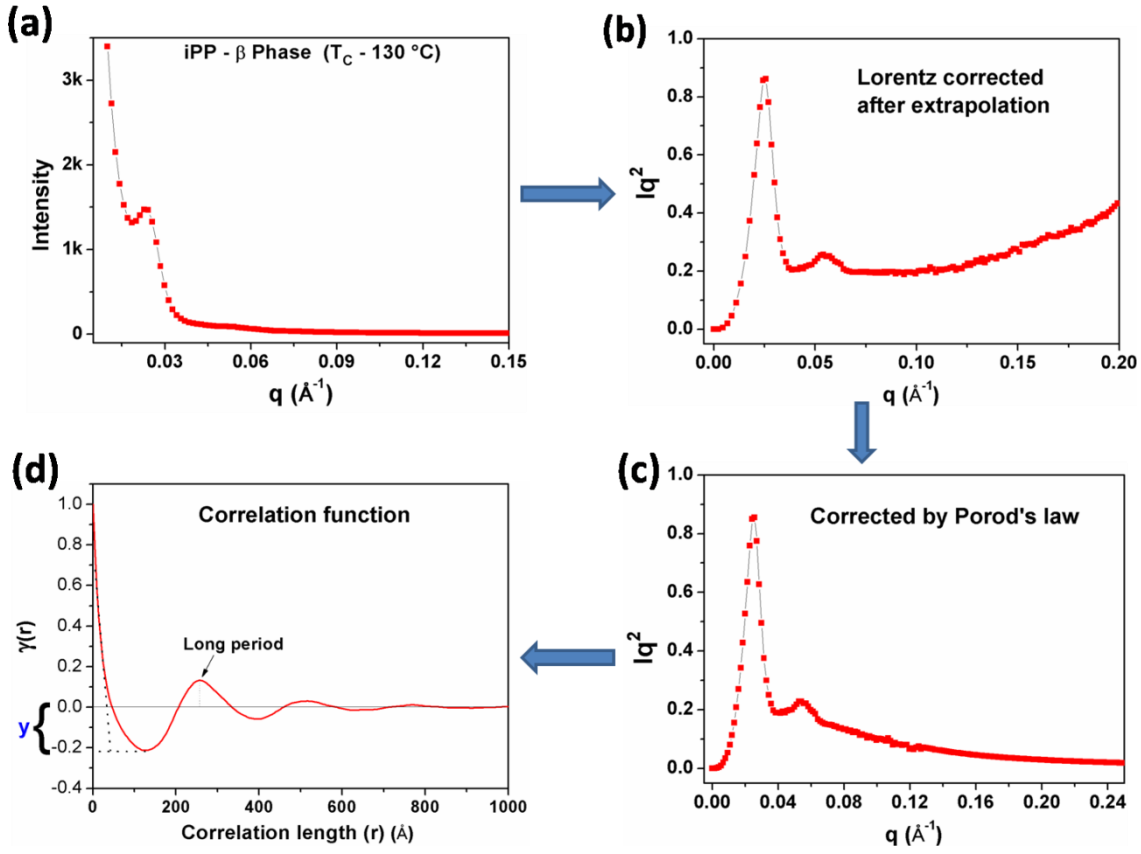

Figure 1. (a) SAXS pattern of *β*-phase of iPP crystallized at 130 °C. (b) Lorentz corrected SAXS pattern (previously the background data points were removed and scattered intensity fixed zero at q=0 by linear extrapolation). (c) Larger q region was corrected by applying Porod's law. (d) Correlation function.

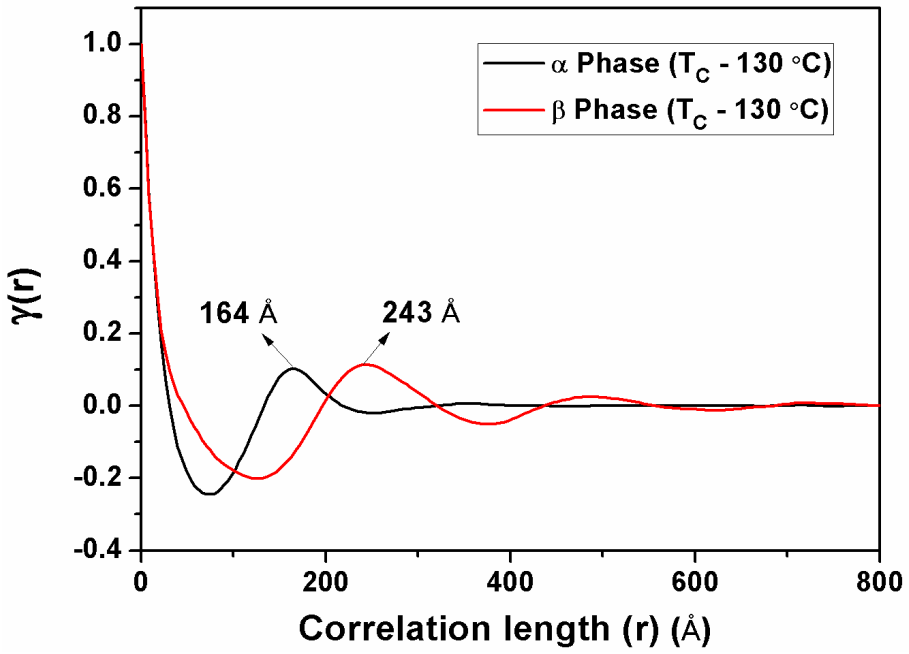

Figure 2. Correlation function of the α and the *β*-phases of iPP non-isothermally crystallized at 130 °C. The respective long periods are indicated in the figure.

References

(1) Hsiao, B.; Verma, R. *J Synchrotron Rad.*, **1998**, *5*, 23.

(2) Strobl, G.; Schneider, M. *J. Polym. Sci. Polym. Phys. Ed.*, **1980**, *18*, 1343.

(3) Cruz, C.; Stribeck, N.; Zachmann, H.; Calleja, F. *Macromolecules*, **1991**, *24*, 5980.

Publications

1. New understanding on regulating the Crystallization and Morphology of β polymorph of isotactic Polypropylene based on carboxylate-alumoxane nucleating agents

   Mohan Raj, M.; Chellaswamy, R.; Marathe, Y.; Pillai, V.

   Macromolecules, **2016**, 49, 2197.

2. Enhanced nucleation of polypropylene by metal organic frameworks (MOFs) based on aluminium dicarboxylates: Influence of structural features

   Mohan Raj, M.; Chellaswamy, R.; Marathe, Y.; Pillai, V.

   RSC Adv., **2016**, 6, 1907.

3. The role of the molecular structure of carboxylate-alumoxanes in the enhanced nucleation of polypropylene

   Mohan Raj, M.; Chellaswamy, R.; Marathe, Y. N.; Pillai, V.

   Chem. Commun., **2015**, 51, 10026.

4. Effect of carboxylate-alumoxane on syndiotactic polystyrene (sPS) crystallization and morphology"

   Mohan Raj, M.; Chellaswamy, R.; Pillai, V.

   (Manuscript in preparation)

Patents filed

1. Carboxylate-alumoxanes nucleating agents and a process for the preparation thereof,

   Mohan Raj, M.; Chellaswamy, R.; Pillai, V.

   US2015/0344672A1, EP2938667A1, WO2014102825A1.